UNIVERSITY OF OKLAHOMA

GRADUATE COLLEGE

# BLOWOFF CHARACTERISTICS OF PARTIALLY PREMIXED FLAMES OF PREVAPORIZED BLENDS OF BIOFUELS AND PETROLEUM FUELS

A THESIS

SUBMITTED TO THE GRADUATE FACULTY

in partial fulfillment of the requirements for the

Degree of

MASTER OF SCIENCE

By

TONČI MALETA
Norman, Oklahoma
2017

Downloaded from SHAREOK. Persistent Handle URL: https://hdl.handle.net/11244/52943

BLOWOFF CHARACTERISTICS OF PARTIALLY PREMIXED FLAMES OF PREVAPORIZED BLENDS OF BIOFUELS AND PETROLEUM FUELS

A THESIS APPROVED FOR THE
SCHOOL OF AEROSPACE AND MECHANICAL ENGINEERING

BY

_____
Dr. Ramkumar Parthasarathy, Chair

_____
Dr. Wilson Merchan-Merchan

_____
Dr. Jivtesh Garg

© Copyright by TONČI MALETA 2017
All Rights Reserved.

*to my family*

**Acknowledgements**

I express my deepest gratitude to my academic advisors Dr. Subramanyam Gollahalli and Dr. Ramkumar Parthasarathy. Your guidance and advice made it possible for me to complete this work. I thank Dr. Parthasarathy for straightforward criticism and immense patience. You thought me valuable life lessons which made me not just a better engineer and scientist, but also a more professional and thoughtful person. Professors had a big influence on me and some even changed the trajectory of my life. I can only hope to be the same inspiration for others.

I would like to acknowledge my labmates Dr. Arun Balakrishnan, Flavio Moreno, Alexander Spens, and Colby Bodkin for their valuable input towards my research as well as making this journey more joyful.

A special appreciation goes to Gallogly College of Engineering Dean Theresa Marks, MEP Executive Director Lisa Morales, and Dr. James Sluss. I will always stay grateful for your support and help.

I thank AME office staff for their kindness, patient help, and cheerful attitude whenever I walked in the office.

Lastly and above all, I give thanks to God for granting me keenness of mind, capacity to remember, skill in learning, lucidity in interpretation, and eloquence in speech.

## Table of Contents

Acknowledgements ..... iv

Table of Contents ..... v

List of Tables ..... vii

List of Figures ..... viii

Abstract ..... xii

Chapter 1 Introduction ..... 1

Chapter 2 Literature Review ..... 5

Flame Stabilization ..... 5

Partially Premixed Flames ..... 9

Biofuel Flame Studies ..... 16

Laminar Flame Speed ..... 20

Chapter 3 Experimental Setup and Technique ..... 26

Combustion Chamber ..... 26

Air and Fuel Delivery System ..... 28

Blowoff Measurement ..... 31

Velocity Profile Measurement ..... 32

Flame Dimensions ..... 35

Flame Temperature Profile ..... 39

Stoichiometric Formula ..... 40

Reynolds Number Calculation ..... 41

Damköhler Number Calculation ..... 42

Chapter 4 Experimental Setup and Technique ..... 45
Operational Range of Burner ..... 45
Blowoff Velocities ..... 51
Damköhler Number ..... 55
Inflame Temperature Measurements ..... 57
Flame Dimensions ..... 60
Chapter 5 Summary and Conclusions ..... 118
References ..... 121
Appendix A: Blowoff Velocities ..... 130
Appendix B: Flame Dimensions ..... 137
Appendix C: Temperature Profiles ..... 157
Appendix D: Laminar Flame Speed Estimation ..... 159
Appendix E: MATLAB code ..... 161

## List of Tables

Table 3.1: Heat tape temperature settings based on fuel type ..... 34

Table 3.2: Parts and Instrumentation ..... 34

Table 3.3: Typical range of Reynolds number (example of Jet A at all three coflow velocities) ..... 42

Table 3.4: Uncertainties of various parameters ..... 44

Table 4.1: Properties of tested fuels ..... 48

Table 4.2: Experimental conditions ..... 49

Table 4.3: Damköhler number for Jet A flames at blowoff ..... 75

Table 4.4: Damköhler number for CME flames at blowoff ..... 75

Table 4.5: Damköhler number for PME flames at blowoff ..... 76

Table 4.6: Damköhler number for SME flames at blowoff ..... 76

## List of Figures

Figure 3.1: Photograph of experimental set-up ..... 26

Figure 3.2: Schematic diagram of experimental set-up ..... 28

Figure 3.3: Photograph of the burner ..... 29

Figure 3.4: Schematic diagram of the fuel/air delivery to the burner ..... 30

Figure 3.5: Schematic illustration of blowoff representing the flame velocity and gas velocity above the burner rim; Curves A, B, C are flame velocities at heights A, B, C; Curve 1 – flashback limit, curve 2 – stable flame, curve 3 – blowoff limit, curve 4 – blowoff (Lewis and von Elbe, 1987) ..... 32

Figure 3.6: An example of a flame and its binary image with the brightness threshold set for inner cone; Fuel: Jet A, Re = 2800, U = 3.8 m/s, Φ = 0.74 ..... 36

Figure 3.7: An example of a flame and its binary image with the brightness threshold set for outer cone; Fuel: Jet A, Re = 2800, U = 3.8 m/s, Φ = 0.74 ..... 37

Figure 3.8: An example of a lifted flame and its binary image with the brightness threshold set for a lifted flame; Fuel: Jet A, Re = 2800, U = 3.8 m/s, Φ = 0.74 ..... 38

Figure 3.9: Illustration of inflame temperature measurement ..... 40

Figure 4.1: Air temperature rise at burner exit with time at coflow velocity of 2.3 m/s (heat tape set to 520 K) ..... 47

Figure 4.2: Air temperature at the burner exit at coflow velocity of 2.3 m/s ..... 47

Figure 4.3: The first flame achieved in the experimental setup; Jet A at a flow rate of 2 ml/min with 14,800 ml/min of primary airflow rate and 5.95E-3 $m^3$/s of coflow ..... 50

Figure 4.4: Images of typical blowoff for various fuels ..... 69

Figure 4.5: Oscillations between attached and detached phase, t = 0.67 seconds,..... 70
Figure 4.6: Typical blowout of a lifted flame; constant change in flame dimensions and shape can be observed, time interval is 0.67 seconds,..... 71
Figure 4.7: Axial velocity profiles at 6 mm above burner at temperature of 523 K ..... 73
Figure 4.8: Change in velocity gradient with coflow ..... 74
Figure 4.9: Change in blowoff velocity with equivalence ratio for pure fuels at different coflow velocities..... 78
Figure 4.10: Change in blowoff velocity with equivalence ratio for flames of pure CME and Jet A and their blends at different coflow velocities ..... 80
Figure 4.11 Change in blowoff velocity with equivalence ratio for flames of pure PME and Jet A and their blends at different coflow velocities ..... 82
Figure 4.12: Change in blowoff velocity with equivalence ratio for flames of pure SME and Jet A and their blends at different coflow velocities ..... 84
Figure 4.13: Change in inner cone height with equivalence ratio for flames of pure fuels at different coflow velocities..... 86
Figure 4.14: Change in outer cone height with equivalence ratio for flames of pure fuels at different coflow velocities..... 87
Figure 4.15: Change in outer cone width with equivalence ratio for flames of pure fuels at different coflow velocities..... 89
Figure 4.16: Change in liftoff height with equivalence ratio for flames of pure fuels... 89
Figure 4.17: Change in inner cone height with equivalence ratio for flames of CME blends at different coflow velocities..... 91

Figure 4.18: Change in inner cone height with equivalence ratio for flames of PME blends at different coflow velocities..... 92
Figure 4.19: Change in inner cone height with equivalence ratio for flames of SME blends at different coflow velocities..... 94
Figure 4.20: Change in outer cone height with equivalence ratio for flames of CME blends at different coflow velocities..... 95
Figure 4.21: Change in outer cone height with equivalence ratio for flames of PME blends at different coflow velocities..... 97
Figure 4.22: Change in outer cone height with equivalence ratio for flames of SME blends at different coflow velocities..... 98
Figure 4.23: Change in outer cone width with equivalence ratio for flames of CME blends at different coflow velocities..... 100
Figure 4.24: Change in outer cone width with equivalence ratio for flames of PME blends at different coflow velocities..... 101
Figure 4.25: Change in outer cone width with equivalence ratio for flames of SME blends at different coflow velocities..... 103
Figure 4.26: Change in liftoff height with equivalence ratio for flames of blends ..... 104
Figure 4.27: Example of heights at which the temperature profiles were measured (Jet A flame)..... 105
Figure 4.28: Temperature profile across the burner in absence of flame measured at 3 mm above the burner for two different conditions: without coflow and at coflow velocity of 2.3 m/s; temperature was set to 493 K and primary airflow velocity of 4.3 m/s ..... 106

Figure 4.29: Inflame temperature profiles of pure fuels at no coflow..... 108

Figure 4.30: Jet A inflame temperature profiles at different coflow rates ..... 109

Figure 4.31: CME inflame temperature profiles at different coflow rates..... 111

Figure 4.32: PME inflame temperature profiles at different coflow rates ..... 112

Figure 4.33: CME blends inflame temperature profiles at no coflow..... 114

Figure 4.34: PME blends inflame temperature profiles at no coflow ..... 115

Figure 4.35: SME blends inflame temperature profiles at no coflow ..... 117

## Abstract

The laminar partially premixed flames of prevaporized Jet A, canola methyl ester (CME), palm methyl ester (PME), soy methyl ester (SME), and blend flames of Jet A and CME-PME-SME were studied over a range of equivalence ratios of 0.53-0.83 with and without heated coflow. Coflow velocity ranged up to 3.5 m/s. Measurements of blowoff velocities, flame temperature profiles, and flame dimensions were made. The injector was designed to produce a uniform inner flow and had an inner diameter of 12.7 mm. The flames were laminar and blue in color (dominated by homogeneous gas-phase reactions). The temperature profiles in all the flames were similar, with a peak temperature of 1740 K. Inner cone height and outer cone height both increased with equivalence ratio. Lifted flames were obtained at coflow velocity of 3.5 m/s; the liftoff height stayed approximately constant regardless of equivalence ratio. The blowoff velocity increased with equivalence ratio for all the flames; the difference in blowoff velocity of pure biodiesel flames and pure Jet A flames was within experimental uncertainty. The blowoff velocity of the blend flames ranged around the values for the pure fuel flames. A Damköhler number (based on the velocity gradient at the jet boundary and chemical reaction time scale estimated from laminar flame velocity) of 2-8 characterized the blowoff velocity. As the coflow velocity was increased, the blowoff velocity was increased and the differences between the values for the various flames became smaller.

# Chapter 1 Introduction

## Flame Extinction and Stability

Flame extinction is one of the most fundamental phenomena studied in the combustion field (Glassman and Yetter, 1996). It is governed by chemistry, mass transport and other combustion processes. The extinction of jet diffusion flames is described in terms of liftoff and blowout. Liftoff occurs when the emerging jet velocity is high enough so the flame lifts off from the burner and stabilizes at some location downstream. Blowout occurs when a lifted flame can no longer stabilize downstream of the burner; instead, the flame gets extinguished. A flame can blow off immediately as it detaches from the burner without stabilizing at some location downstream as a lifted flame. Opposite from liftoff, a flame can also flash back into the burner tube if the jet velocity is too small. It is highly undesirable to have a flame flash back as it can have detrimental safety consequences (Turns, 2011). The blowoff characteristics are one of the important criteria in designing burners for various applications such as in boilers and gas turbines. It is important to understand flame stabilization in order to control combustion in various applications.

The surrounding airflow can affect the combustion and resulting flame configuration significantly. The studies on liftoff and blowoff are often carried out in a coaxial environment. In this arrangement, the primary burner tube is housed coaxially within a larger tube which delivers air (coflow). There is also a transverse arrangement in which the primary jet nozzle is perpendicular to airflow (crossflow). The

characteristics of coflow (or crossflow), such as velocity and temperature, can have a significant impact on the flame behavior and stability parameters.

A variety of different studies have focused on the extinction of premixed, partially premixed, and non-premixed flames. Partially premixed flames are a 'hybrid' type of a flame possessing characteristics of both non-premixed and premixed flames. These flames include a wide range of flames such as double, tribrachial and edge flame structures. Examples of partially premixed flames can be found in diesel engines (Higgins and Siebers 2001) and gas turbine combustors (Mongia 2004). It is, therefore, important to study extinction characteristics of partially premixed flames specifically.

## Partially Premixed Flames

Partially premixed flames are formed by mixing air and fuel in less than stoichiometric proportions. Many home appliances and industrial furnaces operate with partially premixed flames. Air can be added to fuel jet to increase stability. Additionally, partially premixed flames are present in turbulent combustion due to reignition effects. The focus of this thesis is on the blowoff characteristics of partially premixed flames. Partially premixed combustion has been studied as a way to reduce NOx emissions and soot formation in engines and gas turbines. Premixed and non-premixed flames contain a single dominant reaction zone, whereas partially premixed flames contain multiple reaction zones. A lifted non-premixed flame often contains a partially premixed structure prior to blowout. A double flame contains two reaction zones one of which is rich premixed zone on the fuel side and the other zone which is non-premixed zone on the oxidizer side. A triple flame contains three reaction zones,

two premixed reaction zones and a non-premixed zone between them. The overall flame structure is strongly dependent on interaction of these zones. Consequently, there are important differences in flame liftoff and blowoff between premixed, non-premixed, and partially premixed flames.

## Biofuel Flames

The need for fuel continues to increase, and researchers are seeking to increase the energy independence and simultaneously decrease environmental impact. In recent years, the search for alternative fuels which are environmentally-friendly and which could replace petroleum fuels has grown significantly.

Biofuels are a renewable energy source produced from various feedstock which can be grown domestically. Biodiesels (a subcategory of biofuels) are produced by the transesterification of vegetable oils, residual fry oil or animal fats with alcohol and alkaline catalysts. Some of the biofuels have been suggested as a viable option for petroleum fuel replacement and have been experimentally investigated and are commercially available. Canola, palm, and soy methyl esters (CME, PME, SME) are biodiesels which are produced by the transesterification of canola, palm, and soy oil, respectively. Rapeseed and soybean oil are most common feedstock used for biodiesel production in United States and Europe. These biodiesels are nearly carbon-neutral and their physical properties are nearly similar to those of petroleum-based fuels; therefore, they can be blended with petroleum fuels and can be readily used in existing engines with little or no modifications (Balakrishnan, 2016). While the performance of these fuels and their petroleum fuel blends in engines has been well-documented

(Balakrishnan, 2016, Durbin, 2000, Labeckas, 2006, Muralidharan, 2001), fundamental knowledge of the stabilization mechanism and blowoff of the blends of biofuels with petroleum fuels is still lacking. Thus, the motivation for this study was to improve our understanding of the stabilization mechanism and blowoff of these fuels.

## The Scope of This Work

The objective of this investigation is to study the stabilization mechanism and blowoff phenomena of pre-vaporized blends of Jet A fuel and biofuels (CME, PME, SME) in the fuel-lean regime. Fuel-lean conditions are preferred in operation due to lower pollutant emissions.

# Chapter 2 Literature Review

## Flame Stabilization

Flame stabilization mechanism has been studied for decades. Some of the early research in this field involved qualitative observations. Wohl et al. (1949) performed a number of experiments involving butane-air flames (lean mixtures and diffusion flames) in laminar and turbulent flow in still air. The authors concluded that a lifted diffusion flame stabilized at a height above the burner and this height depended on the local physical and chemical parameters. For a given burner diameter and a fuel gas, a lifted diffusion flame could only exist between two limiting values of the gas flow. If the gas flow was lower than the gas flow at drop back, the flame dropped back and attached to the burner (or even flashed back in the tube). If the gas flow was higher than the gas flow at blowout, the flame extinguished. The stabilization height depended on the gas flow and it lied somewhere between these two limits.

Vanquickenbourne and van Tiggelen (1966) were among the first to investigate the stabilization mechanisms of lifted diffusion flames in still air. The experiment involved methane as fuel emerging from a circular burner. They reported that a turbulent lifted diffusion flame stabilized at a certain height above the burner where the local methane concentration corresponded to the stoichiometric value. The assumption was that at this point the gas velocity was equal to turbulent flame speed. Blowout occurred when the flame was at a height far upstream where the local fuel concentration was too lean to support the combustion.

The most comprehensive experimental study of blowout was performed by Kalghatgi (1984). The study involved different fuels (hydrogen, propane, methane, and ethylene) tested over a range of burner diameters (up to 8 mm diameters) and jet velocities with no coflow. Jet velocities ranged up to 2,000 m/s in case of hydrogen, and about 250 m/s for other fuels. Particularly, liftoff heights of turbulent jet diffusion flames in still air were measured. It was reported that liftoff height increased linearly with jet velocity. The study showed that there was no noticeable change in the liftoff height when different burner diameters were used. Additionally, the liftoff height was found to be inversely proportional to the square of the maximum laminar flame speed.

Broadwell et al. (1985) investigated the blowout of turbulent diffusion flames in still air. No experiments were conducted in this study. Rather, their analysis was based on already published literature, primarily that of Kalghatgi (1984). It was proposed that flame stabilization resulted when hot gases were re-entrained and ignited the non-combusting eddies of the jet. They argued that the blowout occurred when the combustion began far in the axial direction so the re-entrained, hot gases were mixed so rapidly with the jet that there was not enough time for the mixture to reignite before the temperature and fuel concentration fell below some critical value. The ratio of a characteristic chemical reaction time and a time associated with mixing of hot products and fresh reactants was the single parameter which determined the blowout velocity. When this ratio was less than some critical value, the blowout occurred. Average value of the critical blowout parameter was 4.8.

Savas and Gollahalli (1986) conducted experiments with laminar propane diffusion flames in still air. The Reynolds number was sufficiently low to ensure

laminar flow (ranged less than 250). It was reported that combustion occurred within a laminar region outside the jet. It was observed that a lifted flame reattached quickly back to the burner when the jet velocity was decreased. However, the authors observed hysteresis as the liftoff velocities and reattachment velocities were significantly different. The difference was described in terms of Strouhal number which was 2.8 and 1.30 during liftoff and reattachment, respectively.

The Damköhler number has been used to characterize the blowoff of flames. The Damköhler number is the ratio of the flow time scale and the chemical reaction time scale. As noted by Lewis and von Elbe (1987), blowoff occurred when the gas velocity gradient at the jet edge became higher than the flame velocity near the jet edge (which reduces to zero steeply). Thus, the blowoff-limit was reached when the gas velocity near the edge was tangential to the flame velocity variation with distance from the boundary. Thus, the gradient of velocity near the edge was an important factor in determining the flow time scale.

Pitts (1988) compared many competing theories which characterized the stabilization mechanism and blowout of lifted diffusion flames in turbulent regime. In addition, the author compared the theories with the actual turbulent behavior of unignited fuel jets. The conclusion of the study was that none of the currently available theories accurately predicted the stabilization and blowout mechanism and that further experimentation was required to gain a better understanding of this matter.

Tieszen et al. (1996) conducted experiments on blowout phenomena of turbulent jet diffusion flames. The experiment involved ethylene and ethane as fuels. Reynolds number (based on turbulent integral length scale) was 2,500 and 6,000 for ethane and

ethylene, respectively. Unlike in the case of lifted flames where combustion occurred near the outer edge of the jet, it was observed that most of the jet of diffusion flame was combusting in a premixed flame near blowout. They concluded that the blowout occurred when the local flow velocity exceeded the premixed turbulent flame speed, which was first proposed by Vanquickenbourne and van Tiggelen. Under this assumption, they developed a model which was in agreement with the conclusion of Broadwell et al. (1985) that large-scale turbulent structures were involved in the stabilization process. However, they argued that these rotational structures played a role to enhance the turbulent flame speed near blowout, which happened in the interior of the jet.

Montgomery et al. (1998) studied the effect of coflow velocity on lifted diffusion flames. The experiment was conducted in turbulent regime and it involved methane as the fuel. They experimented with a wide range of jet (20 m/s – 50 m/s) and coflow (0.1 m/s – 15 m/s) velocities. The photographs of flow visualization illustrated that the jet spread out more slowly with higher coflow velocities. Thus, the coflow did not contribute to the mixing of the jet and surrounding air.

Brown et al. (1999) investigated the dependence of liftoff height on turbulent jet exit velocity and coflow velocity of a non-premixed jet flame. The maximum jet exit velocity was three times the laminar flame velocity. The coflow velocity was varied (between 0 and 2.5 m/s) while the gas flow velocity of methane or ethylene was kept constant. The study was conducted with the maximum gas flow velocity reaching up to 43 m/s. The results showed that the liftoff height increased in linear fashion with increase in coflow velocities. The flame became more sensitive to changes in coflow

velocities when it stabilized farther away from the burner. For instance, a change of 0.1 m/s in coflow velocity increased the liftoff height from 3.0 to 3.5 inches, but a change of only 0.03 m/s in coflow was necessary to lift the flame from 4.0 to 4.5 inches. Their results support the initial proposal by Vanquickenbourne and van Tiggelen (1966) that lifted flames in the near-blowout region stabilized at stoichiometric contours where the local jet velocity equaled the turbulent flame speed.

It is important to understand the physical processes in which a flame approaches blowoff in order to obtain a correlation for the blowoff phenomenon. Lean blowoff is often not an abrupt process. Zhang (2008) investigated lean blowoff characteristics of swirling $H_2$/CO/$CH_4$ premixed flames. The author reported that before the lean blowoff, the flame oscillated between extinction and re-ignition phases. Nicholson and Field (1951) reported large scale pulsations in the flame as it approached lean blowoff in their paper regarding flame stabilization mechanism in the wake of bluff bodies. They observed that the flame detached and reattached to the burner repeatedly before the lean blowoff occurred. This kind of behavior was also observed by Hertzberg (1991).

## Partially Premixed Flames

Peters and Williams (1983) described the behavior of lifted turbulent jet diffusion flames. The jet velocity was increased until it reached a sufficiently high Reynolds number and the flame became turbulent. The reaction took place at the nozzle exit. As the jet velocity was increased further the flame detached from the nozzle and stabilized at some location downstream. The liftoff height increased with increase in jet velocity, but the overall flame height stayed nearly constant. As the jet velocity was

increased further to some critical value, the flame blew off. When a flame was stabilized near the nozzle the reaction took place only in the thin strained flames. It was quenched when the mixture was above the rich limit (strain rates being low enough only in fuel-lean regions). At the flame end the reaction occurred in both the flame sheets and as the entire flame was homogenized as the air entered the mixture and made it combustible.

Rokke et al. (1994) performed a study with unconfined turbulent partially premixed propane/air flames emerging from a straight tube into quiescent air at atmospheric pressure and temperature. Six different nozzle diameters (up to 29.5 mm diameters) were used and the fuel mass fraction ranged from 0.15 – 1.0. Jet outlet velocities varied from 1 m/s to 130 m/s and the flame height reached up to 2.5 m. It was proposed that the liftoff height was inversely proportional to the square root of the mass fraction in the partially premixed jet. This correlation was in good agreement with experimental results. Additionally, increase in air/fuel ratio resulted in smaller flame heights.

Gore and Zhan (1996) reported measurements of visible flame heights and radiative heat loss fractions in experiment with partially premixed laminar flames of methane in fuel-rich regime (equivalence ratio range of 1.4 – 19). The experiments were conducted with presence of coflow (up to 1442 mg/s of coflow rate). The air/fuel mixture flow rate reached up to 515 mg/s. The visible flame height decreased (by approximately 30%) and the flame color changed from yellow to blue as the level of partial premixing increased. The radiative heat loss fractions initially decreased to 12%

with the increase in level of partial premixing, but then it stayed approximately constant.

A triple flame is a partially premixed flame which contains three reaction zones, two premixed reaction zones and a non-premixed zone between them. The overall flame structure is strongly dependent on interaction of these zones. Azzoni et al. (1999) studied the characteristics of the triple flames using methane as fuel in a fuel rich mixture. A Wolfhard-Parker slot burner was used to achieve laminar triple flames. The flow consisted of a rich mixture of methane and air emerging from the inner slot (equivalence ratio ranged from 1.6 to 1.9) and a lean mixture from two symmetric outer slots (equivalence ratio ranged from 0.33 to 0.39). The results from a detailed numerical model were in good agreement with experimental results. All three different reactions zones were clearly identifiable. As the equivalence ratio in the fuel-rich stream increased or that in the fuel lean stream decreased, the heights of both the innerpremixed and the non-premixed reaction zones increased. Heat release occurred in all three zones, but the magnitude was different depending on the level of partial premixing.

Characteristics of reattachment and blowout of laminar lifted flames in partially premixed jets of propane fuel have been investigated experimentally in a series of studies conducted by Chung and Lee (1991; 1997; 2001; 2003) with and without coflow. They observed that a base of a lifted laminar flame exhibited a tribrachial structure consisting of a lean and a rich premixed flame wings and a trailing diffusion flame, all originating at a same location (Chung and Lee 1991). Propagation speed of tribrachial flame and the local jet velocity speed were the two parameters which

governed the stabilization of lifted laminar flames. It was also shown that the positions of maximum luminosity of lifted tribrachial flames can reasonably be located along the stoichiometric contour. The authors reported that as flow rate decreased from a lifted flame, liftoff height decreased nonlinearly and the flame reattached to a nozzle at a certain liftoff height (Lee and Chung 2001).

Puri et al. (2001) performed a numerical and experimental study on the similarity between lifted and methane-air burner-stabilized triple laminar flames with no coflow. The reaction zone of the flame consisted of the outer lean premixed zone, an inner rich premixed zone, and a central nonpremixed zone. The overall equivalence ratio was 0.6, inner equivalence ratio was 1.8, and outer equivalence ratio was 0.35. The highest temperature was found to be between the inner rich and central nonpremixed zone. A lifted flame was simulated by varying the boundary conditions used for investigating the burner-stabilized flames. The shape and separation distance of three reaction zones were found to be very similar for lifted and burner-stabilized flames. In addition, the heat-release distribution was almost identical for both kinds of flames.

Effects of coflow on reattachment and blowout were also inspected in a study with lifted propane flames in laminar jets (Lee et al., 2003). The liftoff height in coflow jets was found to increase highly nonlinearly with jet velocity and was sensitive to coflow velocity. The blowout and reattachment velocities decreased in linear fashion with the increase in coflow velocity. At coflow velocity of 15 cm/s (which was maximum coflow velocity used in the study), a burner attached flame lifted off at a liftoff velocity of 9.7 m/s. As the jet velocity was increased further, the liftoff height increased until the flame blew out at the velocity of 11.0 m/s. When jet velocity was

decreased, a lifted flame reattached to the burner at a velocity of 7.4 m/s. Thus, the liftoff and reattachment velocities were different. As noted earlier, this behavior was also observed by Savas and Gollahalli (1986).

Choi and Puri (2003) examined flame stretch effects on two-dimensional 'regular' and 'inverted' flames in experiments with methane-air and propane-air mixtures without coflow. The regular flames had a negative curvature and they were concave to the unburned mixture, while the inverted flames had a positive, convex curvature. The curvature had a significant effect on the flame speed. In case of inverted flames, the positive curvature decreased local reaction and heat generation rates, which resulted in lower flame speed. For example, laminar flame speed decreased by approximately 8 cm/s (from 25 cm/s to 17 cm/s) when the curvature decreased by about 20%. Base of triple flames had a smaller radius of curvature when compared to double flames. Smaller radius of curvature resulted in flames which were more readily lifted and extinguished through blowout.

Lock et al. (2007) investigated the difference in liftoff phenomena between partially premixed and non-premixed laminar flames in lifted methane-air coflow flames. Equivalence ratio in partially premixed flames was 1.5 and 2.25. The results showed that, in fuel stream dilution, partially premixed flames stabilized at higher liftoff heights than non-premixed flames. In contrast, in air stream dilution, non-premixed flames stabilized at higher heights than partially premixed flames. The liftoff height ranged up to 110 mm. The difference in the liftoff height between partially premixed and non-premixed flames depended on the level of dilution (air stream dilution or fuel stream dilution).

Wu et al. (2009) presented an experimental study on the liftoff and blowout stability mechanism of pure hydrogen, hydrogen/propane and hydrogen/methane jet flames using a 2 mm burner without coflow. In addition to hydrocarbon fuels, carbon dioxide and argon gas were used for comparison. Jet exit velocity varied from 700 m/s to 1400 m/s. It was observed that the flame liftoff height of the pure hydrogen diffusion flame increased with the jet velocity. The flame was at approximately 17 mm liftoff height at about 730 m/s of jet exit velocity. As the velocity increased to about 1350 m/s, the liftoff height increased to 29 mm. Hydrogen/methane required highest liftoff, blowoff, and blowout velocities, while hydrogen/propane resulted in highest liftoff height (it ranged from 50 mm to 70 mm). Propane addition was more effective in hydrogen flame blowout than carbon dioxide addition. Methane effects on hydrogen flames were similar to those of carbon dioxide. At high concentration, direct blowoff of the methane/hydrogen was achieved.

Following Pitts' review (1988) which concluded that none of the currently available theories accurately predicted the stabilization and blowout mechanism, there was a large number of papers published which added to better understanding of this matter. In a majority of these papers, computational modelling techniques, which were not available before, were used to expand our knowledge of flame stabilization. Nonetheless, the fundamental understanding of flame stabilization and blowout phenomena was still lacking. Lawn (2009) focused on additional complexity of the matter when coflow was present. The author reviewed three competing theories for the stabilization of lifted flames on fuel jets with presence of coflow. These theories were discussed in numerous studies such as the ones presented in this section, and can be

divided in the premixed model, the extinction model, and large eddy model. It was concluded that presence of coflow moved the stoichiometric contour and the contour of maximum flame velocity to a smaller radius at the same height in the jet. Thus, the flame stabilized further downstream.

Choi and Chung (2013) performed an experimental study on turbulent lifted flames of methane in coflow jets by varying the initial temperature. The authors used the premixed flame model (initially proposed by Vanquickenbourne and van Tiggelen, 1966) for liftoff height prediction. Thermal diffusivity of unburned gas temperature was used rather than burned gas temperature in their predictions. The Reynolds number ranged from 1766 to 3139. They reported that the liftoff height decreased with the jet velocity in the transition regime, and increased linearly with the jet velocity in the turbulent regime. For example, liftoff height increased from approximately 50 cm to 133 cm when fuel jet velocity increased from approximately 20 m/s to 60 m/s.

Kedia and Ghoniem (2015) performed a numerical study on blowoff mechanism of laminar premixed flames stabilized on a confined bluff-body. Reynolds number was kept constant at 500 while the equivalence ratio was decreased until the blowoff occurred. The equivalence ratio range was 0.42 – 0.8. They concluded that a flame would not blow off if it was in a state of static and dynamic stability. Static stability was achieved when the local flame displacement speed was equal to the flow speed. Dynamic stability was achieved when the gradient of the flame displacement speed normal to its surface was higher than the gradient of the flow speed along the same direction. As the equivalence ratio was reduced, the difference between the displacement gradient and flow gradient decreased, violating the dynamic stability,

which led to blowoff. Blowoff was initiated at a location along the flame where the violation of dynamic stability first occurred. This location was far downstream from the flame anchoring zone, near the recirculation zone. The authors confirmed that Damköhler number correlated well with blowoff indicating once more that Damköhler number encompasses well the basic physical mechanism responsible for blowoff.

## Biofuel Flame Studies

Biodiesel is a renewable, safer, less pollutant, biodegradable alternative fuel which could substitute petroleum fuels. Fuel properties of biodiesel and petroleum fuels are comparable, but due to the differences in physical and chemical properties, pure biodiesel cannot be readily used in existing industrial and domestic machines. However, this problem can be temporarily overcome by blending the biodiesel with petroleum fuels. Due to its oxygen content, using biodiesel is expected to promote a more complete combustion which would reduce the amount of unburned hydrocarbon, particulate matter, and carbon monoxide. Net carbon dioxide emission is also expected to reduce, but studies have shown that NOx emission was higher in biofuel combustion. A brief review of these studies is given in this section.

Wang at al. (2000) analyzed exhaust emissions of nine heavy trucks fueled by diesel and biodiesel blends. Soybean methyl ester was used as a biofuel in the study. The biodiesel/diesel blend was a mixture of 35% biodiesel and 65% petroleum diesel. There was no noticeable difference in fuel economy (miles per gallon) between the blend and the pure diesel. The trucks fueled with the blend produced significantly lower particulate matter (by 25%). Biodiesel has higher oxygen content then petroleum diesel

(which contains almost no oxygen), which enables more complete combustion. This effectively leads to lower emissions. Emission of carbon monoxide was reduced by about 12% when trucks operated with blend fuel rather than petroleum diesel alone. Hydrocarbon emission decreased very slightly (by 7% on average) for trucks operating with blend fuel. Biodiesel has longer carbon chains which improves overall cetane value. This promotes complete combustion which reduces the level of unburned fuel. NOx emission was about the same for both fuels.

Jha et al. (2008) investigated the effect of component methyl ester in biodiesels on the open air flame temperature. Flame temperature of biodiesel blends (blends of biodiesel with diesel and ethanol and methyl acetate) was also analyzed. Soybean was the biodiesel used in this study. It was found that blends of ethanol and methyl acetate with diesel resulted in higher flame temperatures (approximately 120 K and 180 K higher, respectively) when compared to pure diesel. The authors also reported that greater flame temperature (by approximately 10-30 K) resulted from saturated methyl esters when compared to unsaturated methyl esters. Additionally, shorter chained fatty acid methyl ester produced higher flame temperature than long chained ones.

Lim et al. (2009) studied low temperature properties (e. g. pour point and cloud point) of blends of palm oil methyl esters and petrodiesel. Pour point is defined as the lowest temperature at which a liquid can flow. Cloud point is defined as temperature at which a cloud of wax crystals first appears in a liquid form when liquid is cooled under certain conditions. The authors reported that blends of palm oil methyl esters-petrol diesel with 70% - 80% palm oil methyl esters did not result in change of pour point temperature. Lower cloud point temperature (2 $^{o}$C lower) resulted in blends of palm oil

methyl esters-petrol diesel with 90% palm oil methyl esters. Additionally, the blends of palm oil methyl esters and petrodiesel resulted in lower viscosity than the individual components. The change in viscosity ranged from approximately 2.5 to 3.5 cP.

Love at al. (2009) developed a rapid method for characterization of combustion properties such as pollutant emission and flame radiation. They performed a study involving laminar flames of pre-vaporized mixtures of fuel with air, particularly canola methyl ester (CME) and No. 2 diesel. The CME flames resulted in approximately 50% lower radiative heat fraction than petroleum fuels flames. CME flames had 53% lower emission index of CO, but 9% higher emission index of NO when compared to respective emission indexes of petroleum fuels.

Dhamale et al. (2010) investigated the effects of turbulence on the combustion characteristics of blends of canola methyl ester (CME) and No 2 diesel fuel in a partially premixed flames. Three different blends of 25%, 50%, and 75% of CME by volume were at initial equivalence ratio of 7 and burner exit Reynolds numbers of 2700, 3600, and 4500. Reynolds number was calculated using injector diameter and air-fuel mixture velocity at burner exit. Pure diesel fuel resulted in highest soot volume fraction which did not change significantly with Reynolds number. The global NOx emission index was highest (approximately 55% higher than pure diesel) and CO emission index was lowest (approximately 44% lower than pure diesel) for pure CME, which agrees with results of Love et al. (2009). The temperature measured at mid-flame and three-quarter flame heights was 10-20% higher (depending on radial location) for blends than pure fuels. It was shown that the combustion characteristics of CME/diesel blends cannot be predicted accurately based on the blend ratio and properties of CME and

diesel flames. Rather, detailed measurements are needed to gather the relevant information.

In addition to emissions, another aspect which has been studied in combustion of biofuels is soot formation. Merchan-Merchan et al. (2012) studied soot particles derived from laminar diffusion flames of canola methyl ester (CME), soybean methyl ester (SME), a 50% SME and 50% animal fats (AF) mixture, and pure diesel fuel. The experiment was conducted at atmospheric pressure. Carbon particulates produced from tested biodiesels resulted in significantly smaller diameters than those of diesel fuel. Soot particles derived from diesel fuel averaged at 48 nm in diameter, while soot particles of SME and SME/AF had 29 nm diameter. Soot particles derived from CME resulted in smallest diameter of 27 nm. Soot derived from biodiesel had a highly graphitic shell-core arrangement compared to soot from diesel fuel which resulted in far less graphitic structure which consisted of short, disconnected, and not concentrically arranged graphene segments. The present study was done in the lean regime (equivalence ratio range 0.54 - 0.83) so there was no soot formed.

As seen in this section, there have been a number of studies which investigated emissions of biofuel (and blends of biofuel with petroleum fuel) combustion. The results showed that biofuels and their blends produced higher NOx emissions. However, this information was scattered across many different studies under many different configurations and engines. Hence, Balakrishnan et al. (2016) reviewed the available data regarding NOx emissions from engines fueled with blends of biodiesel and petroleum diesel. In total, 542 different studies were considered. From those, 368 studies reported an increase, while 147 studies reported a decrease in NOx emissions

with biodiesel content. The results varied based on the biodiesel content, but biggest number of studies was conducted with 20% of biodiesel in the mixture and with pure biodiesel (265 studies reported increase in NOx at these two conditions and 94 studies reported a decrease). There were 27 studies which reported no change in NOx emissions with biodiesel content. The change in NOx emissions for blends varied non-monotonically with biodiesel content. Hence, NOx emissions cannot be predicted based on biodiesel content, but rather a holistic approach is needed in combining the published data in order to achieve an accurate estimate.

## Laminar Flame Speed

Glassman and Yetter (1996) outlined the flame theories of Mallard and Le Chatelier (1883) whose theory was later expanded by Semenov (1951). His theory, which became known as Semenov theory described work of Zeldovich and Frank-Kamenetskii (1938 - 1940) in great detail; it showed that laminar flame speed is proportional to the ratio of diffusivity and characteristic chemical time. Laminar flame speed of various fuels has been found experimentally in several studies which are presented in this section. The most relevant flame speeds in the present study were those of Jet A, CME, PME, and SME flames.

Chong and Hochgreb (2011) measured laminar flame speeds of premixed flames of Jet A1, diesel, PME, and blends of PME and Jet A1 and PME and diesel. The flame speed was measured using the jet-wall stagnation flame configuration and particle imaging velocimetry (PIV) technique. Three different blends were used with either 10%, 20%, or 50% by volume of PME in the mixture. The experiment was conducted

under atmospheric pressure and temperature of 470 K. The equivalence ratio ranged from 0.74 to 1.5. The authors also compared the experimental results to other experimental and simulation data from the literature for large n-alkanes. It was shown that laminar flame speed of Jet A1 was similar to laminar flame speed of n-decane and n-dodecane. The results on the lean side were very close to simulation results by Kumar et al. (2009), but slightly higher on the rich side (by 5-8 cm/s). Peak laminar flame speed of Jet A1 and PME was about 91 cm/s and 86 cm/s, respectively. Maximum laminar flame speeds occurred at equivalence ratio of 1.1; a change in the equivalence ratio from 1.1 resulted in decrease in laminar flame speed (in seemingly parabolic fashion) whether the equivalence ratio became leaner or richer. Pure diesel flames resulted in slightly higher laminar flame speed than pure PME flames (by about 5 cm/s) on the lean side, whereas the difference became unnoticeable on the stoichiometric and lean side. Increase of PME in blends with either Jet A1 or diesel shifted the laminar flame speed profile to slightly more fuel-rich region (peak shifted from equivalence ratio of 1.08 to 1.2).

Wang et al. (2011) performed a study with laminar premixed and non-premixed methyl ester flames. Particularly, they calculated laminar flame speeds of methyl butanoate, methyl crotonate, and methyl decanoate using digital particle image velocimetry. The experiment was conducted under atmospheric pressure in counterflow configuration at temperature of 403 K. The results for laminar flame speeds were reported for equivalence ratio range of 0.7 – 1.6. Peak laminar flame speed of methyl decanoate and methyl butanoate was 62 cm/s and 58 cm/s, respectively. The peak flame speed was achieved at equivalence ratio of 1.1. Visual observation of reported flame

speed profiles indicated that laminar flame speed profile resembled a negative parabola which reached maximum at equivalence ratio of about 1.1.

Liu et al. (2011) reported their findings on laminar flame speeds of several fuels, particularly of methyl butanoate. Their experiment was with premixed flames of methyl butanoate conducted under initial pressure up to 2 atm and unburned gas temperature of 353 K. The equivalence ratio range was 0.7 – 1.7. Maximum laminar flame speed of methyl butanoate at 1 atm of 44 cm/s was reached at equivalence ratio of 1.1. Laminar flame speed profile resembled a negative parabola. These results of Lie et al. on laminar flame speed of methyl butanoate were on average 13% lower than those of Wang et al. (2011), even after the temperature effect was taken into account assuming that laminar flame speed varies with temperature as $T^{1.5}$. The laminar flame speed was also computationally simulated; this simulation yielded higher laminar speeds (about 15% higher) which are in better agreement with the results of Wang et al.

Gomez-Meyer et al. (2012) measured laminar flame speed of CME and SME biofuels. Laminar flame speed of diesel was also measured to serve for comparison. Bunsen flame method was used to measure the flame speed. Flame speed was computed as a ratio of mass flow of air/fuel mixture and product of the density of the air/fuel mixture and area of the outer cone of the flame. Equivalence ratio ranged from 1.0 to 1.2. Peak flame speed of diesel, CME, and SME was 128.5 cm/s, 110.5 cm/s, and 107.5 cm/s, respectively. The flame speeds of these biofuels are lower than that of diesel by about 12%-15% at each equivalence ratio. The peak value was reached at about equivalence ratio of 1.1, which is the same equivalence ratio as in the study of Chong

and Hochgreb (2011) where the laminar flame speed was maximum. Additionally, in both studies petroleum fuels resulted in higher laminar flame speed than biofuels.

Nilsson and Konnov (2015) measured laminar flame velocities of C2 – C7 esters. The experiment was conducted with premixed flames under atmospheric pressure and unburned gas temperature of 298 K and 338 K. The equivalence ratio range was 0.6 – 1.6. Similar to the aforementioned studies, maximum laminar flame speed was reached at equivalence ratio of 1.1 for all the fuels tested. The peak value of laminar flame speed of methyl butanoate at temperatures of 298 K and 338 K was 35 cm/s and 43 cm/s, respectively. This change in laminar flame speed with temperature is in accordance with the assumption that laminar flame speed varies with temperature as $T^{1.5}$. Besides experimental studies of laminar flame speed, there are also computational models for estimating the laminar flame speed. Sulmon et al. (2016) performed an extensive kinetic modeling study to predict the laminar flame speed of various methyl esters such as methyl butanoate, methyl formate, methyl acetate, and methyl propanoate. They compared their results with experimental data published in the literature, namely the results of Wang at al. (2011) and Nilsson at al. (2015). A good agreement (within 5%) with computational and experimental results indicated that their flame chemistry of each methyl ester has been correctly described.

This literature review described that flame stabilization mechanism has been researched extensively in the last six decades. Nonetheless, our knowledge of flame stabilization and blowout/blowoff phenomena is still lacking. Reviews of Pitts (1988) and Lawn (2009) confirmed that our understanding of flame stabilization mechanism is limited and that further studies are needed in order to improve our knowledge in this

matter. As world is seeking greater energy independence and more environment-friendly energy sources, biofuels have emerged as an alternative to petroleum fuels. Biofuels are renewable, safer, less pollutant, biodegradable alternative fuel which could substitute petroleum fuels. However, even though fuel properties of biodiesel and petroleum fuels are comparable, biodiesels tested in the present study are denser and more viscous so they cannot be readily used in existing industrial and domestic machines. But blends of biodiesel and petroleum fuels can be readily used in existing machines. Performance of biofuels and their blends in engines has been well documented. Emissions of biofuel combustion have also been extensively studied. A few studies have reported laminar flame speed of biofuel flames (mostly for equivalence ratio range of 0.8 to 1.5). However, a little research has been done on flame stabilization of biofuels.

Willingham (2014) examined flame stability mechanism and blowoff phenomena of partially premixed flames of prevaporized pure petroleum fuels (Jet A) and pure biodiesel fuels (CME, PME, SME) over a range of equivalence ratios (2.4 – 3.6) with and without heated coflow. Measurements of flame dimensions, flame temperature profiles, and blowoff velocities were made. It was reported that visible flame height increased with equivalence ratio due to the reduction in the supplied air. The blowoff velocity increased with equivalence ratio and with coflow velocity. The peak temperatures of various flames at corresponding equivalence ratios were comparable. The present study (which was conducted using the same experimental setup used by Willingham, 2014) examined flame stability mechanism and blowoff phenomena of partially premixed flames of blends of prevaporized petroleum fuels (Jet

A) and biodiesel fuels (CME, PME, SME). The combustion properties of pure fuels and blends change non-monotonically which means that properties of blends cannot be predicted based on the properties of the pure fuels from which the blends were composed. Hence, the present study was conducted to expand our knowledge about flame stabilization mechanism of blends of biodiesels and petroleum fuels.

# Chapter 3 Experimental Setup and Technique

This chapter gives a detailed description of the experimental setup and its individual components. The instrumentation and methods used for measuring are also provided. Major calculations and data collection methods are explained.

## Combustion Chamber

All experiments were conducted in a steel test chamber with a cross section of 76 cm x 76 cm x 100 cm as presented in Figure 3.1. A list of all parts and instrumentation used in the present study is shown in Table 3.2.

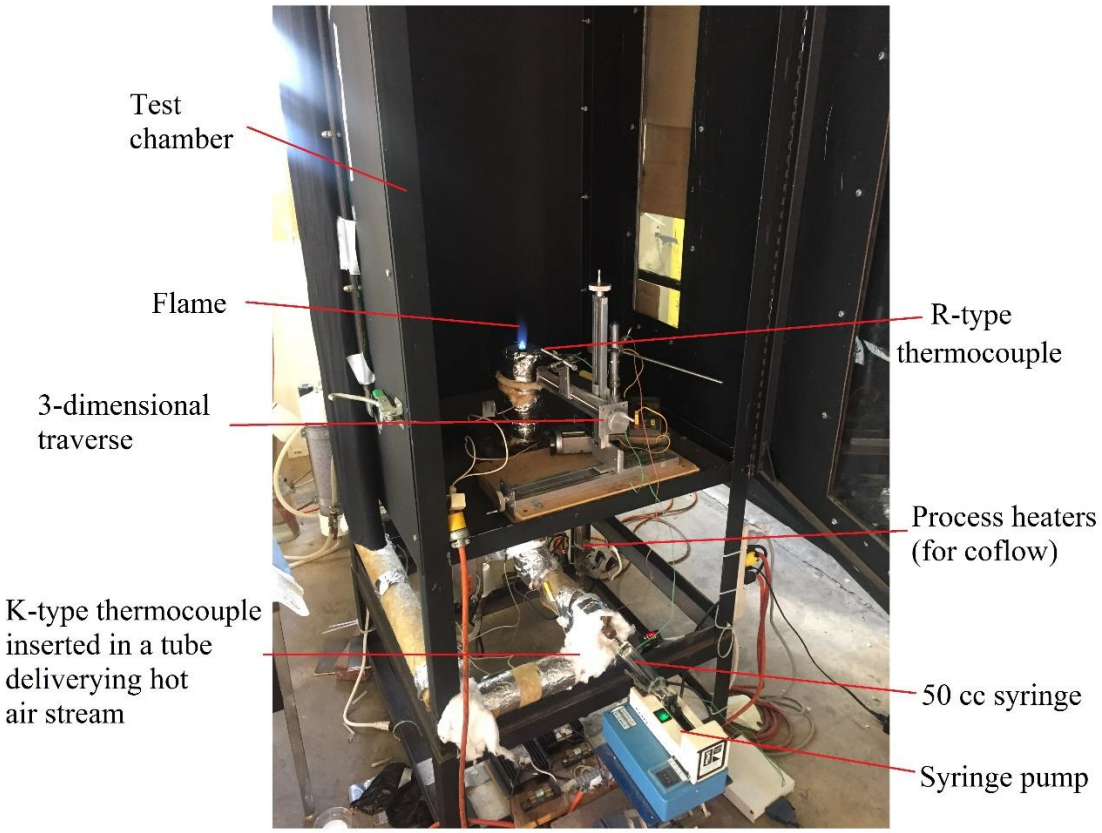


Figure 3.1: Photograph of experimental set-up

The chamber was equipped with windows (20 cm x 90 cm) for optical access to the flames. A schematic diagram of the experimental arrangement is provided in Figure 3.2. The experimental setup was assembled in such way so that the heated air could completely prevaporize the liquid fuel before it was ignited at the burner exit. The ambient pressure was atmospheric and ambient temperature (inside the combustion chamber) within 5 $^{o}$C of the room temperature. An exhaust duct (equipped with a fan) used to vent the combustion products from the test chamber was open to the atmosphere. Initial approach to the research was to ensure that all the equipment and instruments were working properly. The existing setup was first equipped with relays and a controller. After ensuring the relays and controller were working properly (i.e. relay diodes come on/off accordingly, current is supplied to the heat tape, etc.), the controller was set to a certain temperature. Using a thermocouple (K type) it was inspected if the exit air temperature stabilized at a desired point. After ensuring the temperature was stable and could be controlled, the airflow rate was inspected to ensure the rotameters were working properly by measuring velocity profiles which are presented later in this study.

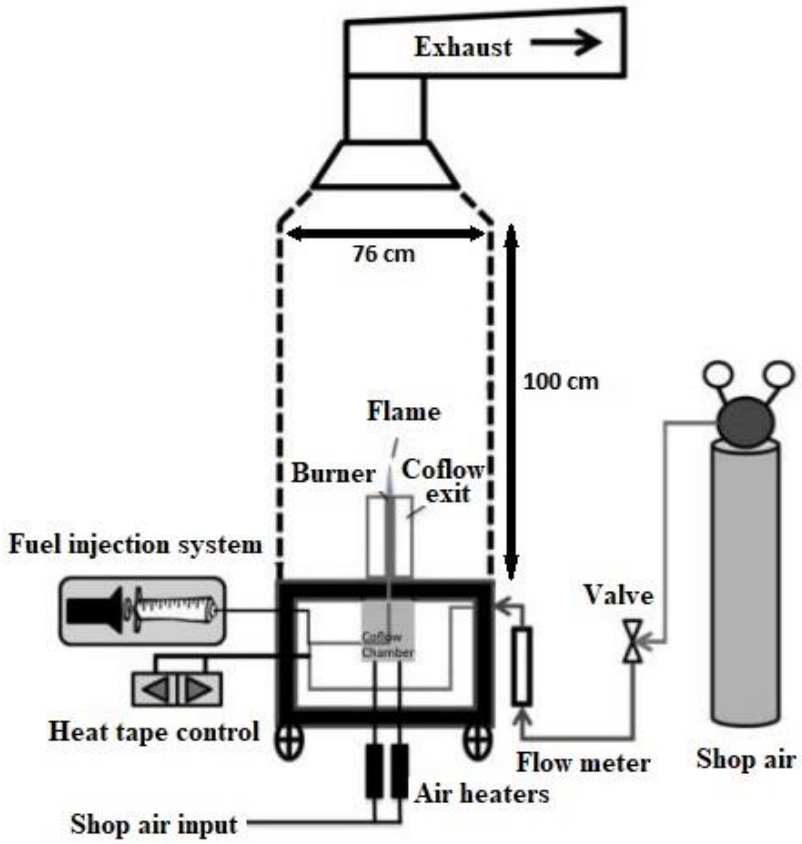


Figure 3.2: Schematic diagram of experimental set-up

## Air and Fuel Delivery System

The burner was located within the test chamber at the bottom center and it was concentrically aligned within a circular tube of inner diameter 6.2 cm which was used to provide a coflow of air. Using a caliper the burner exit diameter (outer and inner) and coflow inner diameter were measured. Besides calculating the exit area of the both cylinders, the burner's inner diameter also served as a reference length for calculating flame dimensions. A stainless steel circular tube 20.3 cm long (tapered $60^{o}$ inward to

provide more uniform flow as shown in Figure 3.4) with 1.27 cm inner diameter served as a burner. A photograph of the burner is presented in Figure 3.3.

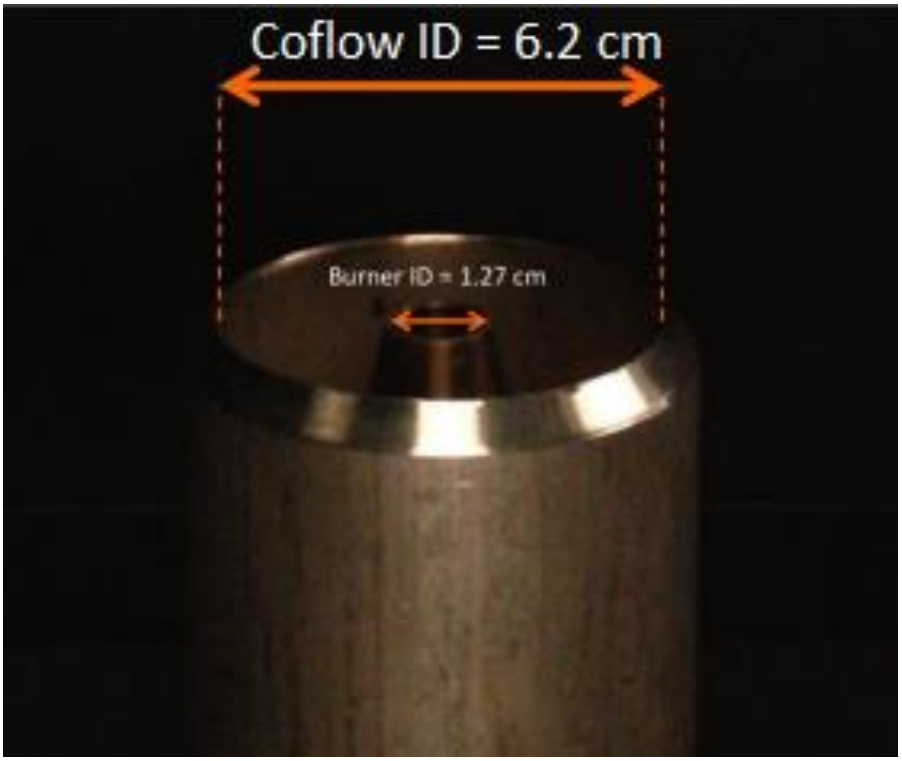


Figure 3.3: Photograph of the burner

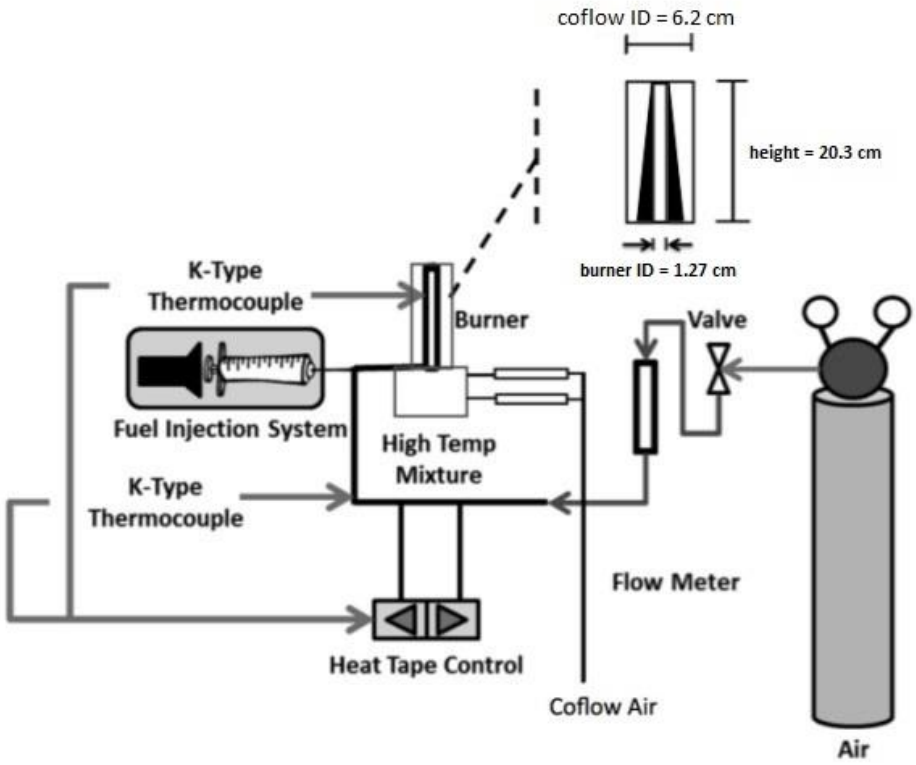


Figure 3.4: Schematic diagram of the fuel/air delivery to the burner

All the fuels used in this study were in liquid form. A closer view of the fuel injection system and heated air delivery is shown in Figure 3.4. The fuel was injected using a syringe pump into a heated stream of air at a location far enough upstream from the burner exit to ensure the fuel was completely vaporized before it was ignited. Table 3.1 indicates the temperature settings for each fuel.

Shop air was used to provide both primary airflow and coflow because there was no noticeable difference between using the shop air or air from compressed cylinder. High temperature heating tape wrapped around the 1.47 outer diameter circular tube was used to heat the air stream. The heating tape was connected to an automatic

temperature controller which was used to obtain the temperature needed to completely vaporize the fuel, but not too high to cause coking. The inside of the burner and tubes was regularly cleaned with a wire brush to remove any unburned fuel and debris. The exit temperature of the air-fuel mixture was measured with a K-type thermocouple. Another K-type thermocouple was used to measure the air temperature at the fuel injection port. The liquid fuel was injected through a high-temperature silica-based septum with a 50 ml syringe inserted into a syringe pump. Two process heaters were used to heat the coflow of air. The exit temperature of the coflow air was about 20 $^{o}$C lower than the exit temperature of the primary airflow. Three different coflow rates were used in this study: 1.985E-3 $m^3$/s (~2 L/s) with a bulk velocity of 1.1 m/s, 3.97E-3 $m^3$/s (~4 L/s) with a bulk velocity of 2.3 m/s, and 5.95E-3 $m^3$/s (~6 L/s) with a bulk velocity of 3.5 m/s. Experiments were also conducted with no coflow. Both primary airflow and coflow were metered using rotameters. Before the shop air reached the rotameters it was passed through a purifier and an ice bath in order to prevent moisture and any particles entering the flow. The air-fuel mixture was ignited at the burner exit using a butane lighter with a flame length of approximately 1 cm.

## Blowoff Measurement

The present study was done with and without heated coflow. Three different coflow rates were used in this study. Measurements were taken at nine discrete fuel flow rates which ranged from 65.1 ml/hr to 100 ml/hr. The experiments were conducted in such way that after the fuel/air mixture was ignited (at approximately stoichiometric condition), for a given fuel flow rate and a given coflow setting, the airflow rate was

increased until the blowoff was reached. As noted by Lewis and von Elbe (1987), blowoff occurred when the gas velocity gradient at the jet edge became higher than the flame velocity near the jet edge (which reduces to zero steeply). Figure 3.5 provides a schematic illustration of this concept.

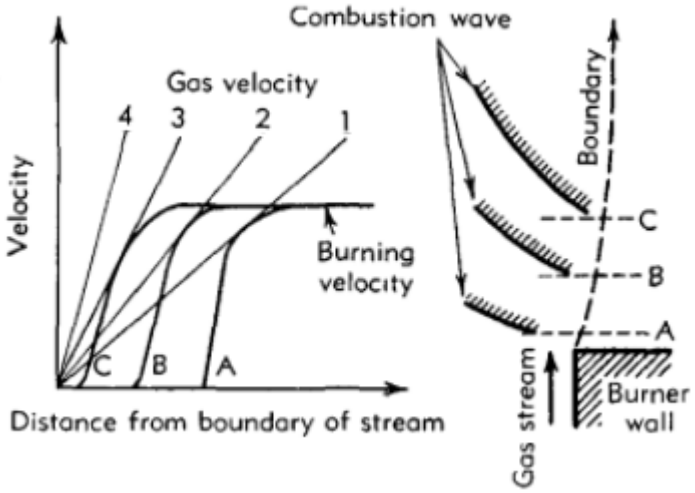


Figure 3.5: Schematic illustration of blowoff representing the flame velocity and gas velocity above the burner rim; Curves A, B, C are flame velocities at heights A, B, C; Curve 1 – flashback limit, curve 2 – stable flame, curve 3 – blowoff limit, curve 4 – blowoff (Lewis and von Elbe, 1987)

At any gas velocity lower than curve 1, the flame flashed back into the tube. Once the gas velocity gradient near the edge was tangential to the flame velocity variation with distance from the boundary, the blowoff-limit was reached (curve 3). If the velocity gradient at the jet edge increased further, the flame blew off. Thus, the gradient of velocity near the edge was an important factor in predicting the blowoff.

### Velocity Profile Measurement

A pitot static probe was used to obtain velocity values of exiting air. The tip of pitot static probe was placed 6mm above the burner while the pitot static probe was

mounted on a traverse and moved radially across the centerline of the burner in increments of 2 mm. The pitot static probe was connected to an inclined manometer which read height of water column corresponding to the dynamic pressure. After obtaining the velocity profile (for both coflow and primary airflow) the volumetric airflow rate was calculated using Riemann sum (since only discrete velocity values). This result was corrected for temperature and pressure using the standard method (Cole-Parmer, 2017)

$$\frac{Q_a}{Q_{ref}} = \sqrt{\frac{T_{ref}}{T_a}\frac{p_a}{p_{ref}}} \tag{3.1}$$

where Q, T, and p are volumetric flow rate, temperature and pressure respectively, and a and ref are actual (measured) and reference (manuf. calibration which was done at atmospheric pressure of 101,325 Pa and room temperature of 25 $^{o}$C; atmospheric pressure in present study ranged from 100,500 Pa to 103,600 Pa). The results were calculated using Riemann sum method (analyzing graphs in Figure 4.7) and then compared to the manufacturer's data. The good agreement in the results (the difference was within 16%) confirmed that instruments worked properly.

Velocity gradients were calculated in order to estimate the time scale associated with the velocity gradient at the edge to determine the Damköhler number. The velocity gradients were calculated between the two velocity measurements on either side of the burner wall. These measurements correspond to radial distance of 6 and 8 mm since the measurements were taken in 2 mm increments and the burner radius is 6.4 mm. Majority of the flames from all the fuels in this study blew off within the range of 15.1 L/min to 22.1 L/min of the primary airflow rate. Thus, the velocity profiles were measured at primary flow rates of 15.1 L/min, 18.7 L/min, and 22.1 L/min

(corresponding to bulk velocities of 3.5 m/s, 4.3 m/s, and 5.1 m/s, respectively). Velocity profiles were measured at three different coflow rates of 2 L/s, 4 L/s, 6L/s, and without any coflow.

Table 3.1: Heat tape temperature settings based on fuel type

| **Fuel** | **Upper Boiling Point (ºC)** | **Heat Tape Setting (ºC)** | **Exit Temp (ºC) (+/- 15 ºC)** |
|---|---|---|---|
| Jet A | 310 | 260 | 220 |
| CME and blends | 380 | 365 | 260 |
| SME and blends | 365 | 360 | 250 |
| PME and blends | 350 | 320 | 240 |

Table 3.2: Parts and Instrumentation

| **Parts and Instrumentation** | **Manufacturer and Model Number** |
|---|---|
| Air Heaters | Process Heater |
| High Temperature Heavy Insulated Heat Tape | Omega Engineering Inc. FGH051-100, FGH051-080, FGH051,060 |
| High Temperature 11 mm Inlet Septa | Agilent 5183 – 4757 |
| 50cc Interchangeable Syringe | B-D Multifit 512135 |
| Syringe Pump | Razel A-99.EMS |
| Rotameter with Glass Ball | Cole-Parmer Lo-Flo with tube 044-40-G |
| Omega Temperature Control | Omega Engineering Inc. CN79000 |
| Type K Thermocouple | Omega Engineering Inc. |
| Type R Thermocouple | Omega Engineering Inc. |
| Digital Thermometer | Tegam 871A |
| Inclinometer | Dwyer Mark II Model 25 |
| Pitot Static Probe | |
| Traversing Mechanism | Unislide / Velmex Inc., Gaertner 132D |
| Viscometer | Gilmont GV-2100 |
| Hydrometer | Fisherbrand 11-582 |
| Caliper | |
| Data Acquisition Hardware | National Instruments Labview Board SCB-68 |
| Data Acquisition Software | National Instruments Labview 2010 |
| Image Processing Software | MATLAB |
| Image Processing Software | GIMP |
| Image Processing Software | VirtualDub |
| Data Acquisition Software | Excel 2013 |
| Data Acquisition Computer | Dell Inspiron |

## Flame Dimensions

Flame dimensions were calculated using MATLAB software. An iPhone 6 8-megapixel camera was used to record the images of stable flames and flame blowoff. The exposure time was set to auto, but the range of the exposure time in iPhone 6 camera is 1/15 to 1/50,000 seconds (Apple.stackexchange.com). The phone was mounted against one of the chamber glass windows 38 cm away from the burner. The flames were axisymmetric (as confirmed by the images and temperature measurements). Videos were recorded at 720p and 30 frames per second under similar lighting conditions and dark background to better observe the flames. Individual frames were extracted from a video using VirtualDub software and thereafter cropped using GIMP software. MATLAB software was used to process the cropped frames based on the brightness of the flame in order to analyze the flame dimensions (outer cone height, width, and inner cone height). MATLAB code can be found in Appendix E. All the photographs were transformed into binary images as shown in Figures 3.6 – 3.8 (only Jet A flames are shown here since all the other fuels resulted in similar flames and these Figures only serve as an example of binary image). This was done in MATLAB with the set brightness threshold. Thereafter, each pixel in a photograph was changed into either black or white pixel, depending if the brightness of the pixel was below or above the set threshold. The threshold value was determined by trial and error method with seeing which threshold produces most accurate flame images. Three different threshold values were used since the brightness of the flame was different for the inner cone, outer cone, and lifted flame. Number of white pixels were counted from top to bottom

and from left to right; the height and width in pixels were converted into centimeters using the burner inner diameter as the reference length.

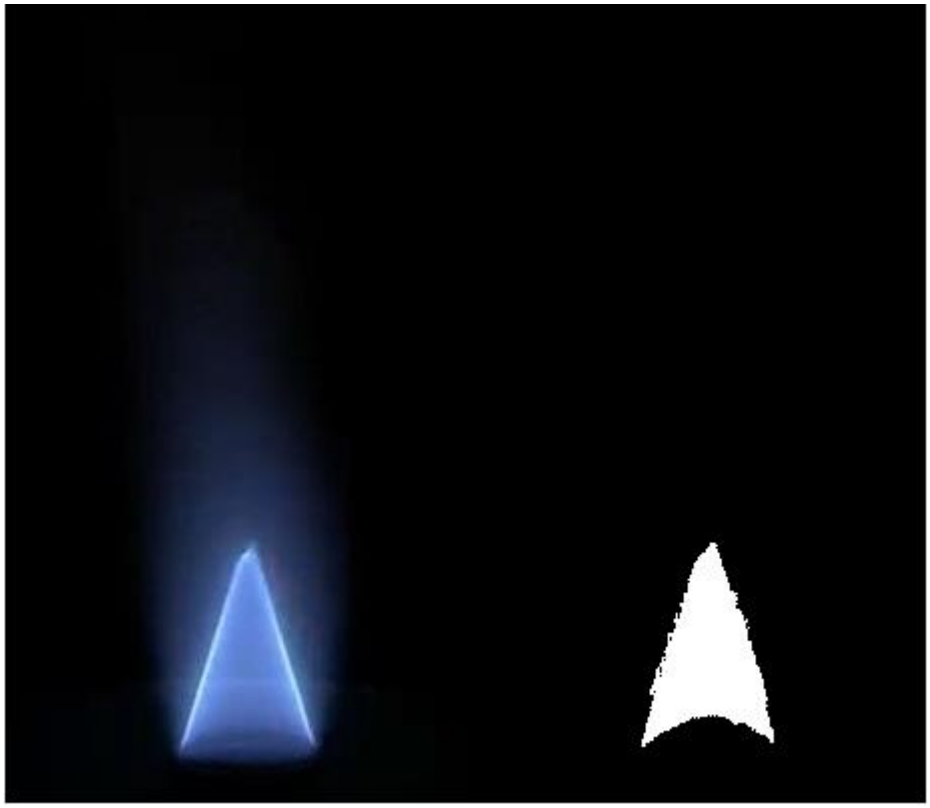

Figure 3.6: An example of a flame and its binary image with the brightness threshold set for inner cone; Fuel: Jet A, Re = 2800, U = 3.8 m/s, Φ = 0.74

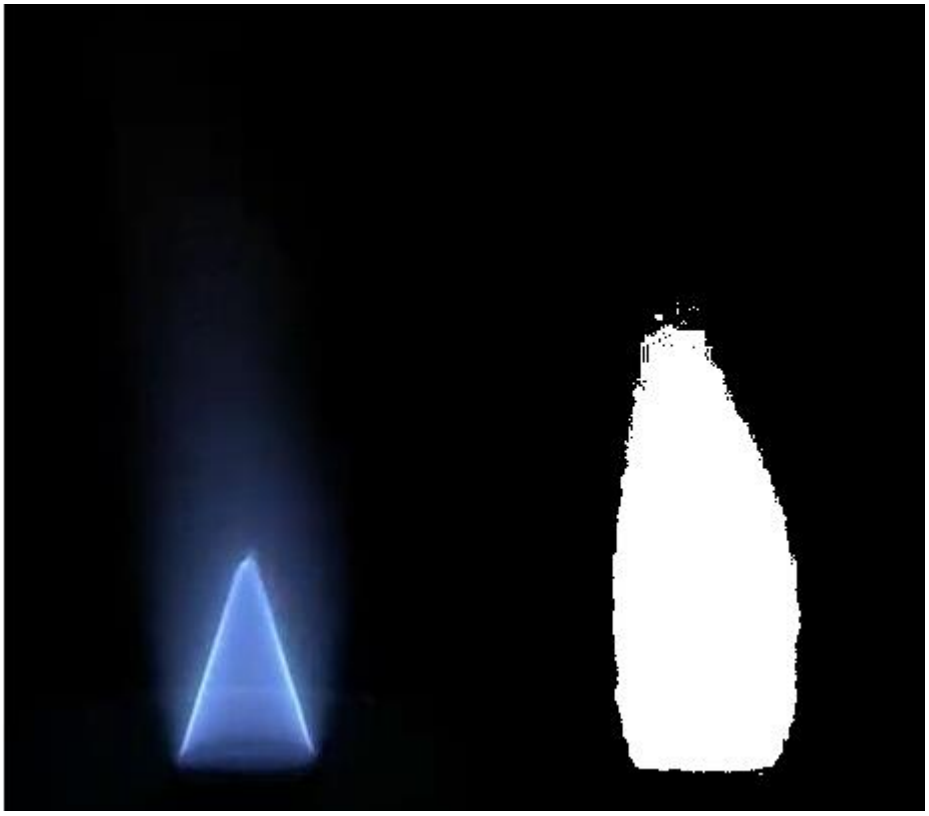

Figure 3.7: An example of a flame and its binary image with the brightness threshold set for outer cone; Fuel: Jet A, Re = 2800, U = 3.8 m/s, Φ = 0.74



Figure 3.8: An example of a lifted flame and its binary image with the brightness threshold set for a lifted flame; Fuel: Jet A, Re = 2800, U = 3.8 m/s, Φ = 0.74

The outer cone height and inner cone height were determined by counting the number of pixels from the tip of the burner to the tip of the flame of the binirized flame image. The width was calculated at the widest point of the outer cone by counting the number of white pixels from one side to the other. The liftoff height was calculated by counting the number of black pixels from the tip of the burner to the base of the lifted flame. Lastly, the fully attached flame prior to blowoff was used to calculate the flame outer cone height, width at the widest point, and inner cone height. The last 20 frames or images of a lifted flame prior to blowoff were averaged to achieve more accurate liftoff height. The burner's inner diameter was used as the reference length.

## Flame Temperature Profile

Figure 3.9 illustrates how the inflame temperature profiles were measured. A two-dimensional traverse was used to hold an R-type thermocouple (Platinum/Platinum-87%, Rhodium-13%) to collect data at three different flame heights while traversing radially through the flame in increments of 2 mm. The bead diameter of the thermocouple was 0.2 mm. The bead was coated with silica before every experiment to reduce the catalytic effects. A 1.6 mm outer diameter ceramic tube was used to provide structural support to very thin thermocouple wires (0.03 mm diameter). The collected temperature measurements were corrected for radiation and conduction losses according to procedures outlined by Jha et al. (2008) which are also included in Appendix C. Temperature data from the thermocouple was collected using the LabVIEW data acquisition software and a personal computer. The readings were taken at 1 Hz at each point and averaged over 5 seconds as there was no noticeable difference when averaged over a longer time period.

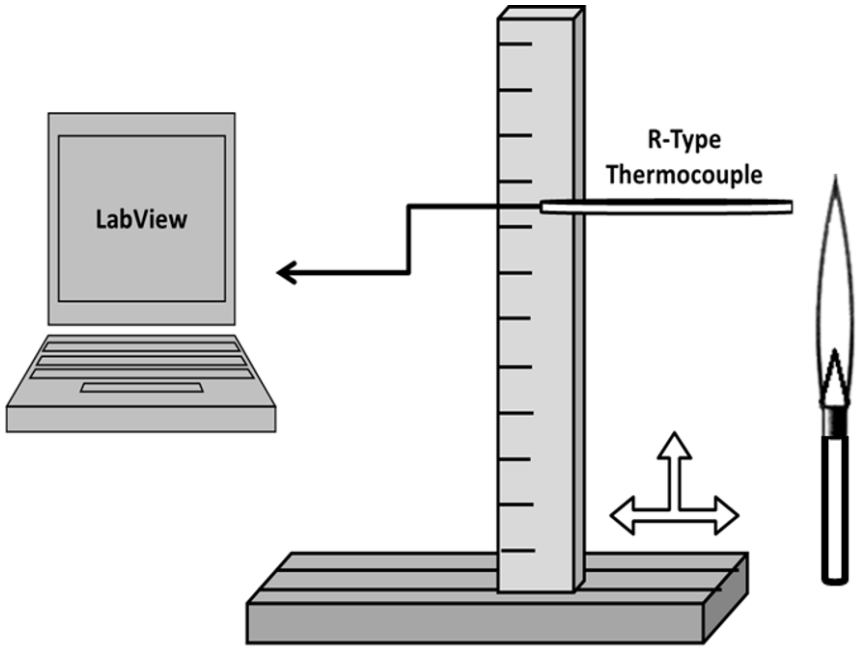


Figure 3.9: Illustration of inflame temperature measurement

**Stoichiometric Formula**

Air was assumed to be 21 percent oxygen and 79 percent nitrogen (by volume). The fuels used in these experiments were assumed to have a general chemical formula based on the average composition of hydrocarbons or fatty acids methyl ester components the fuel comprised. The chemical formula used to calculate the stoichiometric air/fuel ratio is presented in equation 3.2

$$C_xH_{2y}O_{2z} + a(O_2 + 3.76\,N_2) \rightarrow xCO_2 + H_2O + (3.76a)N_2 \quad (3.2)$$

where

$$a = x + \frac{y}{2} - z \quad (3.3)$$

Stoichiometric air/fuel ratio by mass can be calculated using the equation 3.4.

$$AF_{stoic} = \left(\frac{\dot{m_{air}}}{\dot{m_{fuel}}}\right)_{stoic} = \frac{4.76a}{1}\frac{MW_{air}}{MW_{fuel}} = \frac{a(32+3.76*28)}{12x+2y+32z} \quad (3.4)$$

Equivalence ratio is one of the most commonly used parameters in combustion science to indicate quantitatively whether a fuel-oxidizer mixture is fuel rich, lean, or stoichiometric. The equivalence ratio is defined as

$$\Phi = \frac{(A/F)_{stoic}}{(A/F)_{actual}} \tag{3.5}$$

where

$$(A/F)_{actual} = \left(\frac{\dot{m_{air}}}{\dot{m_{fuel}}}\right) \tag{3.6}$$

If equivalence ratio is greater than 1 the mixture is fuel-rich, whereas for the equivalence ratios lower than 1 the mixture is fuel-lean. Stoichiometric mixture corresponds to equivalence ratio equal to unity. The equivalence ratio was calculated based on the primary airflow alone, without taking the coflow into account.

## Reynolds Number Calculation

Reynolds number (Re) is a dimensionless quantity which gives a ratio of inertial forces and viscous forces. It is defined as

$$Re = \frac{\rho UL}{\mu} \tag{3.7}$$

where ρ is density, U is burner exit velocity, L is burner inner diameter, and μ is the viscosity of vaporized air/fuel mixture. In case of circular tubes, laminar flow occurs for Reynolds number less than 2000. Due to the nature of the experiments conducted in this study, the results presented here correspond to transitional Reynolds number. The Reynolds number was a dependent variable based on the blowoff velocity. The blowoff was achieved at airflow velocities corresponding to transitional Reynolds number. An example of typical range of Reynolds number in this study is shown in Table 3.3.

Table 3.3: Typical range of Reynolds number (example of Jet A at all three coflow velocities)

| Airflow rate at blowoff (ml/min) | Primary flow bulk velocity at blowoff (m/s) | Equivalence ratio at blowoff | Reynolds number |
|---|---|---|---|
| 14919 | 3.27 | 0.54 | 2402 |
| 22661 | 4.95 | 0.84 | 3646 |

Viscosity (μ) of the vaporized air/fuel mixture was calculated with data from Maxwell (1950) and equations below from Kanury (1975).

$$\mu_{mixture} = \sum_{i=1}^{n} \frac{X_i \mu_i}{\sum_{j=1}^{n} X_j \Omega_{ij}} \tag{3.8}$$

$$\Omega_{ij} = \frac{1}{\sqrt{8}}\left(1 + \frac{MW_i}{MW_j}\right)^{1/2}\left(1 + \left(\frac{\mu_i}{\mu_j}\right)^{1/2}\left(\frac{MW_i}{MW_j}\right)^{1/4}\right)^2 \tag{3.9}$$

where X is the molar fraction and MW is molecular weight. Viscosity of fuel vapor was estimated based on the fuel molecular weight (Maxwell 1950).

## Damköhler Number Calculation

The Damköhler number (Da) is the ratio of the flow time scale to that of the chemical reaction time scale.

$$\mathrm{Da} = \frac{\mathrm{t_{flow}}}{\mathrm{t_{chem}}} \tag{3.10}$$

where $t_{flow}$ represents flow or residence time scale and $t_{chem}$ represents chemical reaction time scale. Flow time scale was calculated by taking the inverse of the velocity gradient at the flame edge (Equation 3.11). Lewis and von Elbe (1987) illustrated in Figure 3.5 that the gradient of velocity near the edge was an important factor in predicting the blowoff. Chemical reaction time scale was calculated using the equation 3.12

$$t_{flow} = \frac{1}{\text{velocity gradient (at jet edge)}} \quad (3.11)$$

$$t_{chem} = \frac{\alpha}{S_L^2} \quad (3.12)$$

where α represents thermal diffusivity and $S_L$ represents laminar flame speed. Lima et al. (2000) reported that thermal diffusivity of a fuel/air mixture decreased by 17% when the molar fraction of fuel in the mixture was 2.1%. Molar fractions of fuel in the fuel/air mixture in the present study were 1% or less. Thus, the thermal diffusivity of air was used as estimation of the thermal diffusivity of the mixture since the mixture was about 99% air.

The information on laminar flame speed at very low equivalence ratios (such as those obtained in this study) is very limited, particularly for CME, PME, and SME. Therefore, the laminar flame speed of these fuels at low equivalence ratio was estimated assuming a parabolic correlation between laminar flame speed and equivalence ratio (based on results of Gomez-Meyer et al., 2012 and Chong and Hochgreb, 2011). As discussed in chapter 2, all the studies reported laminar flame speed profiles which resembled a parabolic function. The published information about laminar flame speed of other biofuels such as methyl butanoate and methyl decanoate was also used to improve the estimation (Liu et al., 2011 and Wang et al., 2011). Additionally, the temperature of the unburned gas mixture affects the laminar flame speed. Laminar flame speed was assumed to vary with temperature as $T^{1.5}$ (Gomez-Meyer et al. 2012). The parabolic correlations used to estimate the laminar flame velocity ($S_L$) for various fuels are given in equations 3.13 – 3.16. These equations were obtained by fitting a parabolic trendline to data points reported in the aforementioned studies about laminar

flame velocity (Appendix D). The units of laminar flame velocity in these equations are cm/s.

$$\text{Jet A:} \quad S_L = -212.71\,\Phi^2 + 464.96\,\Phi - 165.13 \tag{3.13}$$

$$\text{CME:} \quad S_L = -166.44\,\Phi^2 + 424.25\,\Phi - 160.72 \tag{3.14}$$

$$\text{PME:} \quad S_L = -133.64\,\Phi^2 + 336.46\,\Phi - 126.04 \tag{3.15}$$

$$\text{SME:} \quad S_L = -352.62\,\Phi^2 + 761.70\,\Phi - 301.49 \tag{3.16}$$

Uncertainties in the measurements were calculated at 95% confidence using standard procedures by Wheeler and Ganji (1996). The maximum uncertainties for various calculated quantities are presented in Table 3.4.

Table 3.4: Uncertainties of various parameters

| **Calculated parameter** | **Uncertainty (95% confidence)** |
|---|---|
| Blowoff velocity | ±0.41 m/s |
| Equivalence ratio | ±0.01 |
| Inner cone height | ±0.57 cm |
| Outer cone height | ±2.59 m |
| Outer cone width | ±0.77 m |
| Velocity gradient | ±264 $s^{-1}$ |
| Inflame temperature | ±165 K |

# Chapter 4 Experimental Setup and Technique

## Operational Range of Burner

Before any scientific measurements were performed the operational range of the experimental setup had to be determined. The maximum temperature which could be reached was monitored. It was found that the maximum temperature achievable with the existing setup was not sufficient (about 15% or 30 K higher temperature was needed). To remedy this, the setup was modified with an extra layer of insulation being added to prevent heat loss through the tube walls. This insulation layer wrapped around the coflow tube in the test chamber can be seen in Figure 3.1. Thereafter, the time needed to reach the desired temperature was monitored. Figure 4.1 shows the temperature rise with time at a coflow velocity of 2.3 m/s; the experiment was repeated 3 times on different days and yielded similar results. About 1.5 hours was needed to reach the desired temperature of 500 K. Additionally, it was inspected if the temperature of the air at the burner exit was dependent on airflow rate. Figure 4.2 shows that the temperature varied insignificantly with the airflow rate. The measurements were repeated on two separate days to verify the trend in the figure.

Experiments conducted for this thesis were performed with biofuel and petroleum fuel blends. Therefore, it was important to measure the physical properties such as density and viscosity of each fuel separately, and then the properties of their blends. The measured properties of liquid fuels used during this study are shown in Table 4.1. Density and viscosity of liquid fuels were measured using instruments (hydrometer and viscometer) listed in Table 3.1. Biofuels (CME, PME, SME) have

about 10% higher density and are on average 3.5 times more viscous than Jet A fuel. The viscosity and density measurements of the blends are in between the values of the pure fuels. Calculated vapor viscosity of air/fuel mixture based on the molecular weight of the fuel (using data from Maxwell, 1950) ranged from 1.32E-5 $(N.s)/m^2$ (with vaporized Jet A) to maximum of 1.40E-5 $(N.s)/m^2$ (with vaporized biodiesels). Molecular weight of Jet A is about 35% lower than molecular weight of the tested biofuels. Biofuels, as their molecular formula shows, contain oxygen unlike Jet A which is a petroleum fuel. Hence, stoichiometric air/fuel ratio is lower for biofuels than for Jet A. PME has lowest stoichiometric air/fuel ratio because it contains highest molar fraction of oxygen. The stoichiometric air/fuel ratio of the blends decreases with increase in biofuel portion. Lower heating value of biofuels is slightly lower (about 7% lower) than that of Jet A (Willingham 2014).

Experimental conditions are shown in Table 4.2. In the present study the range of Reynolds number was 2100 – 3700. All flames blew off/out at air/fuel flow velocity range of 3.3 – 5.0 m/s and equivalence ratio of 0.53 – 0.83.

After verifying all instruments and equipment were operating correctly, the operational range of the burner was inspected. The first flame ignited in the setup is shown in Figure 4.3. It was found that no stable flame could be achieved below 13,300 ml/min of primary airflow rate.

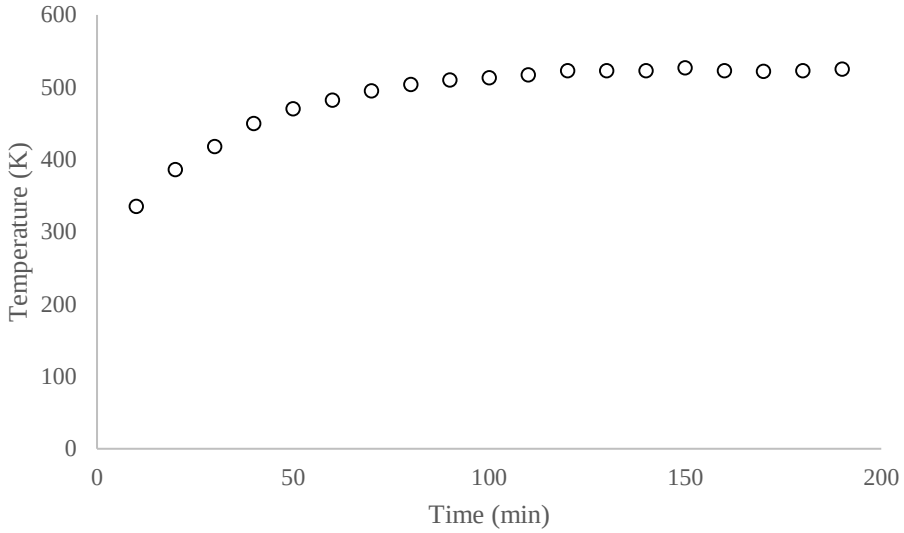


Figure 4.1: Air temperature rise at burner exit with time at coflow velocity of 2.3 m/s (heat tape set to 520 K)

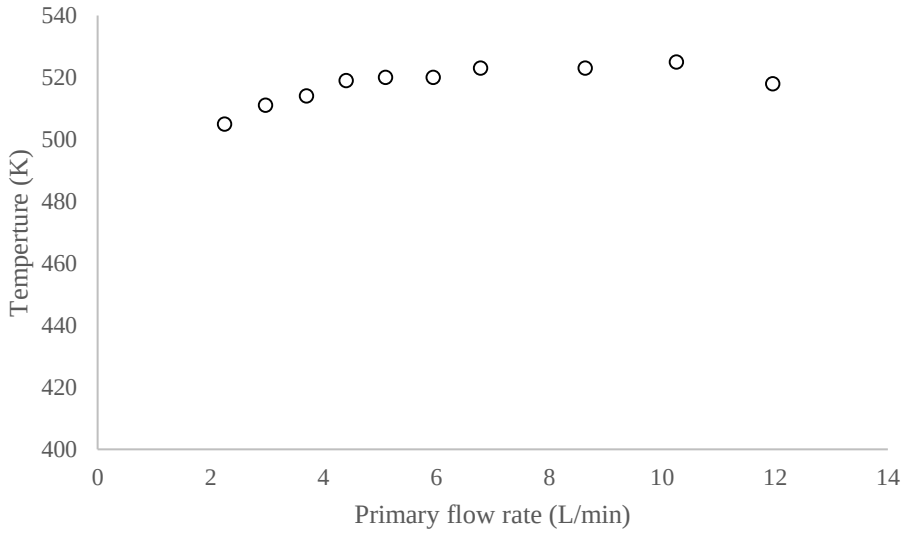


Figure 4.2: Air temperature at the burner exit at coflow velocity of 2.3 m/s (heat tape set to 520 K)

Table 4.1: Properties of tested fuels

| Fuel | Equivalent Molecular Formula | Molecular weight | Liquid density | Viscosity (at 23 $^{o}$C) | $(A/F)_{Stoic}$ by Mass | Lower Heating Value |
|---|---|---|---|---|---|---|
| | | kg/kmol | kg/m$^3$ | cP | | MJ/kg |
| Jet A | $C_{13}H_{23}$ | 179 | 793 | 1.54 | 14.38 | 42.8 |
| CME | $C_{19}H_{36}O_2$ | 296 | 878 | 5.92 | 12.52 | 39.4 |
| CME25 JETA75 | $C_{14.1}H_{25.4}O_{0.4}$ | 201 | 815 | 1.69 | 13.88 | 40.3 |
| CME50 JETA50 | $C_{15.4}H_{28.2}O_{0.8}$ | 226 | 837 | 2.55 | 13.4 | 41.1 |
| CME75 JETA25 | $C_{17.0}H_{31.9}O_{1.4}$ | 258 | 858 | 3.52 | 12.96 | 42.0 |
| PME | $C_{17.05}H_{32.90}O_2$ | 269 | 867 | 5.61 | 11.17 | 39.4 |
| PME25 JETA75 | $C_{13.79}H_{24.93}O_{0.39}$ | 197 | 814 | 1.75 | 13.84 | 40.3 |
| PME50 JETA50 | $C_{14.7}H_{27.16}O_{0.84}$ | 217 | 830 | 2.40 | 13.33 | 41.1 |
| PME75 JETA25 | $C_{15.77}H_{29.78}O_{1.37}$ | 241 | 848 | 3.19 | 12.83 | 42.0 |
| SME | $C_{18.8}H_{34.6}O_2$ | 292 | 883 | 5.25 | 12.43 | 39.7 |
| SME25 JETA75 | $C_{14.1}H_{25.1}O_{0.4}$ | 201 | 816 | 1.79 | 13.82 | 42.3 |
| SME50 JETA50 | $C_{15.3}H_{27.7}O_{0.8}$ | 224 | 840 | 2.58 | 13.26 | 41.3 |
| SME75 JETA25 | $C_{16.9}H_{30.8}O_{1.3}$ | 254 | 861 | 3.68 | 12.79 | 40.5 |

Table 4.2: Experimental conditions

| Fuel | Exit Reynolds number | Equivalence ratio at blowoff | Heat tape temperature | Airflow rate at blowoff | Primary flow bulk velocity at blowoff |
|---|---|---|---|---|---|
| | | | $^{o}$C | ml/min | m/s |
| Jet A | 2400 - 3650 | 0.54 - 0.79 | 270 | 14900 - 22700 | 3.3 - 5.0 |
| CME | 2100 - 3100 | 0.56 - 0.81 | 365 | 14300 - 20400 | 3.4 - 4.9 |
| CME25 JETA75 | 2200 - 3300 | 0.55 - 0.82 | 365 | 14400 - 20700 | 3.4 - 5.0 |
| CME50 JETA50 | 2200 - 3200 | 0.57 - 0.82 | 365 | 14500 - 20500 | 3.5 - 4.9 |
| CME75 JETA25 | 2200 - 3200 | 0.56 - 0.82 | 365 | 14500 - 20500 | 3.5 - 4.9 |
| PME | 2300 - 3250 | 0.53 - 0.81 | 320 | 14500 - 20450 | 3.3 - 4.7 |
| PME25 JETA75 | 2400 - 3200 | 0.56 - 0.81 | 320 | 15300 - 20450 | 3.5 – 4.7 |
| PME50 JETA50 | 2300 - 3150 | 0.57 - 0.82 | 320 | 14950 - 20250 | 3.4 - 4.7 |
| PME75 JETA25 | 2300 - 3200 | 0.54 - 0.79 | 320 | 14650 - 20400 | 3.4 - 4.7 |
| SME | 2200 - 3200 | 0.55 - 0.81 | 360 | 14350 - 20450 | 3.3 - 4.8 |
| SME25 JETA75 | 2300 - 3200 | 0.55 - 0.82 | 360 | 14800 - 20450 | 3.5 – 4.8 |
| SME50 JETA50 | 2200 - 3200 | 0.56 - 0.83 | 360 | 14200 - 20550 | 3.3 - 4.8 |
| SME75 JETA25 | 2250 - 3200 | 0.55 - 0.80 | 360 | 14500 - 20450 | 3.4 - 4.8 |



Figure 4.3: The first flame achieved in the experimental setup; Jet A at a flow rate of 2 ml/min with 14,800 ml/min of primary airflow rate and 5.95E-3 $m^3/s$ of coflow

## Blowoff Velocities

A typical blowoff sequence for various fuels is presented in Figure 4.4. The blowoff velocity is the jet velocity at which the flame blew off. All the flames blew off within a narrow equivalence ratio range (0.53 - 0.83) in the present experiments. The blowoff velocity increased approximately linearly with equivalence ratio in case of all tested fuels.

Lean blowoff is not an abrupt process. Chapter 2 reviewed several studies which have reported that a flame oscillated between attached and detached phase before the lean blowoff occurred. The same behavior was observed in this study. Similarly, Nicholson and Field (1951) observed that the flame detached and reattached to the burner repeatedly before the lean blowoff occurred. This kind of behavior was also observed by Hertzberg (1991). Figure 4.5 shows a sequence of images extracted from a video which was recorded during the blowoff; it can be clearly seen that the flame detached and reattached a number of times to the burner rim before the blowoff occurred which further confirmed that the lean blowoff is not an abrupt process.

The flame blowoff velocity of pure fuels plotted as a function of equivalence ratio is presented in Figure 4.9 for different values of coflow velocity. In the case of no coflow (Figure 4.9a), the blowoff velocity for Jet A flames increased from 3.3 m/s at an equivalence ratio of 0.67 to 4.3 m/s at an equivalence ratio of 0.79. The blowoff velocities for pure PME flames were almost identical to those corresponding to Jet A: 3.3 m/s at an equivalence ratio of 0.66 to 4.3 m/s at an equivalence ratio of 0.79. The blowoff velocity for pure SME flames varied from 3.4 m/s to 4.5 m/s at an equivalence ratio of 0.68 and 0.79, respectively. Pure CME flames had the greatest blowoff velocity

compared to the other fuels: 3.6 m/s at an equivalence ratio of 0.66 to 4.7 m/s at an equivalence ratio of 0.78.

The blowoff velocity increased with the presence of coflow. This can be more clearly seen in Appendix A (Figures 6.01 – 6.13) where the flame blowoff velocities of all the tested fuels at different coflow velocities are shown separately for each fuel. The presence of coflow increased the velocity near the inner jet edge, resulting in a reduced velocity gradient at the edge. At the coflow velocity of 1.1 m/s (Figure 4.9b), the blowoff velocity of the Jet A flame varied from 3.4 m/s at an equivalence ratio of 0.66 to 4.5 m/s at an equivalence ratio of 0.77; the corresponding numbers for the pure PME flame were 3.4 m/s and 4.5 m/s at an equivalence ratio of 0.65 and 0.76, respectively. The blowoff velocity for pure SME flames increased from 3.4 m/s at an equivalence ratio of 0.68 to 4.6 m/s at an equivalence ratio of 0.77. Similarly, pure CME flames had the greatest blowoff velocity compared to the other fuels even though it stayed the same as in the case of no coflow.

As the coflow velocity was increased to 2.3 m/s (Figure 4.9c), the maximum blowoff velocities increased by 0.1 m/s for all the fuels; the corresponding equivalence ratio was 0.75 for Jet A and pure PME, and 0.76 for pure CME and SME. Interestingly, pure CME also had the smallest minimum blowoff velocity of 3.5 m/s at an equivalence ratio of 0.68. The minimum blowoff velocity was 3.6 m/s for other three pure fuels.

The maximum coflow velocity used in this study was 3.5 m/s. The flames of all the fuels experienced a liftoff prior to blowout at coflow velocity of 3.5 m/s. The lifted flames were not stable – continues change in flame shape was observed. However, the flames always remained lifted without sudden reattachment to the burner. A significant

difference in the blowout velocity was not observed at this condition for the various fuels as illustrated in figure 4.9d. Note that Jet A flames had the highest maximum blowout velocity of 5.0 m/s at an equivalence ratio of 0.69 which was just slightly greater than 4.9 m/s which was the maximum blowout velocity of pure CME flames at an equivalence ratio of 0.75. Additionally, Jet A flames blew off at an equivalence ratio ranging from 0.55 to 0.69, which was slightly more lean compared to biodiesel fuels. Overall, all the flames blew off at a more lean equivalence ratio compared to lower coflow velocities.

The flame blowoff velocity of biodiesel blends with Jet A plotted as a function of equivalence ratio is presented in Figures 4.10 – 4.12 for different values of coflow velocity.

Figure 4.10 represents the blowoff velocity for the flames of CME blends. In the case of no coflow, the blowoff velocity for Jet A flames increased from 3.3 m/s at an equivalence ratio of 0.67 to 4.3 m/s at an equivalence ratio of 0.79. Pure CME flames had the blowoff velocity of 3.6 m/s at an equivalence ratio of 0.66 which ranged to 4.7 m/s at an equivalence ratio of 0.78. At no coflow, the blowoff velocity of the CME blend flames was in between values for the pure fuels. However, CME blend flames blew off at a slightly higher range of equivalence ratio from 0.68 to 0.82. At the coflow velocity of 1.1 m/s and 2.3 m/s, the CME blend flames blowoff velocity was in between those of the pure fuels. Similarly, the CME blend flames blew off at a slightly higher range of equivalence ratio. At the coflow velocity of 3.5 m/s both the blowout velocity and the corresponding equivalence ratio of the CME blend flames fell in between the values for the pure fuels. It is noteworthy that the minimum blowoff velocity of the

CME blend flames was always slightly higher than the minimum blowoff velocity of the pure fuels. Furthermore, the maximum blowoff velocity of the CME blend flames was always equal or less than the maximum blowoff velocity of the pure fuels. However, these differences were within experimental uncertainty. It was not possible to discern any trend in the blowoff velocity as the amount of CME was increased in the fuel.

Pure Jet A and PME had identical blowoff velocity ranging from 3.3 m/s to 4.3 m/s at no coflow as shown in Figure 4.11. At that condition, the PME blends had higher blowoff velocity ranging from 3.5 m/s at an equivalence ratio of 0.67 to 4.5 m/s at an equivalence ratio of 0.80. Similar trend was observed at coflow velocities of 1.1 m/s and 2.3 m/s. Figure 4.11c indicates that PME75 JETA25 flames had slightly higher blowoff velocity than pure fuels and other PME blends at the coflow velocity of 2.3 m/s. The PME75 JETA25 flames achieved the maximum blowoff velocity at this condition of 4.7 m/s at an equivalence ratio of 0.74. At the maximum coflow velocity of 3.5 m/s, there was no significant difference in blowout velocity among pure PME and PME blend flames except that PME blend flames blew off at a slightly higher equivalence ratio (on average, 7% higher). Interestingly, the minimum blowoff velocity of the PME50 JETA50 flames was 4.0 m/s which is slightly lower than 4.1 m/s which is the minimum blowoff velocity of both pure Jet A and PME. However, this difference is within experimental uncertainty.

The blowoff velocity of SME blend flames was more scattered than for other fuels, except at one condition corresponding to the maximum coflow rate of 3.5 m/s. At

no coflow, the blowoff velocities of the SME blend flames varied in between the values obtained for the pure fuels.

## Damköhler Number

As reported in Chapter 2, the Damköhler number has been used to characterize the blowoff of flames. As seen in chapter 3, Damköhler number is the ratio of the flow time scale to that of the chemical reaction time scale. For small Damköhler numbers, the chemistry is slow compared to reaction time and well–stirred flames may occur. For large values of Damköhler number, the reaction time is long compared to chemistry time scale which is fast. Blowoff occurs when the gas velocity gradient at the jet edge becomes higher than the flame velocity near the jet edge. Thus, the blowoff-limit is reached when the gas velocity near the edge is tangential to the flame velocity variation with distance from the boundary. Thus, the gradient of velocity near the edge is an important factor determining the flow time scale. Axial velocity profiles for three different primary airflow rates without coflow and with three different coflow rates are provided in Figure 4.7. Majority of the flames from all the fuels in this study blew off within the range of 15.1 l/min to 22.1 l/min of the primary airflow rate (corresponding to velocity range 3.5 m/s to 5.1 m/s).

Several conclusions can be drawn from Figure 4.7. Primary air jet entered into quiescent air when there was no coflow. Dashed lines in Figure 4.7a illustrate the method of calculating the velocity gradients at the edge of the jet. When coflow was increased to 1.1 m/s, the velocity of primary jet was still always greater than the coflow velocity. With further increase of coflow to 2.3 m/s, the lower limit of primary airflow

velocity was about the same, or slightly higher (by about 5%) than the coflow velocity. Figure 4.7d shows that, at coflow bulk velocity of 3.5 m/s, the maximum coflow velocity was significantly higher than the lower limit of primary airflow velocity. In fact, the peak coflow velocity was 4.02 m/s whereas the peak primary flow velocity (corresponding to primary flow of 18.7 l/min) was 4.09 m/s. Thus, with coflow bulk velocity of 3.5 m/s, only primary flows higher than 18.7 l/min resulted in higher primary flow velocity compared to coflow velocity. This is noteworthy because velocity gradients change with coflow. The velocity gradients decreased with increase in coflow as shown in Figure 4.8. Thus, the flow time scale increased, or became longer, with increase in coflow. The chemical time scale is independent of coflow since both thermal diffusivity and laminar flame speed are independent of coflow. However, the laminar flame speed is a function of equivalence ratio and equivalence ratio was significantly lower at 3.5 m/s of coflow velocity compared to other coflow rates and no coflow at all.

Tables 4.3 – 4.6 show the Damköhler number variation for Jet A, CME, PME, and SME with equivalence ratio and coflow rate. Jet A flame blowoffs resulted in highest Damköhler number of about 8. Damköhler number was about 3 to 4 in the case of CME, PME, and SME flame blowoff. Note that Damköhler number seemed to slightly increase with increase in coflow rate; however, it was smallest when the coflow velocity was 3.5 m/s which was the maximum coflow velocity used in this study. All flames at coflow velocity of 3.5 m/s were always lifted before the blowout occurred, which may explain the significant difference in Damköhler number. All lifted flames blew out at leaner equivalence ratio (ranging 0.53 – 0.75), whereas the attached flames blew off at more rich equivalence ratio (ranging 0.62 – 0.82). Many studies which are

briefly reviewed in Chapter 2 have shown that laminar flame speed in lean regime decreases in parabolic fashion with decrease in equivalence ratio. Thus, chemical time scale increases with decrease in laminar flame speed which leads to smaller Damköhler number. Overall, Damköhler number ranged from about 2 to 8 with the range being even narrower if only biofuels are considered (~2-4). Given a significant degree of estimation due to the limited information about laminar flame speed, and the range of Damköhler number being relatively narrow, it can be concluded that Damköhler number can be used for predicting flame blowoff.

## Inflame Temperature Measurements

This section discusses inflame temperature radial profiles. The measurements were taken at the coflow velocities of 1.1 m/s, 2.3 m/s, and at no coflow. The temperature was measured at three different heights – at the half of the inner cone, at the tip of the inner cone, and at the twice the height of the inner cone (which was approximately slightly higher than half of the outer cone height). Figure 4.27 depicts the approximate locations of these heights in a flame. In this study the fuel flow rate ranged from 65.1 ml/hr to 100 ml/hr. Preliminary measurements shown in Figure 6.53 (Appendix C) indicate that there was no noticeable difference in temperature profiles when the fuel flow rate was changed. Thus, the inflame temperature profiles for all the pure fuels and their blends were measured at a fuel flow rate of 78.2 ml/hr. It was initially attempted to measure the inflame temperature profiles of a flame just prior to the blowoff. However, flames which were near the blowoff were very sensitive to the smallest disturbances such as the presence of the thermocouple or even breathing. Thus,

they would often blow off as a result of these disturbances in the midst of a measurement, which required starting over from the beginning. In order to expedite the measurements, the inflame temperature measurements were performed at approximately stoichiometric condition (equivalence ratio about 0.9) where the flame was more stable and less sensitive to aforementioned disturbances. These measurements were compared to the temperature measurements of the flame just before the blowoff (those few measurements which were successfully completed without the flame blowing off) and they were identical. Thus, the inflame temperature measurements reported in this study were collected at equivalence ratio of 0.9.

The temperature measurement in the absence of any flame is shown in Figure 4.28. The two vertical black lines represent the burner wall. The temperature of the primary airflow is only slightly higher (10 K) than the coflow temperature at coflow velocity of 2.3 m/s. However, the temperature difference between primary flow and surrounding air was significant (about 100 K) when there was no coflow. The temperature continued to decrease with the distance away from the burner. The suggested reason is that the surrounding air was not heated directly by the heaters. Instead, it was heated by the heat transfer (conduction) from the primary flow tube.

The flame temperature profiles of pure fuels at heights corresponding to half the inner cone height, at the inner cone height (tip of inner cone), and at twice the inner cone height are presented in Figure 4.29. The temperatures at all three heights are almost identical for all fuels. At half the inner cone height, the peak temperature was reached around 6 mm from the center, indicating that the reaction zone was present at this distance at this height. The temperature profile was symmetric, with a peak

temperature of 1740 K. The temperature profile became flat at the height corresponding to the inner cone; the peak temperature here was 1710 K. The peak temperature at twice the inner cone height was 1660 K. The aforementioned peak temperatures were all measured in Jet A flames; biofuel flames had peak temperature of about 40 K lower than that of Jet A.

Figures 4.30 – 4.32 represent the variation in flame temperature profiles of Jet A, PME, and CME with coflow. There was no significant difference in temperature profiles at different coflow settings. The only noticeable difference is that temperature profiles at coflow velocity of 2.3 m/s seem to be narrower at all three heights at which the flame temperature was measured. This would indicate that coflow caused the flame to become narrower. However, results of the width of the flame do not show any pattern which would suggest that coflow caused the flame to become narrower. Given the significant uncertainty in the flame width, the coflow did not have a significant effect on flame width.

Flame temperatures of CME blends, PME blends, and SME blends at no coflow are presented in Figures 4.33 – 4.35. Flames of blends did not have any significant difference in temperature. The peak temperatures were around the values of pure fuels.

Overall, there was no significant difference in the temperature profiles of the various flames including pure fuels and blends. The adiabatic flame temperature for CME and SME was 2286 K and 2266 K as reported by Gomez-Mayer (2012). The adiabatic flame temperature for Jet A and PME was 2587 K and 2564 K as reported by Chong and Hochgreb (2012). The differences in adiabatic flame temperatures of tested fuels were not significant, so there was no significant difference in temperature profiles.

## Flame Dimensions

This section discusses the visible flame dimensions determined from the photographs extracted from the videos which were recorded during the experiments. The flame dimensions (inner cone height, outer cone height, maximum width, and liftoff height) were very similar across all the flames tested. Uncertainties are presented as error bars.

The outer cone height, inner cone height, and the maximum width are reported for three different coflow settings: no coflow, 1.1 m/s, and 2.4 m/s of coflow bulk velocity. The effect of coflow on flame dimensions of each fuel separately can be seen in Appendix B (Figures 6.14 – 6.52). Since all the flames were lifted at coflow velocity of 3.5 m/s, only the liftoff height is reported.

Figure 4.4 illustrates various flames approaching blowoff. All the flames were laminar and blue in color, indicating the dominance of homogeneous gas-phase reactions. It was observed that flames were very bright and aqua-marine blue in color at around stoichiometric equivalence ratio; as the equivalence ratio became leaner approaching the blowoff, the flame became less bright and the blue color contained tints of violet. At certain instances the flame color was very pale just before the blowoff. Flame pulsation was also observed when a flame would periodically become dimmer and pale in color. The pulsation occurred in irregular intervals so it was not possible to discern any patterns.

Inner cone height and outer cone height both increased roughly linearly with equivalence ratio. The width of the outer cone (measured at the widest point) seemed to

stay constant regardless of equivalence ratio for a given fuel. Uncertainty for outer cone height and width was significant as shown by the error bars.

Coflow did not affect the flame dimensions significantly apart from causing the liftoff when coflow velocity was 3.5 m/s (maximum coflow velocity in this study).

Figure 4.13 provides the comparison in inner cone height of Jet A, CME, PME, and SME at different coflow settings. At no coflow, inner cone height of Jet A varied from 1.7 cm at equivalence ratio of 0.67 to 2.2 cm at equivalence ratio of 0.79. CME and PME inner cone height varied almost identically to Jet A. SME was slightly more scattered with minimum inner cone height of 1.7 cm at equivalence ratio of 0.72. Increase in coflow velocity to 1.1 m/s and 2.3 m/s did not have noticeable effect on inner cone height. Jet A inner cone height at 1.1 m/s of coflow velocity varied form 1.9 cm at equivalence ratio of 0.66 to 2.3 cm at equivalence ratio of 0.77. Thus, a small increase in the inner cone height of Jet A. The biofuels had insignificant changes in inner cone height with coflow velocity. Changes, if any, were within experimental uncertainty.

Figure 4.14 provides the comparison in outer cone height of Jet A, CME, PME, and SME at different coflow settings. While the outer cone height increased roughly linearly with equivalence ratio for all coflow settings, the slope became steeper with increase in coflow velocity. At no coflow, outer cone height of Jet A flames varied from 4.0 cm at equivalence ratio of 0.67 to 6.0 cm at equivalence ratio of 0.79. CME flames outer cone height varied almost identically to Jet A. PME outer cone was slightly shorter than other pure fuels; it varied from 3.7 cm at equivalence ratio of 0.68 to 5.3 cm at equivalence ratio of 0.79. SME flames outer cone height varied at similar values

to those of PME flames; it increased linearly from 3.4 cm at equivalence ratio of 0.68 to 5.7 cm at equivalence ratio of 0.76. Results indicate that the outer cone height increased slightly with increase in coflow velocity but only for more rich equivalence ratios. However, this was not always the case. For example, maximum outer cone height of SME flames dropped from 7.1 cm to 6.7 cm as the coflow velocity increased from 1.1 m/s to 2.3 m/s. Nonetheless, this change is within uncertainty of outer cone height. The possible reason for significant uncertainty in outer cone height is the flame behavior. While not so present at the inner cone which was mostly stationary, the outer cone exhibited typical swaying from one side to another. The outer cone height would be different depending if the flame was swayed to one side or another, or if it was straight at the last instance when the flame was fully attached to the burner before the blowoff.

The variation of outer cone width of pure Jet A, CME, PME, and SME flames measured at the widest point with equivalence ratio is shown in Figure 4.15. It was not possible to determine which flames were the widest. All the flames of all pure fuels varied in width in maximum range of 0.4 cm. At no coflow, CME flames resulted in widest flames; approximately 0.5 cm wider than the flames of Jet A, PME, and SME. The difference became smaller at higher equivalence ratios. At coflow velocity of 1.1 m/s, PME flames had noticeably wider flames (by about 0.5 cm) than the rest of pure fuels flames. No flames had distinctively different width dimensions at coflow velocity of 2.3 m/s. The same reason for significant uncertainty in outer cone height can be suggested to uncertainty in the width.

Figure 4.16 shows the variation in liftoff height of Jet A, CME, PME, and SME with equivalence ratio. Lifted flames were only achieved at maximum coflow velocity

used in this study which was 3.5 m/s. It was not possible to discern any pattern in change of liftoff height with equivalence ratio since it varied unpredictably. However, it seemed to stay somewhat constant. The liftoff height of all flames was mostly clustered between 1.0 and 1.5 cm. Jet A flames had the lowest liftoff height and were scattered the most. The liftoff height of CME, PME, and SME flames seemed to stay fairly constant (varied within 0.4 cm) regardless of equivalence ratio.

Figures 4.17 – 4.19 show the variation in inner cone heights of flames of blends. Flames of CME blends varied around the values of pure fuels. The only noticeable discrepancy is in the case of 2.3 m/s of coflow velocity where CME75 JETA25 flames had slightly lower inner cone height than pure fuels and other blends. Flames of PME blends resulted in inner cone heights which were within the values for pure fuels. SME75 JETA25 flames had slightly higher inner cone heights compared to other SME blends and pure fuels when coflow was present, but this discrepancy was within experimental uncertainty.

Figures 4.20 – 4.22 show the variation in outer cone heights of flames of blends. Outer cone height of flames of CME blends varied around the values of pure fuels. On the other hand, flames of PME blends resulted in significantly more scattered data for outer cone height. PME25 JETA75 flames had the lowest outer cone height for all coflow settings while PME50 JETA50 flames had the tallest outer cone for all coflow settings. Similarly, flames of SME blends resulted in scattered data for outer cone height. SME75 JETA25 had higher outer cone height than other blends and pure fuels when coflow was present. The outer cone heights of flames of SME blends were more clustered when there was no coflow.

Figures 4.23 – 4.25 show the variation in maximum width of outer cone of flames of blends. CME50 JETA50 flames resulted in wider outer cones than other blends and pure fuels for all coflow settings. Width of flames of PME blends was mostly clustered at no coflow. With coflow present, PME75 JETA25 flames resulted in widest flames. Similarly, width of flames of SME blends was mostly clustered at no coflow. At coflow velocity of 1.1 m/s, SME50 JETA50 flames had widest outer cone but also exhibited a very irregular pattern. SME25 JETA75 flames had widest outer cone at coflow velocity of 2.3 m/s.

Liftoff height of flames of blends is shown in Figure 4.26. Liftoff height of flames of CME blends stays fairly constant with equivalence ratio. CME50 JETA50 flames resulted in highest liftoff height of roughly 1.9 cm, while CME25 JETA75 flames had lowest liftoff height of roughly 0.8 cm. The values of pure fuels and other blends were in between these values. The flames of PME blends and SME blends resulted in more clustered liftoff height which varied between 1.0 cm and 1.5 cm.



a) Fuel: Jet A, Re = 2800, U = 3.8 m/s, φ = 0.74, t = 0.2 s



b) Fuel: CME, Re = 2630, U = 4.1 m/s, φ = 0.73, t = 0.2 s

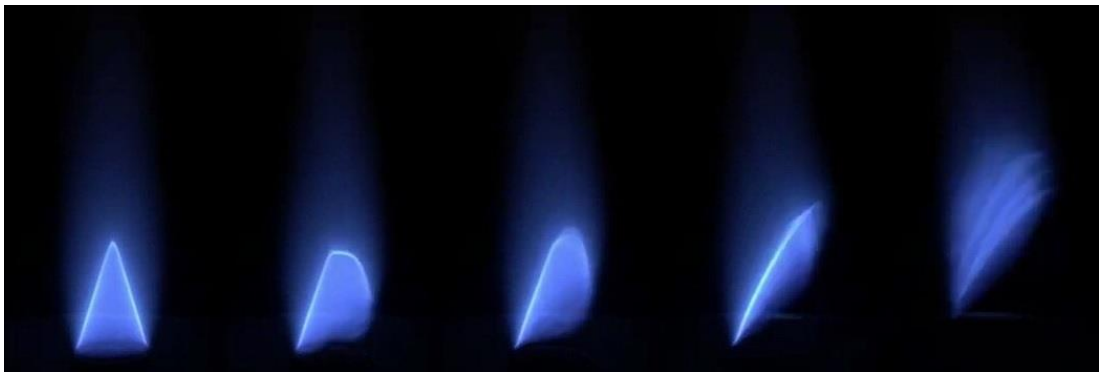

c) Fuel: PME, Re = 2550, U = 3.7 m/s, φ = 0.76, t = 0.2 s

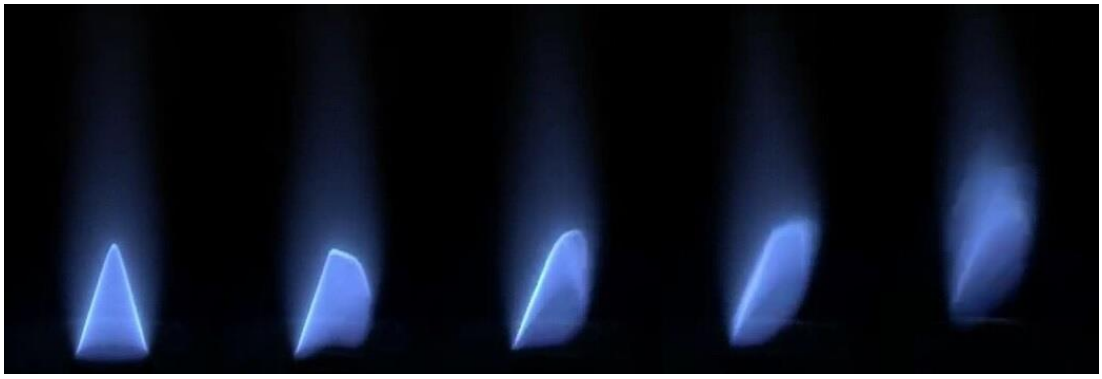

d) Fuel: SME, Re = 2760, U = 4.2 m/s, φ = 0.70, t = 0.4 s



e) Fuel: CME25 JETA75, Re = 2670, U = 4.1 m/s, φ = 0.74, t = 1.17 s

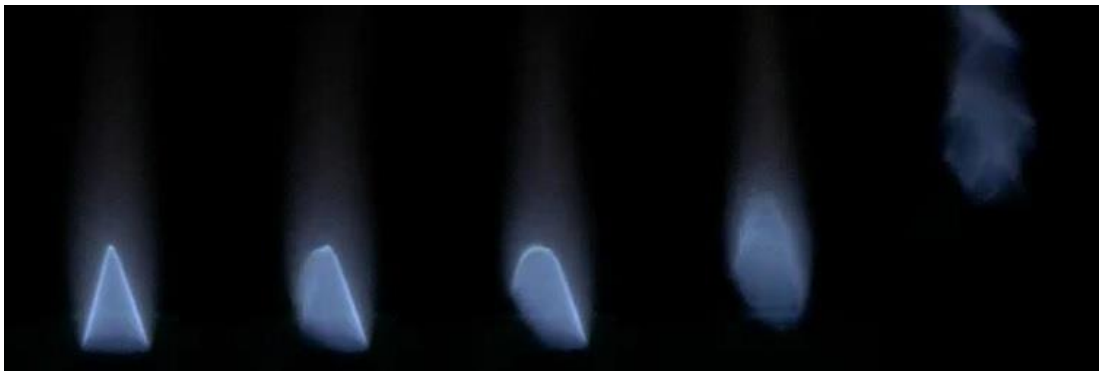

f) Fuel: CME50 JETA50, Re = 2510, U = 3.9 m/s, φ = 0.78, t = 0.17 s

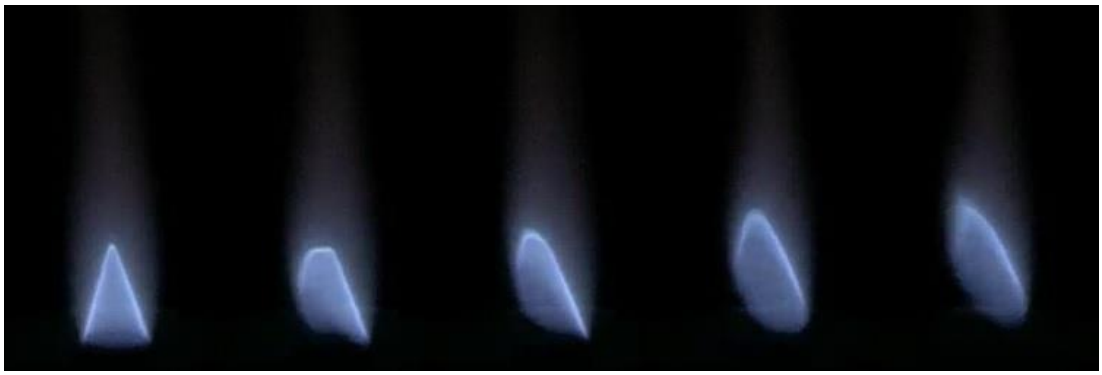

g) Fuel: CME75 JETA25, Re = 2590, U = 4.0 m/s, φ = 0.75, t = 0.33 s



h) Fuel: PME25 JETA75, Re = 2730, U = 4.0 m/s, φ = 0.74, t = 0.4 s



i) Fuel: PME50 JETA50, Re = 2710, U = 4.0 m/s, φ = 0.73, t = 0.73 s



j) Fuel: PME75 JETA25, Re = 2670, U = 3.9 m/s, φ = 0.73, t = 0.27 s



k) Fuel: SME25 JETA75, Re = 2670, U = 4.0 m/s, φ = 0.75, t = 0.2 s

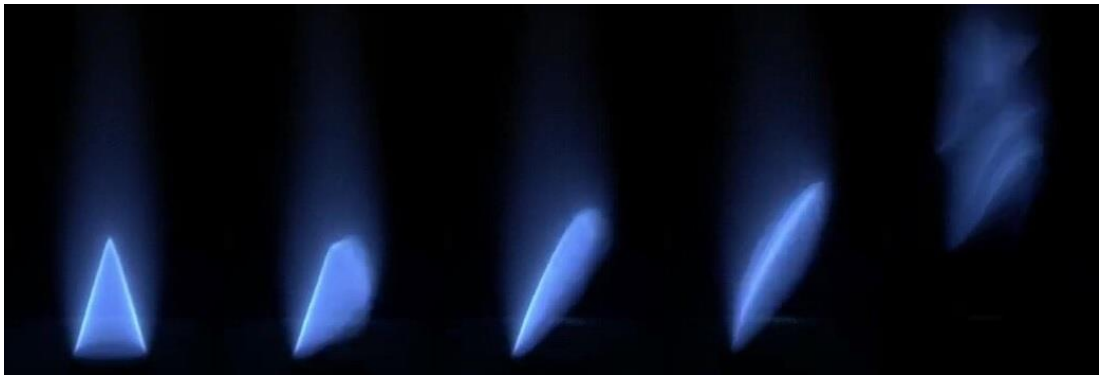

l) Fuel: SME50 JETA50, Re = 2650, U = 4.0 m/s, φ = 0.75, t = 0.23 s

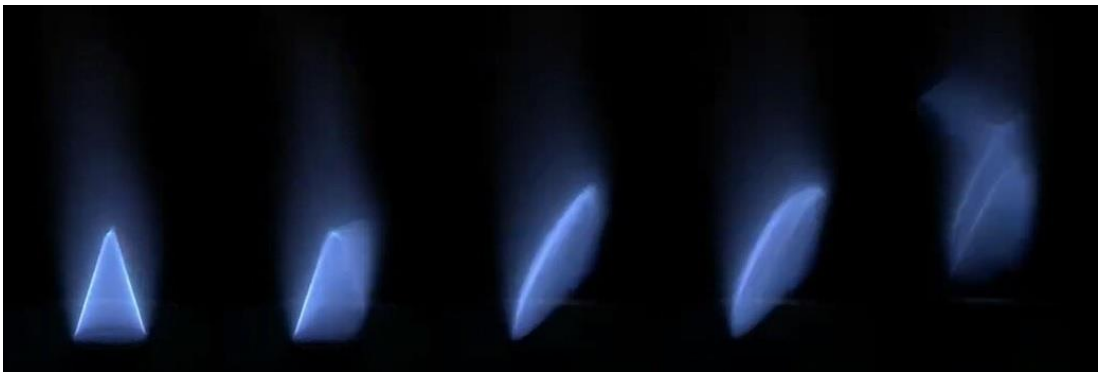

m) Fuel: SME75 JETA25, Re = 2650, U = 3.9 m/s, φ = 0.74, t = 0.2 s

Figure 4.4: Images of typical blowoff for various fuels

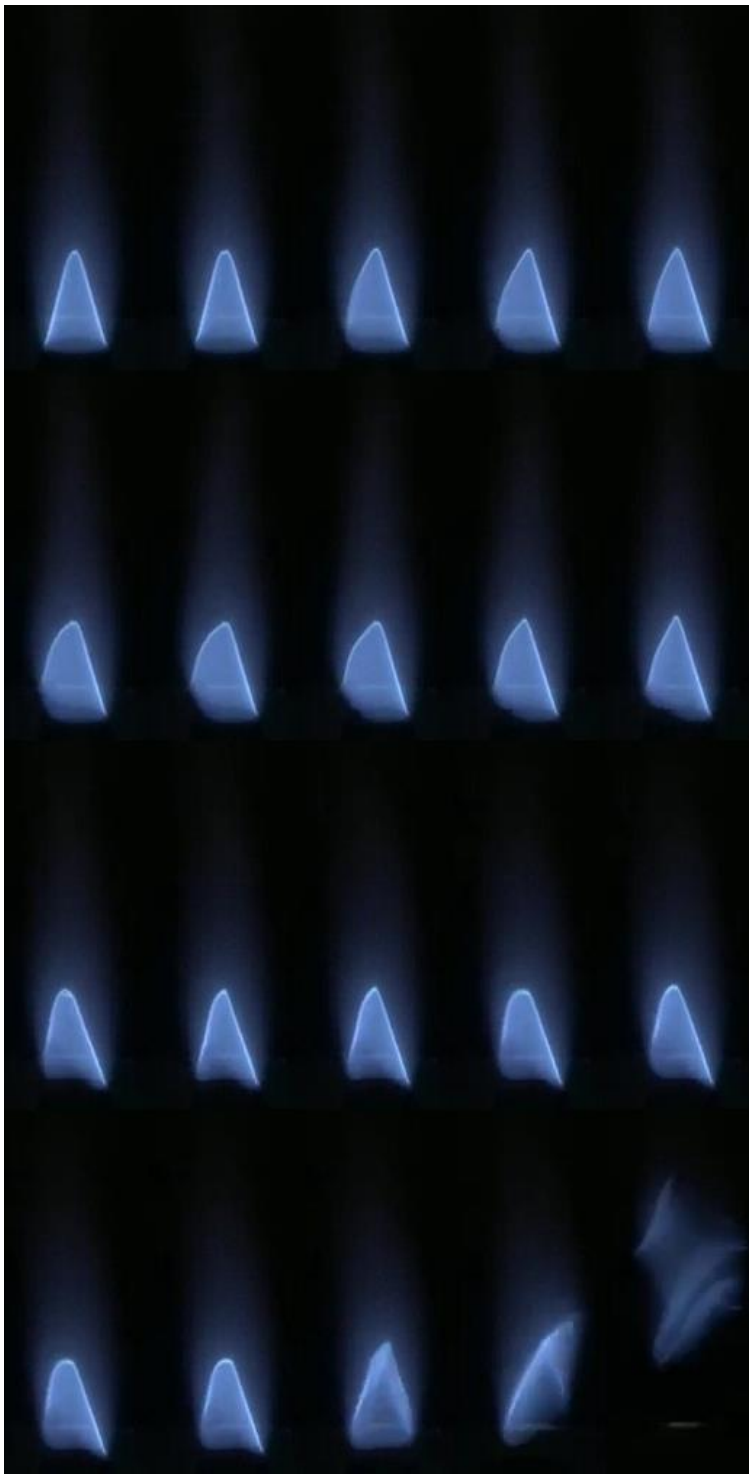

Figure 4.5: Oscillations between attached and detached phase, t = 0.67 seconds, fuel: Jet A

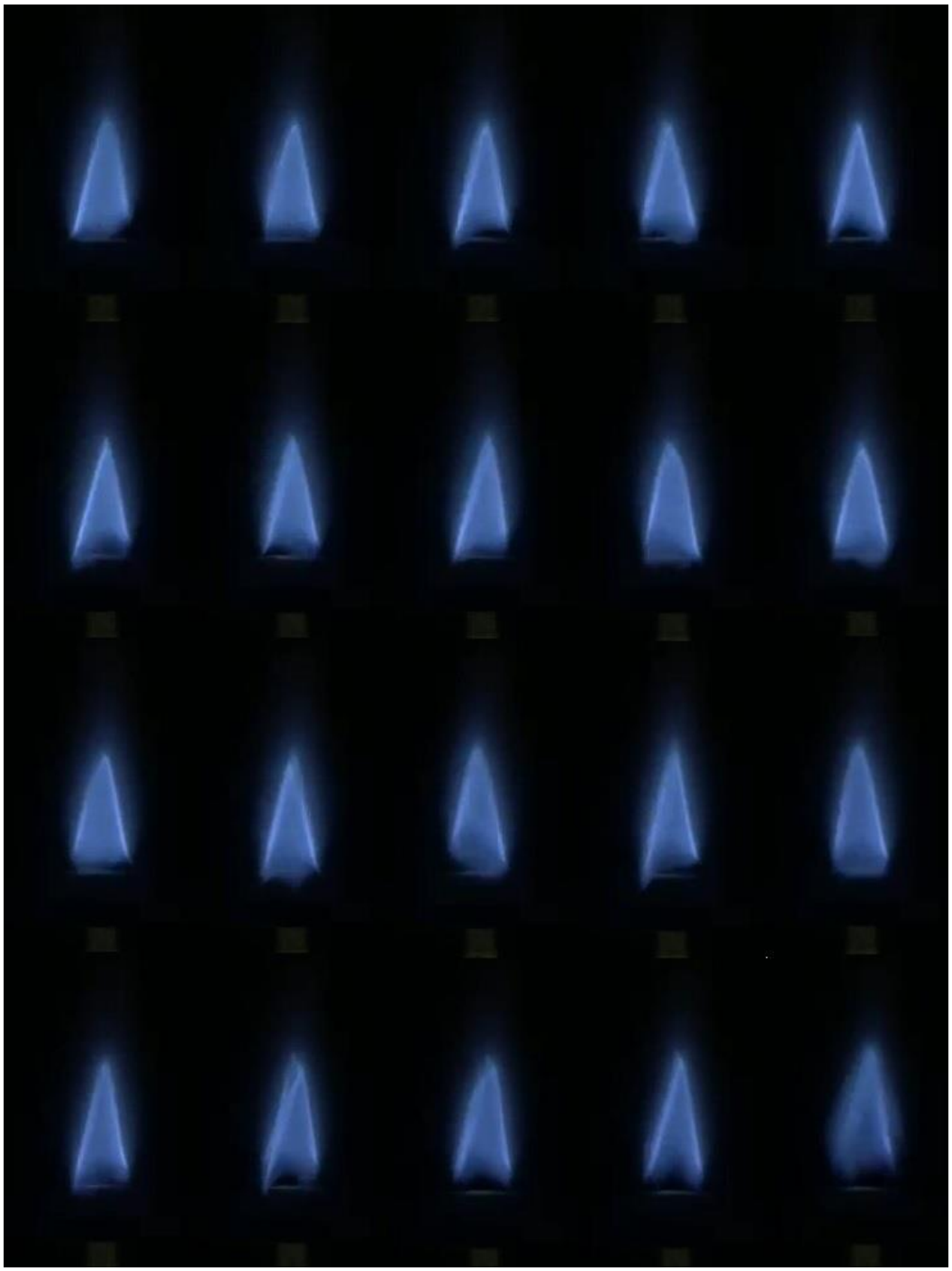

Figure 4.6: Typical blowout of a lifted flame; constant change in flame dimensions and shape can be observed, time interval is 0.67 seconds,
fuel: Jet A

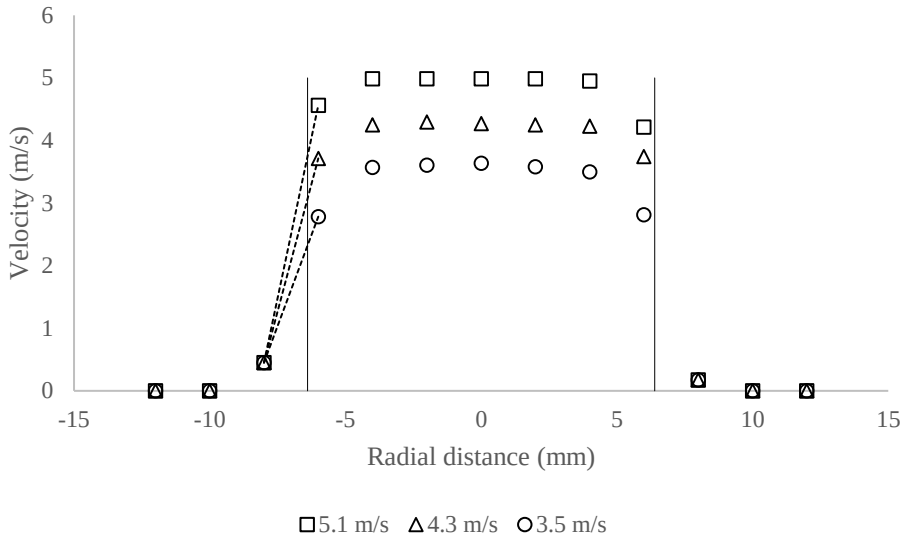


a) no coflow (Gradients: 1880 $s^{-1}$, 1830 $s^{-1}$, 1350 $s^{-1}$)

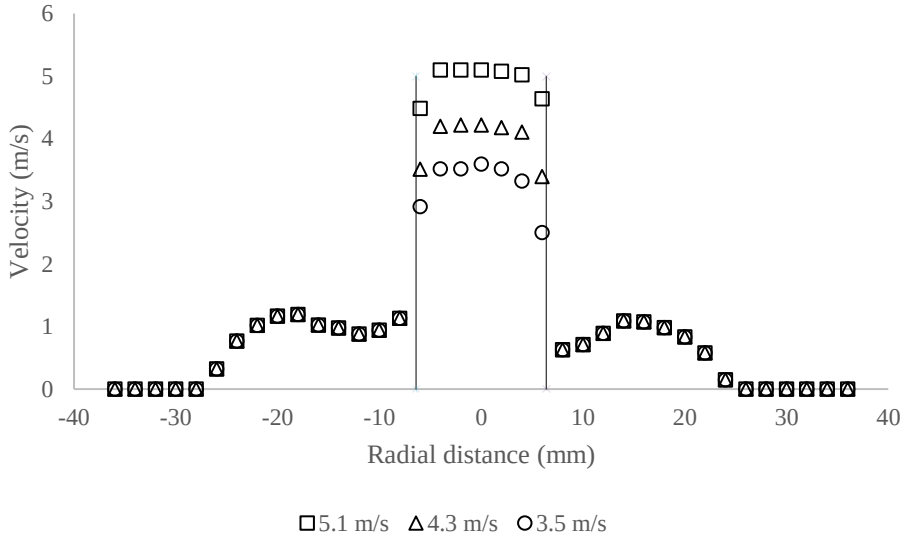


b) coflow velocity of 1.1 m/s (Gradients: 1820 $s^{-1}$, 1350 $s^{-1}$, 1020 $s^{-1}$)

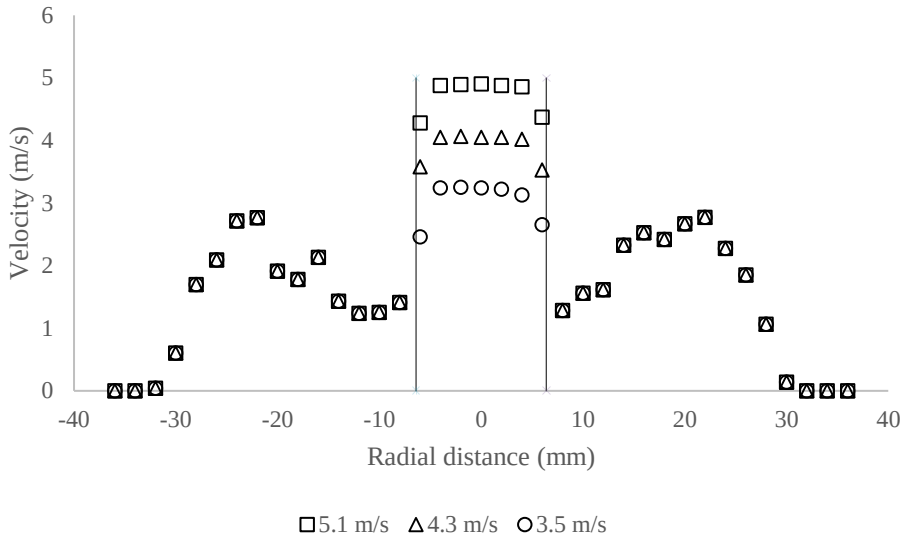


c) coflow velocity of 2.3 m/s (Gradients: 1310 $s^{-1}$, 1120 $s^{-1}$, 890 $s^{-1}$)

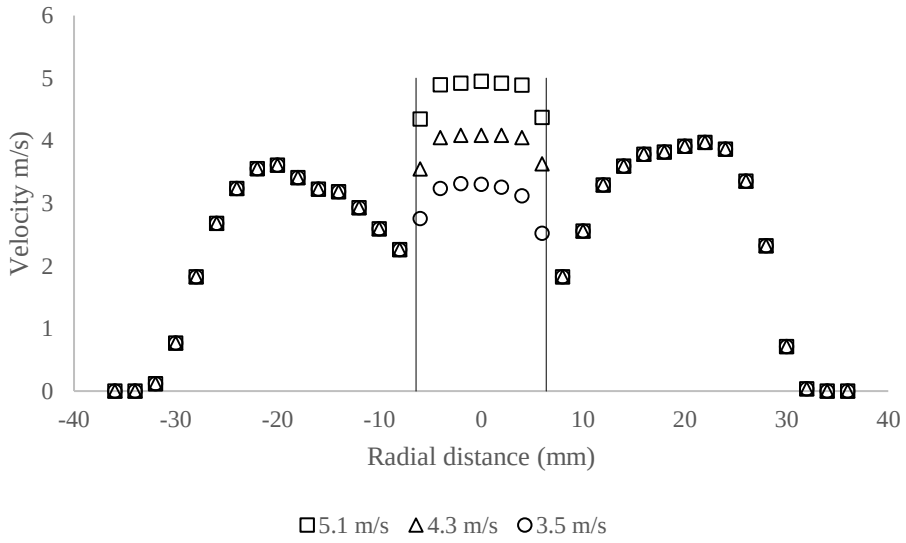


d) coflow velocity of 3.5 m/s (Gradients: 1130 $s^{-1}$, 760 $s^{-1}$, 350 $s^{-1}$)

Figure 4.7: Axial velocity profiles at 6 mm above burner at temperature of 523 K

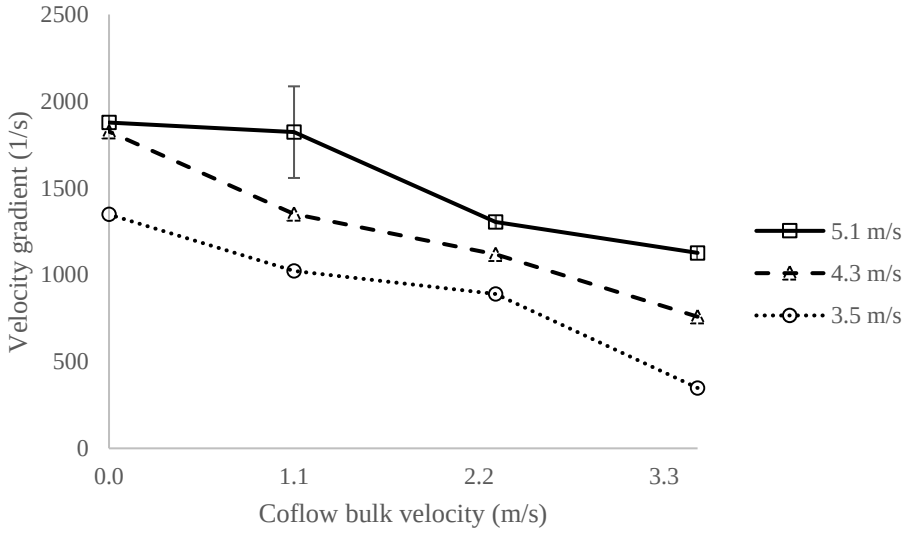


Figure 4.8: Change in velocity gradient with coflow

Table 4.3: Damköhler number for Jet A flames at blowoff

| Coflow (m/s) | 3.5 | | 2.3 | | 1.1 | | 0 | |
|---|---|---|---|---|---|---|---|---|
| | Φ | Da | Φ | Da | Φ | Da | Φ | Da |
| | 0.55 | 2.3 | 0.63 | 6.5 | 0.66 | 7.8 | 0.67 | 5.0 |
| | 0.57 | 3.2 | 0.64 | 6.8 | 0.68 | 8.2 | 0.70 | 5.9 |
| | 0.60 | 4.6 | 0.65 | 7.1 | 0.71 | 9.4 | 0.69 | 5.2 |
| | 0.61 | 4.7 | 0.67 | 8.0 | 0.70 | 7.9 | 0.71 | 5.7 |
| | 0.63 | 5.6 | 0.69 | 8.8 | 0.71 | 7.6 | 0.74 | 6.5 |
| | 0.66 | 6.9 | 0.71 | 9.7 | 0.72 | 7.5 | 0.74 | 6.2 |
| | 0.67 | 7.1 | 0.74 | 10.6 | 0.74 | 8.0 | 0.76 | 6.6 |
| | 0.69 | 7.8 | 0.75 | 10.2 | 0.76 | 8.4 | 0.79 | 7.4 |
| | 0.69 | 7.5 | 0.75 | 9.0 | 0.77 | 8.4 | 0.79 | 7.1 |
| average Da | | 5.5 | | 8.5 | | 8.1 | | 6.2 |

Table 4.4: Damköhler number for CME flames at blowoff

| Coflow (m/s) | 3.5 | | 2.3 | | 1.1 | | 0 | |
|---|---|---|---|---|---|---|---|---|
| | Φ | Da | Φ | Da | Φ | Da | Φ | Da |
| | 0.57 | 1.1 | 0.68 | 2.9 | 0.66 | 2.0 | 0.66 | 1.5 |
| | 0.59 | 1.4 | 0.68 | 2.6 | 0.68 | 2.3 | 0.69 | 1.9 |
| | 0.60 | 1.4 | 0.68 | 2.5 | 0.69 | 2.3 | 0.70 | 1.9 |
| | 0.61 | 1.5 | 0.71 | 3.0 | 0.70 | 2.4 | 0.71 | 1.9 |
| | 0.64 | 2.0 | 0.71 | 2.9 | 0.73 | 2.8 | 0.73 | 2.1 |
| | 0.66 | 2.2 | 0.76 | 3.9 | 0.74 | 2.8 | 0.74 | 2.1 |
| | 0.68 | 2.5 | 0.74 | 3.2 | 0.77 | 3.3 | 0.76 | 2.3 |
| | 0.72 | 3.0 | 0.75 | 3.3 | 0.75 | 2.6 | 0.77 | 2.3 |
| | 0.75 | 3.5 | 0.76 | 3.4 | 0.78 | 3.0 | 0.78 | 2.4 |
| average Da | | 2.1 | | 3.1 | | 2.6 | | 2.1 |

Table 4.5: Damköhler number for PME flames at blowoff

| Coflow (m/s) | 3.5 | | 2.3 | | 1.1 | | 0 | |
|---|---|---|---|---|---|---|---|---|
| | Φ | Da | Φ | Da | Φ | Da | Φ | Da |
| | 0.54 | 1.2 | 0.62 | 2.8 | 0.65 | 3.5 | 0.66 | 3.0 |
| | 0.57 | 2.0 | 0.64 | 3.3 | 0.65 | 3.2 | 0.69 | 3.7 |
| | 0.57 | 1.7 | 0.68 | 4.7 | 0.65 | 3.0 | 0.72 | 4.3 |
| | 0.59 | 2.1 | 0.67 | 4.0 | 0.70 | 4.5 | 0.68 | 2.8 |
| | 0.62 | 3.0 | 0.71 | 5.3 | 0.69 | 3.8 | 0.76 | 4.9 |
| | 0.63 | 3.0 | 0.69 | 4.3 | 0.72 | 4.6 | 0.75 | 4.2 |
| | 0.66 | 3.6 | 0.73 | 5.5 | 0.73 | 4.6 | 0.77 | 4.5 |
| | 0.69 | 4.5 | 0.74 | 5.7 | 0.73 | 4.2 | 0.76 | 4.0 |
| | 0.72 | 5.1 | 0.75 | 5.8 | 0.76 | 5.0 | 0.79 | 4.6 |
| average Da | | 2.9 | | 4.6 | | 4.0 | | 4.0 |

Table 4.6: Damköhler number for SME flames at blowoff

| Coflow (m/s) | 3.5 | | 2.3 | | 1.1 | | 0 | |
|---|---|---|---|---|---|---|---|---|
| | Φ | Da | Φ | Da | Φ | Da | Φ | Da |
| | 0.56 | 0.3 | 0.65 | 2.2 | 0.68 | 2.9 | 0.68 | 2.2 |
| | 0.58 | 0.7 | 0.67 | 2.7 | 0.71 | 3.7 | 0.72 | 3.1 |
| | 0.59 | 0.8 | 0.71 | 4.0 | 0.71 | 3.4 | 0.71 | 2.5 |
| | 0.61 | 1.2 | 0.72 | 4.1 | 0.68 | 2.3 | 0.69 | 1.9 |
| | 0.63 | 1.6 | 0.74 | 4.6 | 0.73 | 3.6 | 0.70 | 2.0 |
| | 0.65 | 2.1 | 0.74 | 4.3 | 0.75 | 3.9 | 0.73 | 2.5 |
| | 0.68 | 2.8 | 0.75 | 4.5 | 0.73 | 3.1 | 0.76 | 3.0 |
| | 0.71 | 3.5 | 0.75 | 4.3 | 0.75 | 3.4 | 0.76 | 2.9 |
| | 0.74 | 4.0 | 0.76 | 4.4 | 0.77 | 3.7 | 0.79 | 3.4 |
| average Da | | 1.9 | | 3.9 | | 3.3 | | 2.6 |

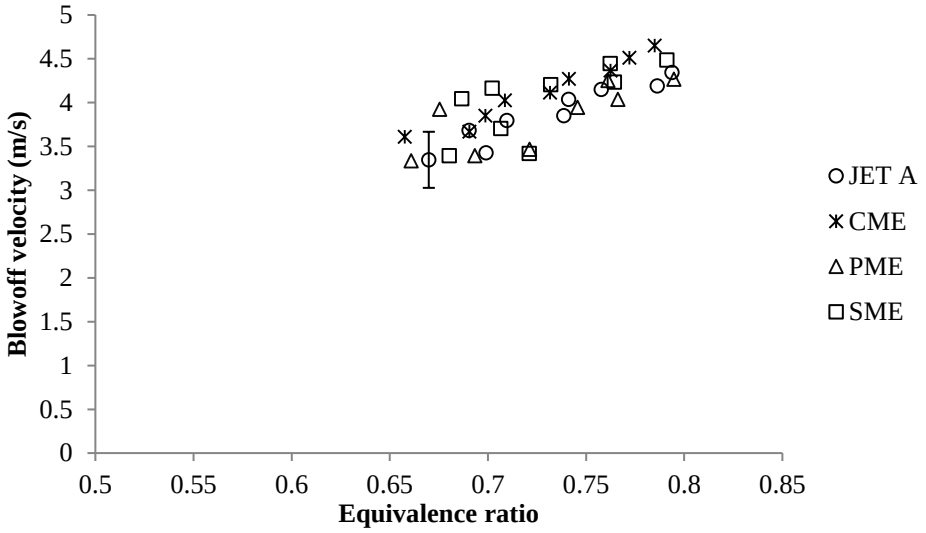


a) no coflow

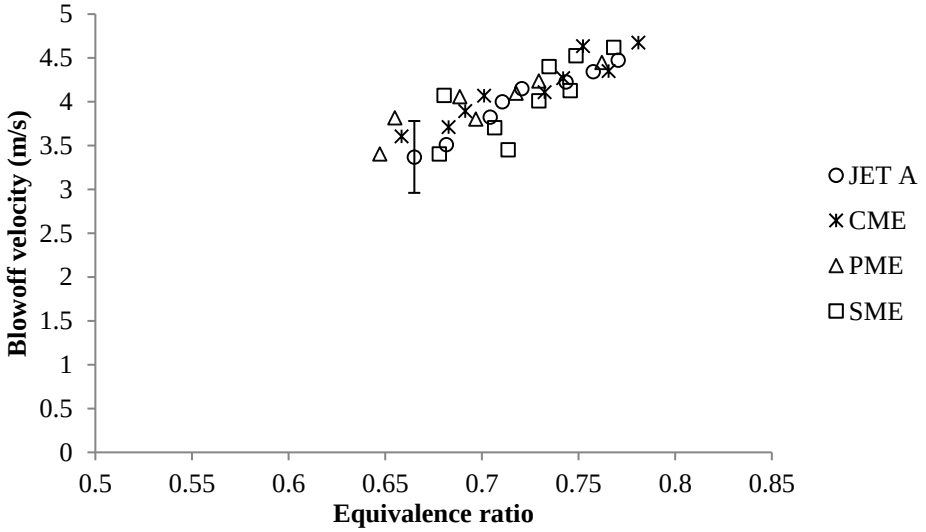


b) coflow velocity of 1.1 m/s

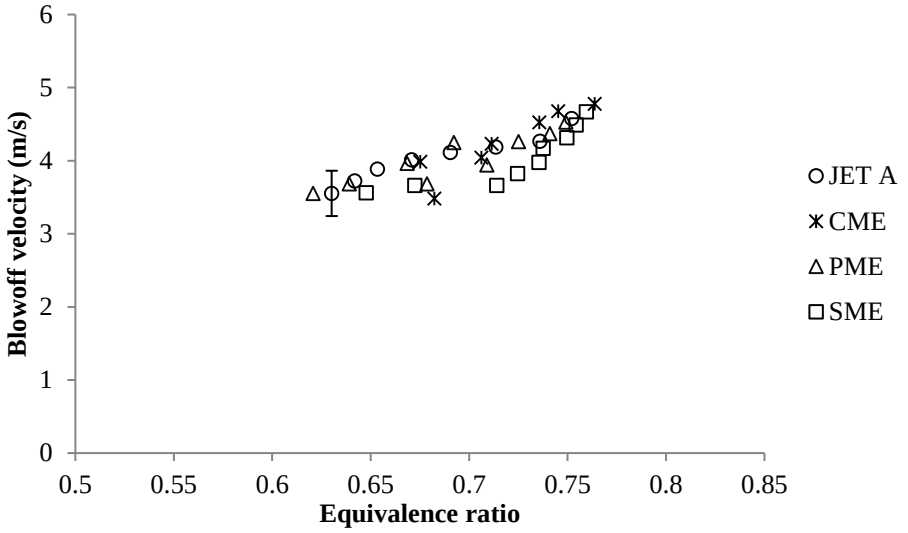


c) coflow velocity of 2.3 m/s

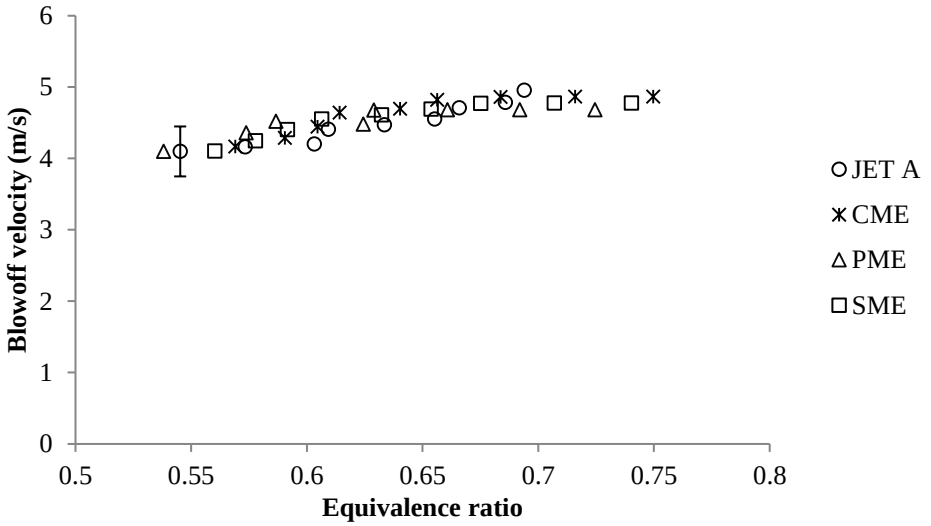


d) coflow velocity of 3.5 m/s

Figure 4.9: Change in blowoff velocity with equivalence ratio for pure fuels at different coflow velocities

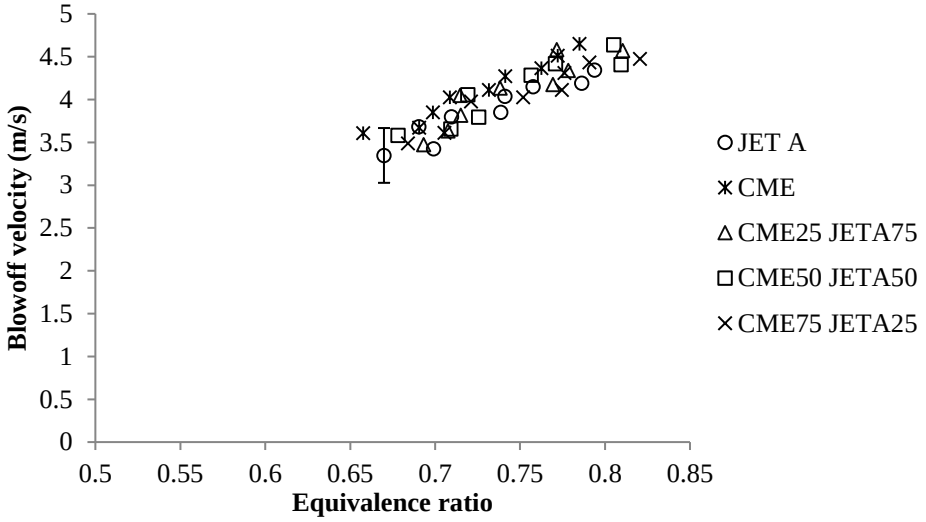


a) no coflow

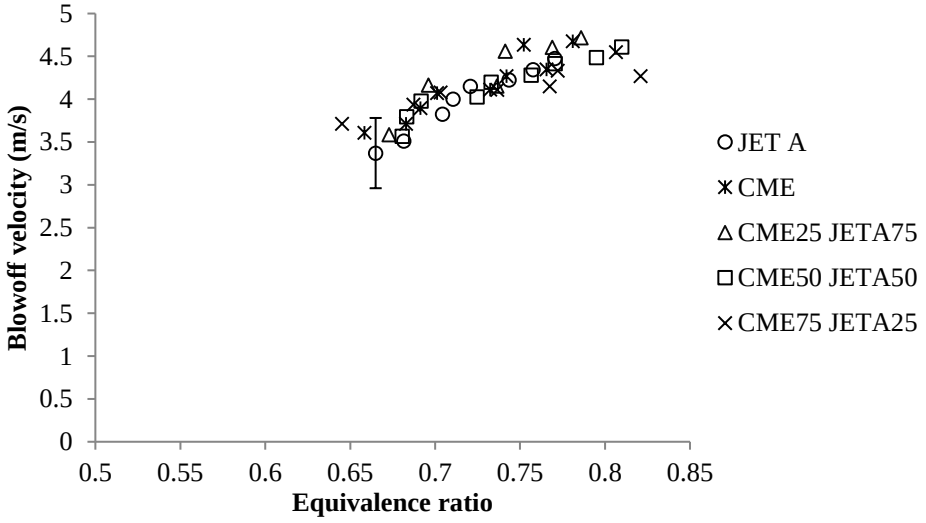


b) coflow velocity of 1.1 m/s

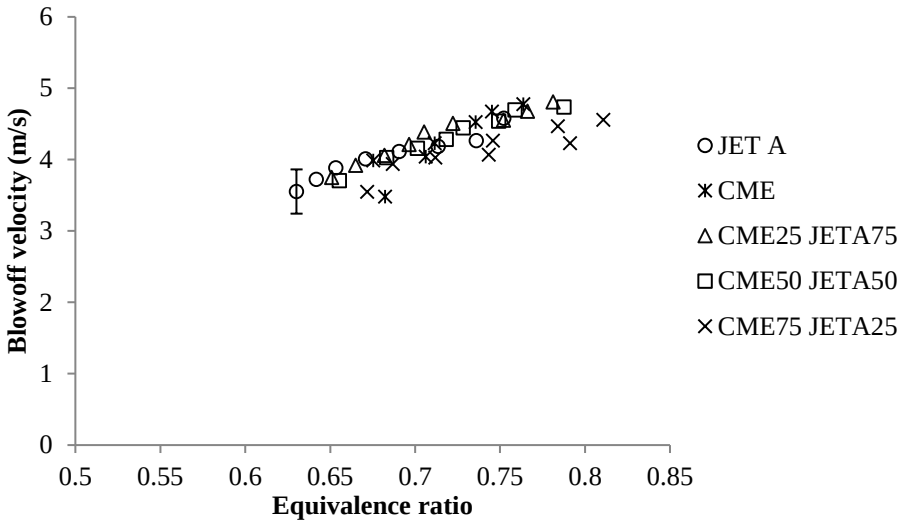


c) coflow velocity of 2.3 m/s

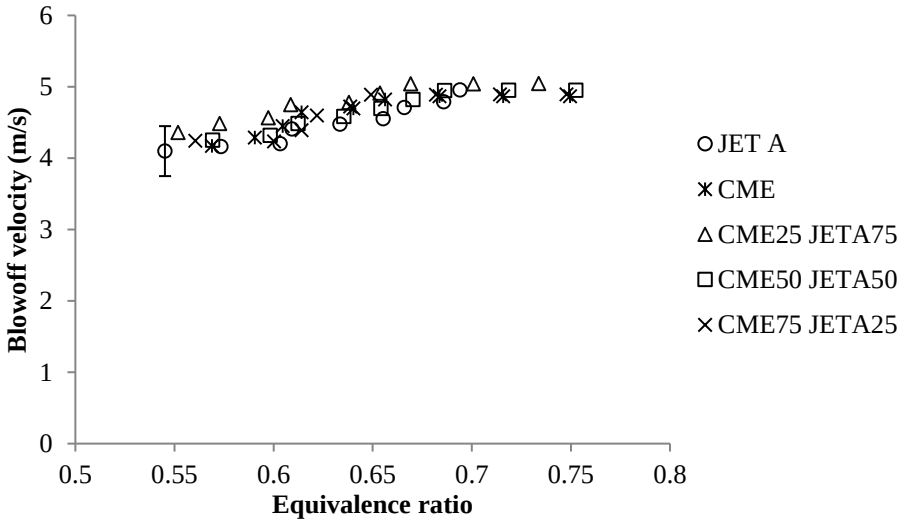


d) coflow velocity of 3.5 m/s

Figure 4.10: Change in blowoff velocity with equivalence ratio for flames of pure CME and Jet A and their blends at different coflow velocities

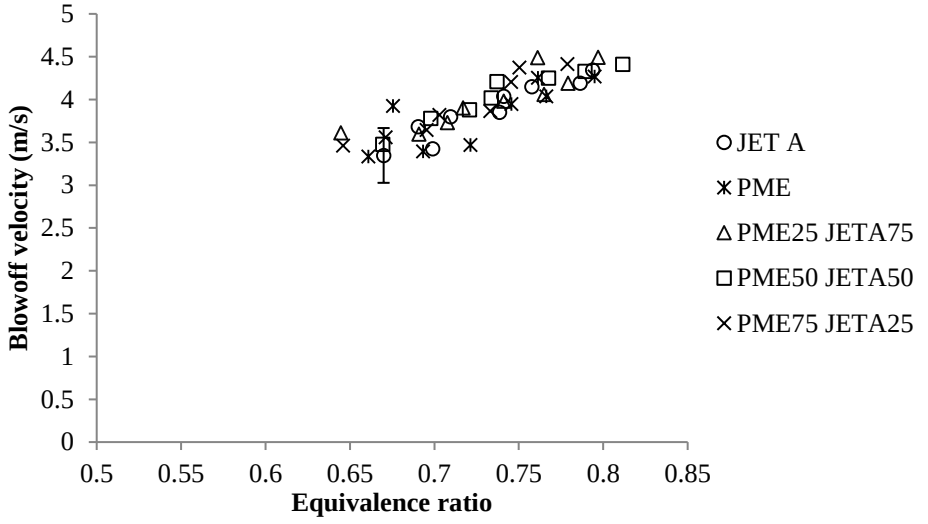


a) no coflow

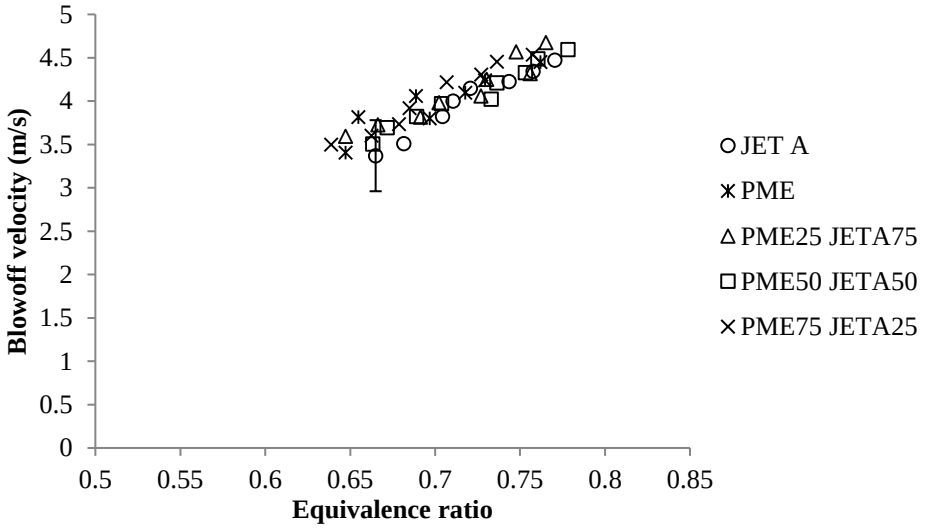


b) coflow velocity of 1.1 m/s

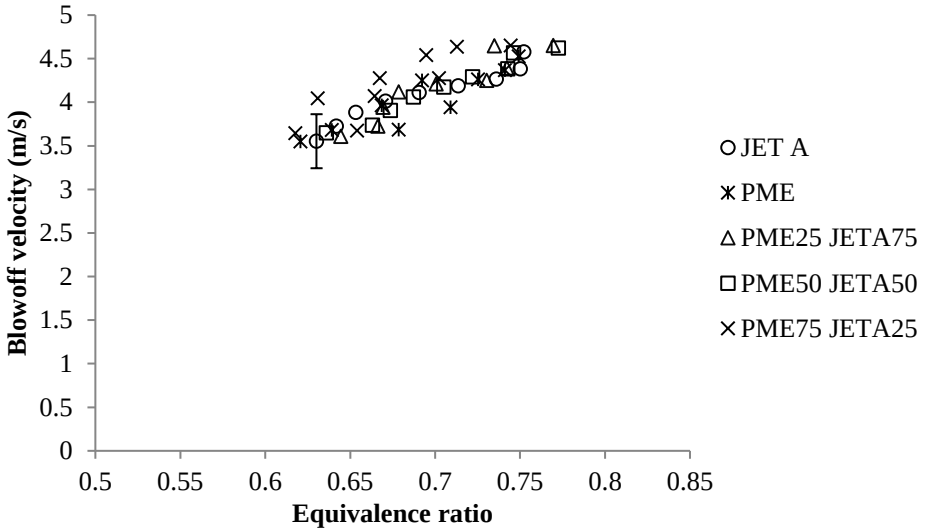


c) coflow velocity of 2.3 m/s

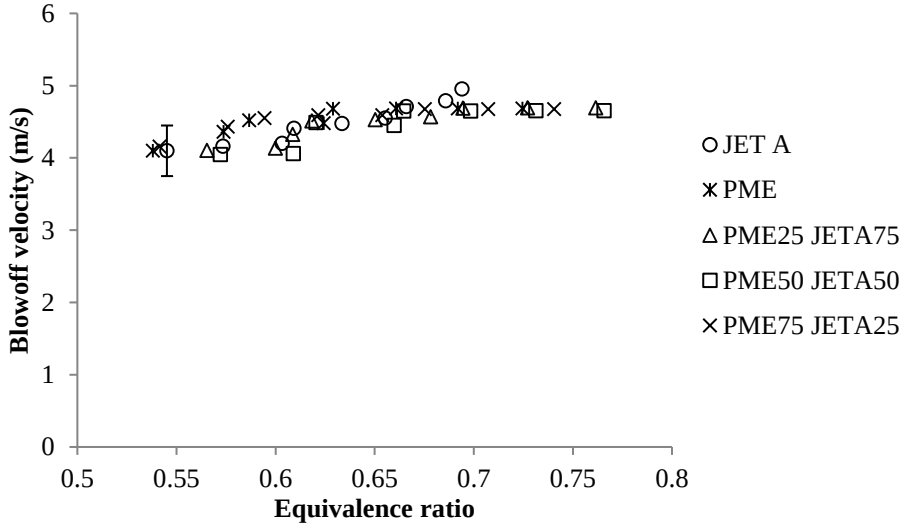


d) coflow velocity of 3.5 m/s

Figure 4.11 Change in blowoff velocity with equivalence ratio for flames of pure PME and Jet A and their blends at different coflow velocities

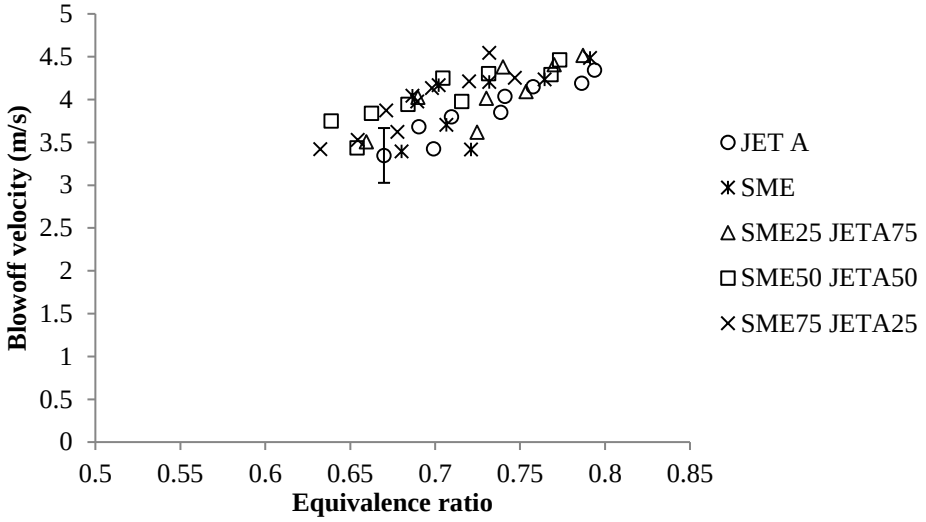


a) no coflow

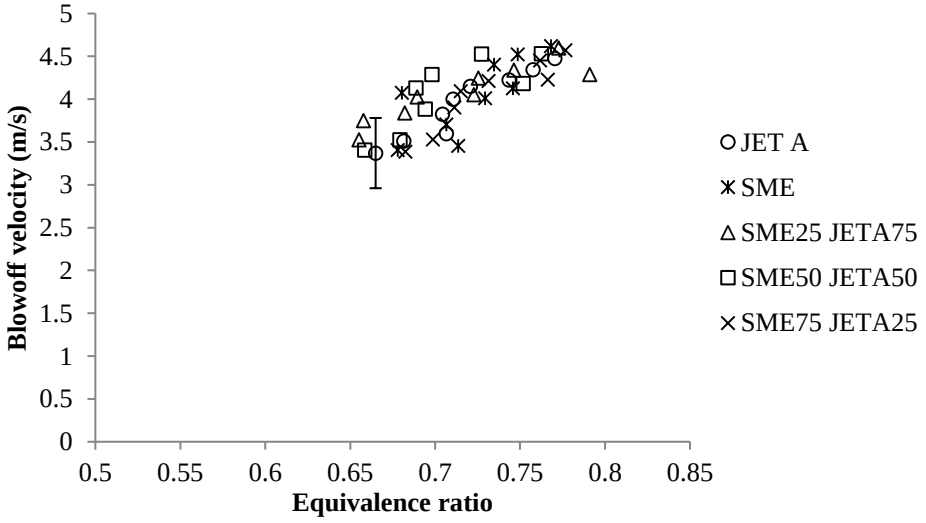


b) coflow velocity of 1.1 m/s

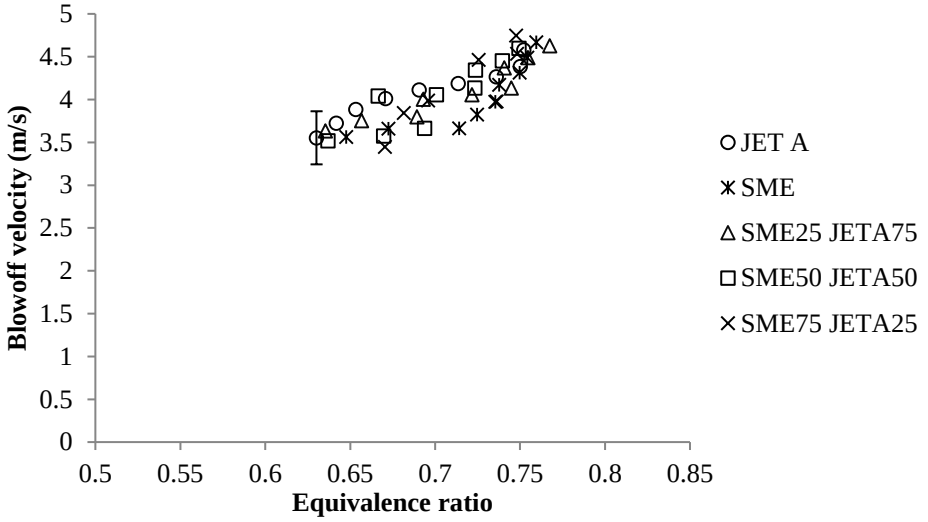


c) coflow velocity of 2.3 m/s

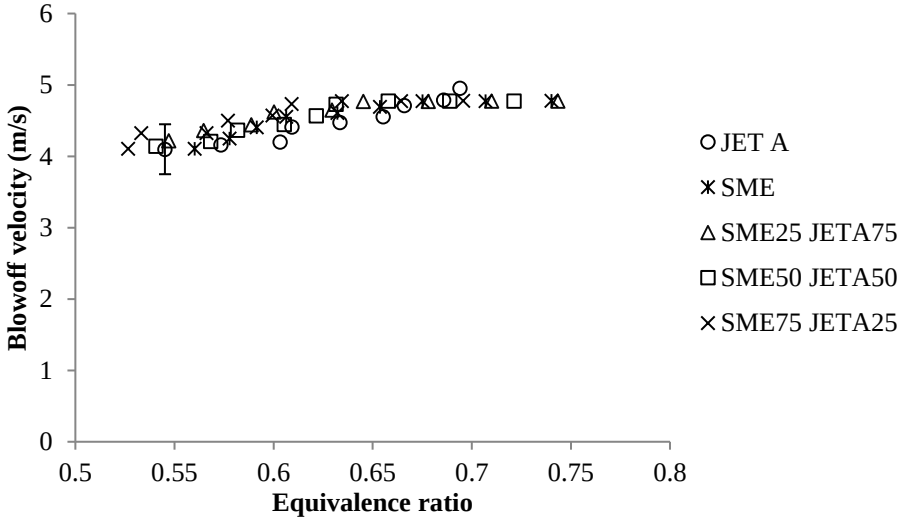


d) coflow velocity of 3.5 m/s

Figure 4.12: Change in blowoff velocity with equivalence ratio for flames of pure SME and Jet A and their blends at different coflow velocities

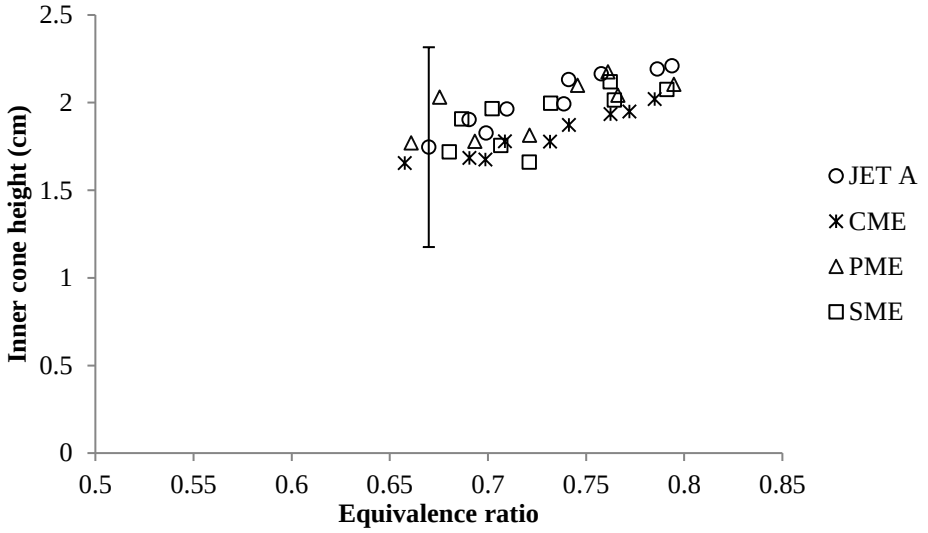


a) no coflow

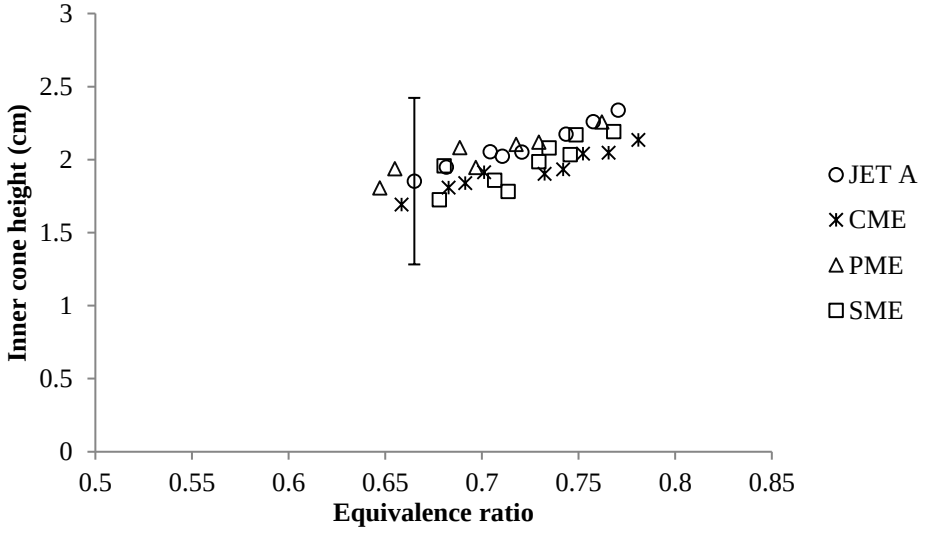


b) coflow velocity of 1.1 m/s

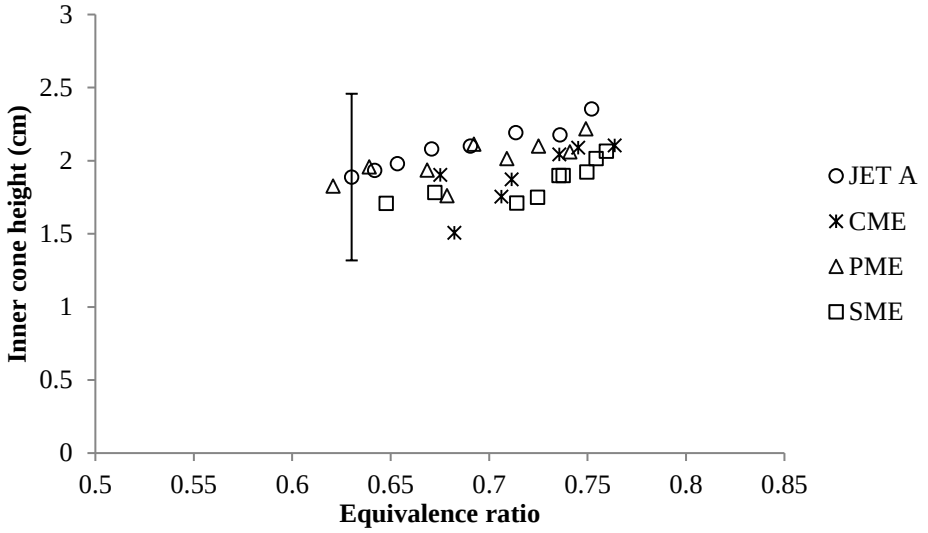


c) coflow velocity of 2.3 m/s

Figure 4.13: Change in inner cone height with equivalence ratio for flames of pure fuels at different coflow velocities

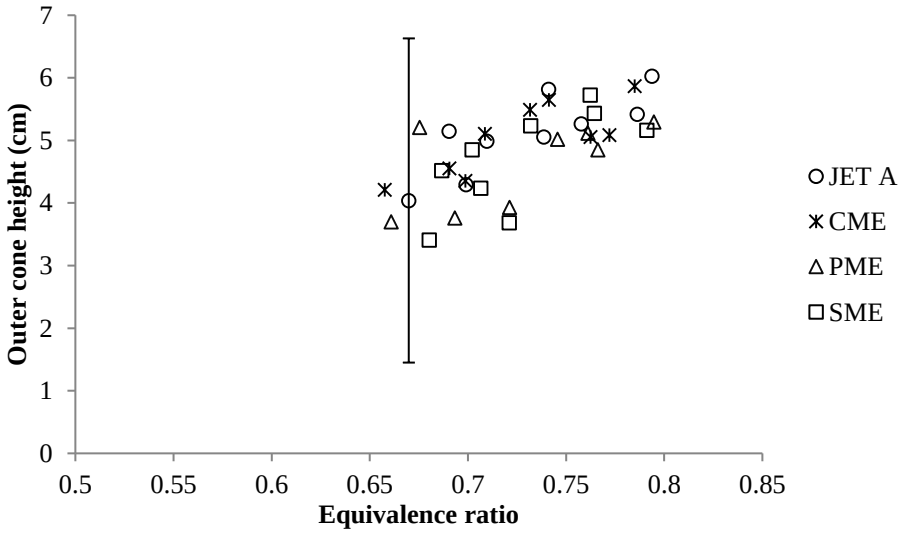


a) no coflow

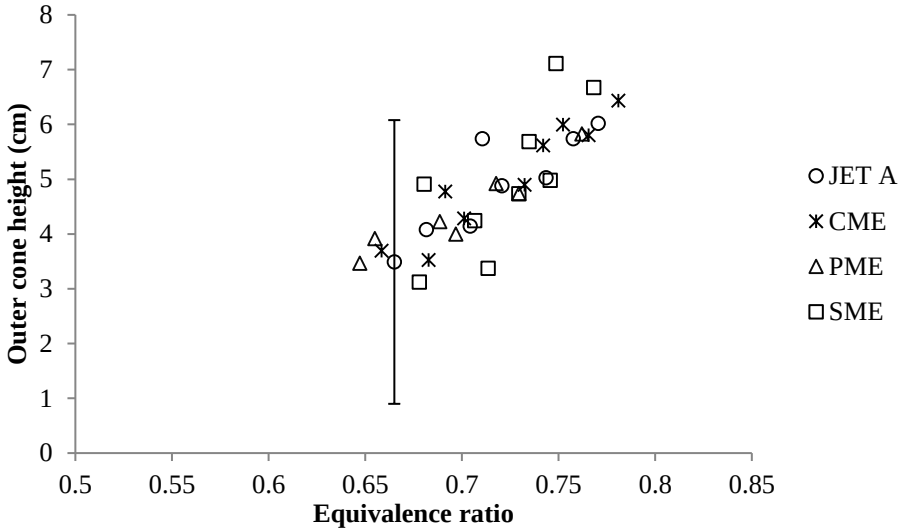


b) coflow velocity of 1.1 m/s

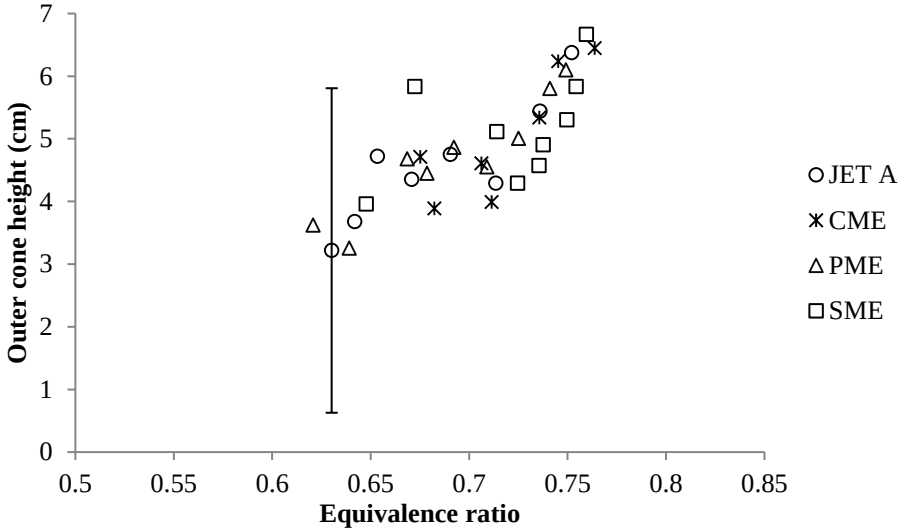


c) coflow velocity of 2.3 m/s

Figure 4.14: Change in outer cone height with equivalence ratio for flames of pure fuels at different coflow velocities

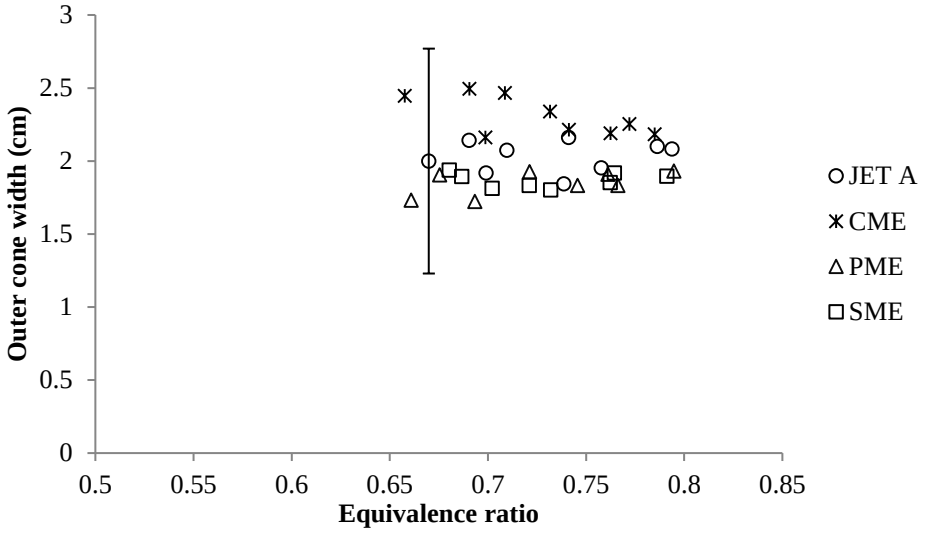


a) no coflow

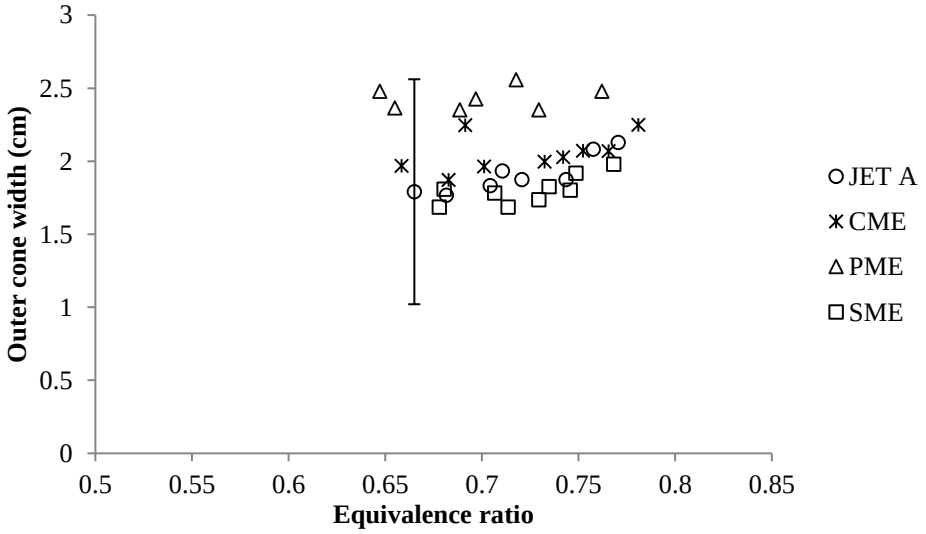


b) coflow velocity of 1.1 m/s

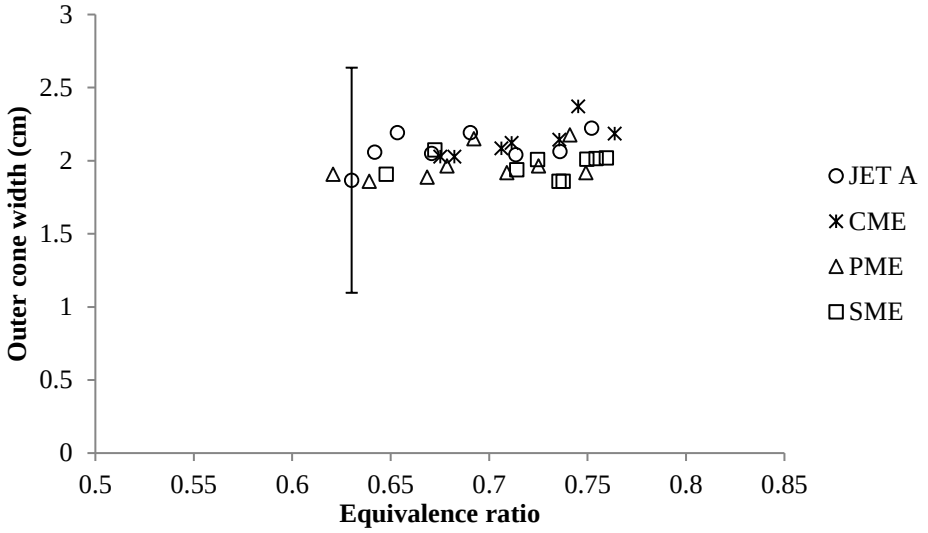


c) coflow velocity of 2.3 m/s

Figure 4.15: Change in outer cone width with equivalence ratio for flames of pure fuels at different coflow velocities

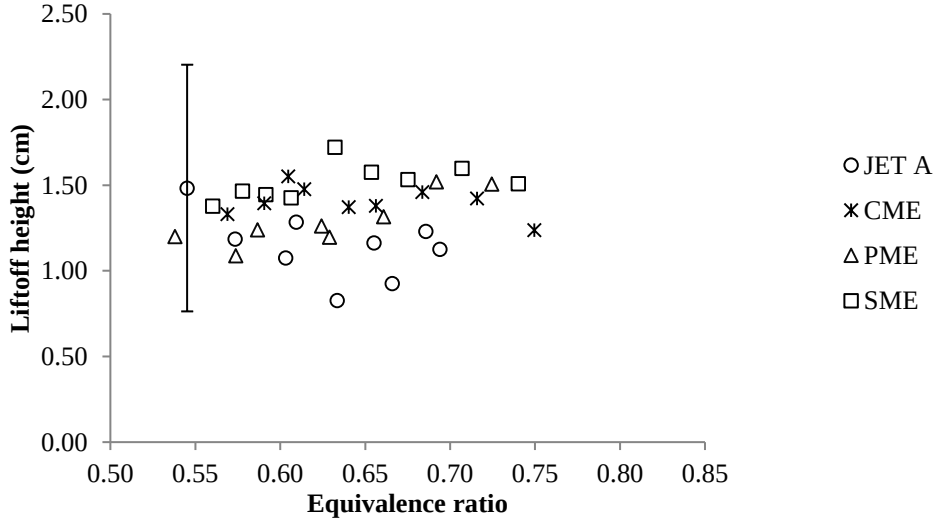


Figure 4.16: Change in liftoff height with equivalence ratio for flames of pure fuels

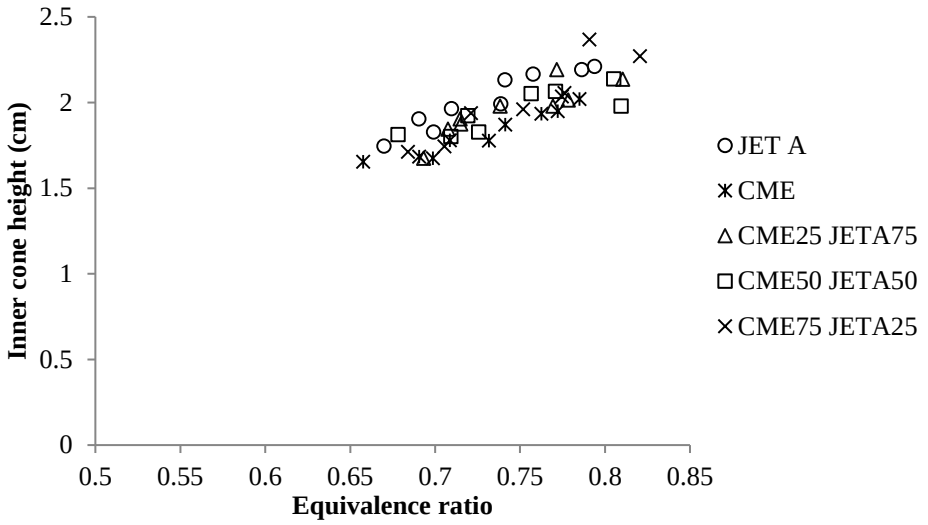


a) no coflow

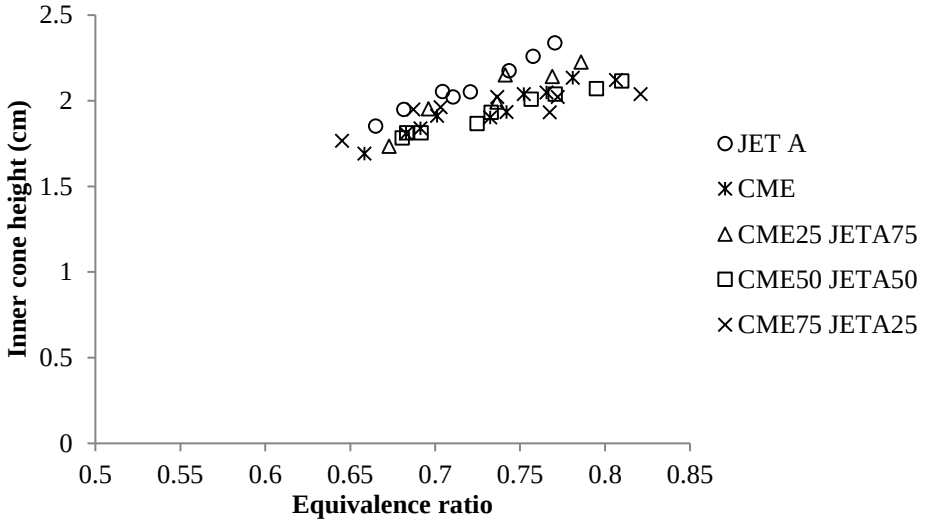


b) coflow velocity of 1.1 m/s

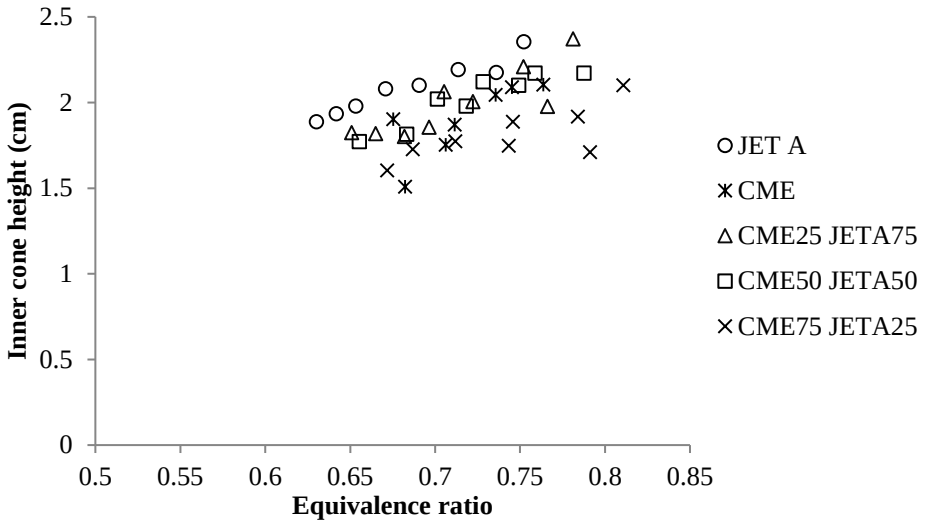


c) coflow velocity of 2.3 m/s

Figure 4.17: Change in inner cone height with equivalence ratio for flames of CME blends at different coflow velocities

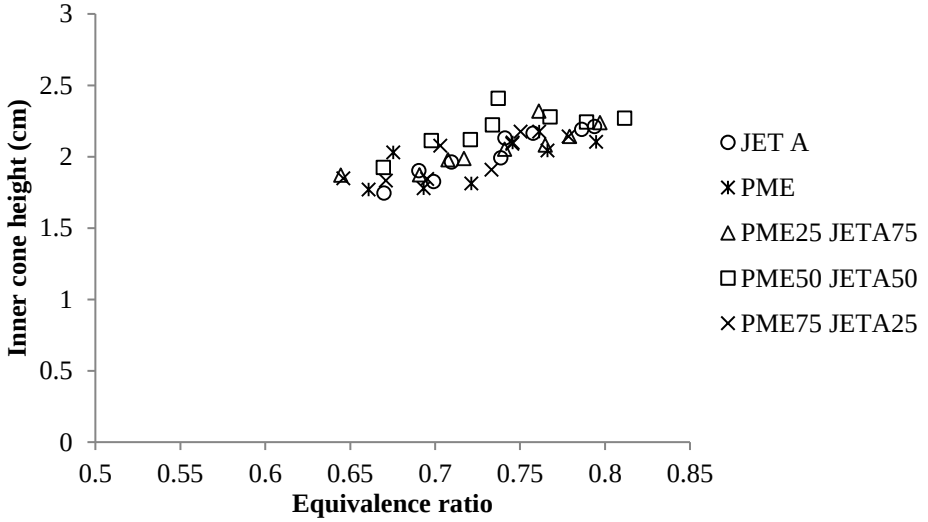


a) no coflow

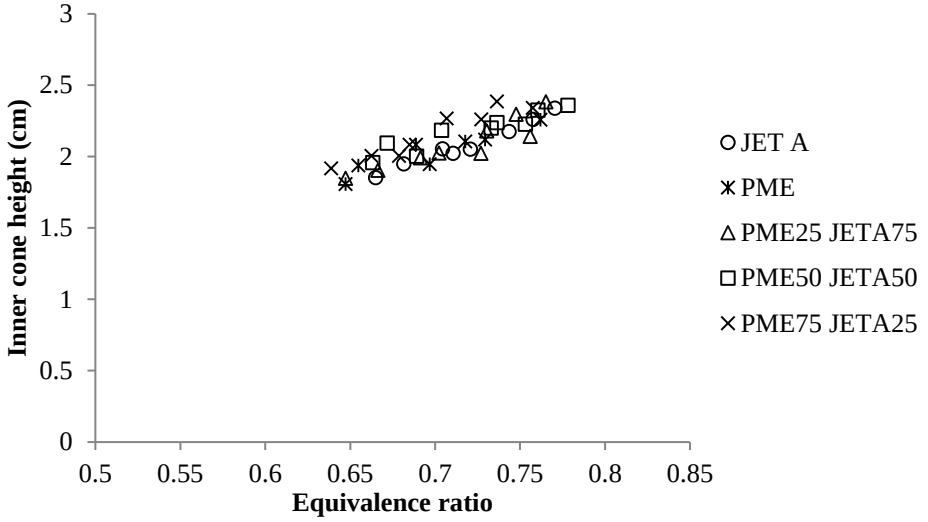


b) coflow velocity of 1.1 m/s

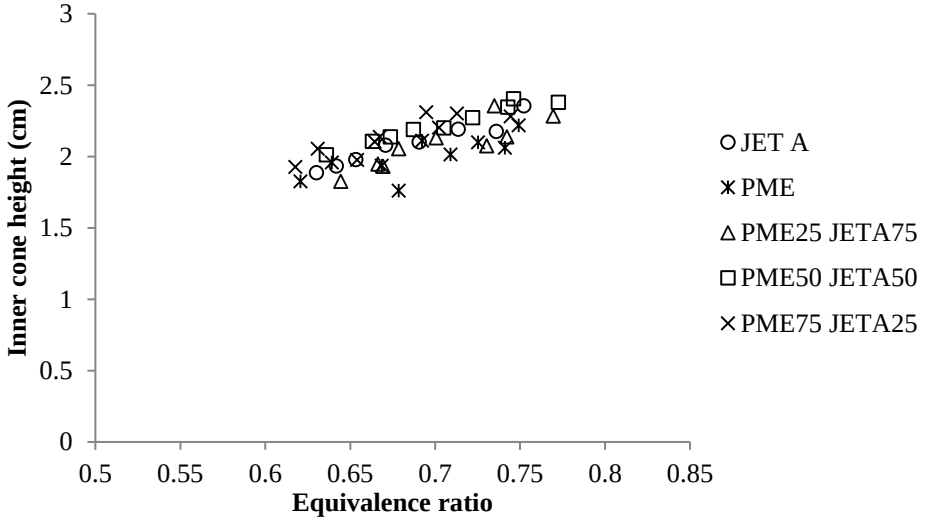


c) coflow velocity of 2.3 m/s

Figure 4.18: Change in inner cone height with equivalence ratio for flames of PME blends at different coflow velocities

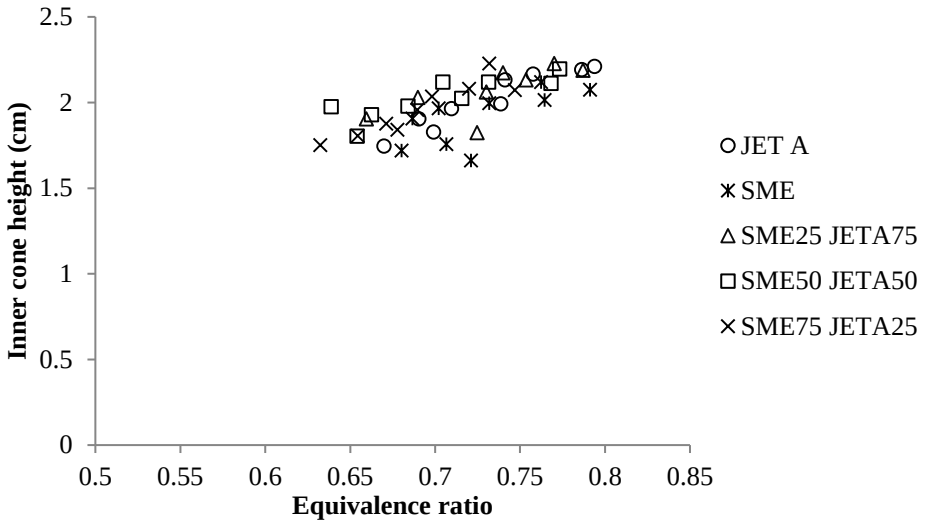


a) no coflow

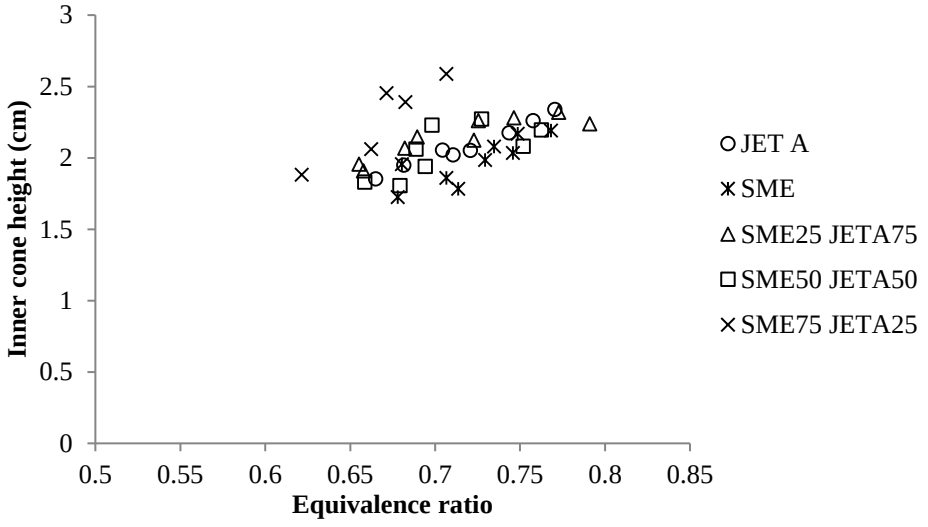


b) coflow velocity of 1.1 m/s

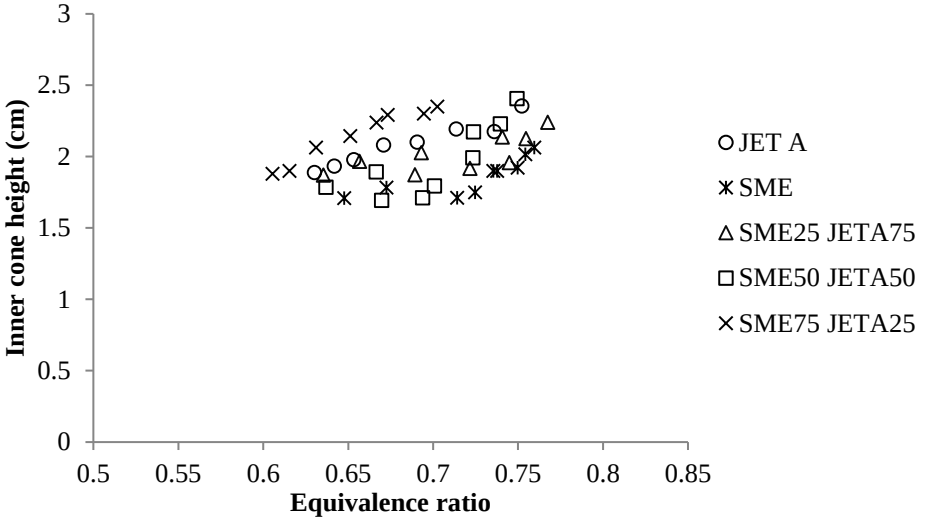


c) coflow velocity of 2.3 m/s

Figure 4.19: Change in inner cone height with equivalence ratio for flames of SME blends at different coflow velocities

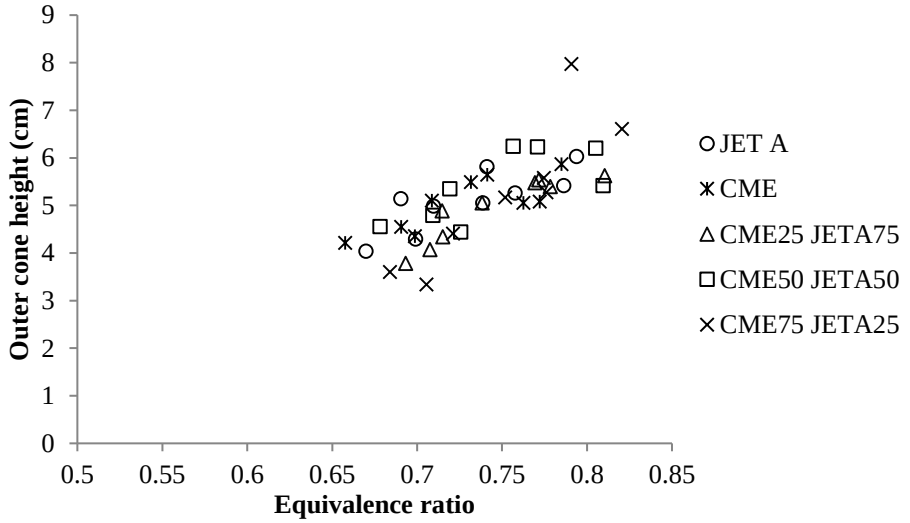


a) no coflow

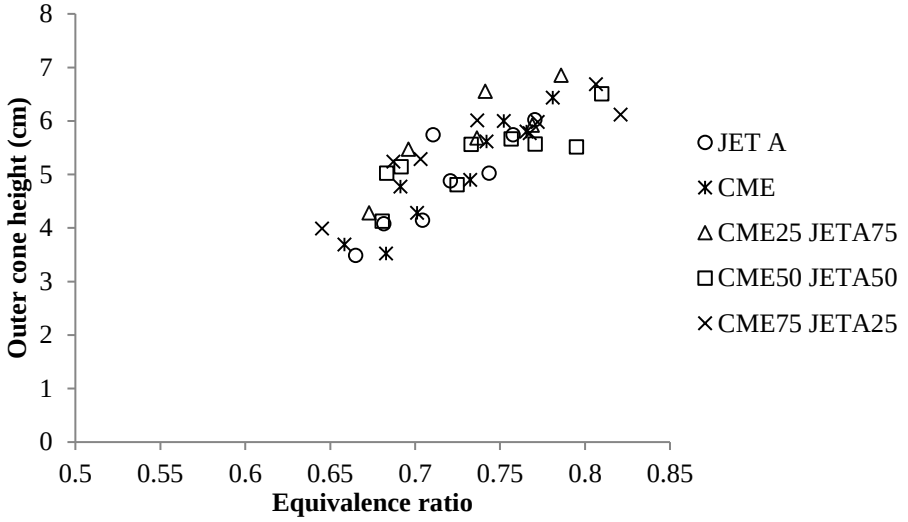


b) coflow velocity of 1.1 m/s

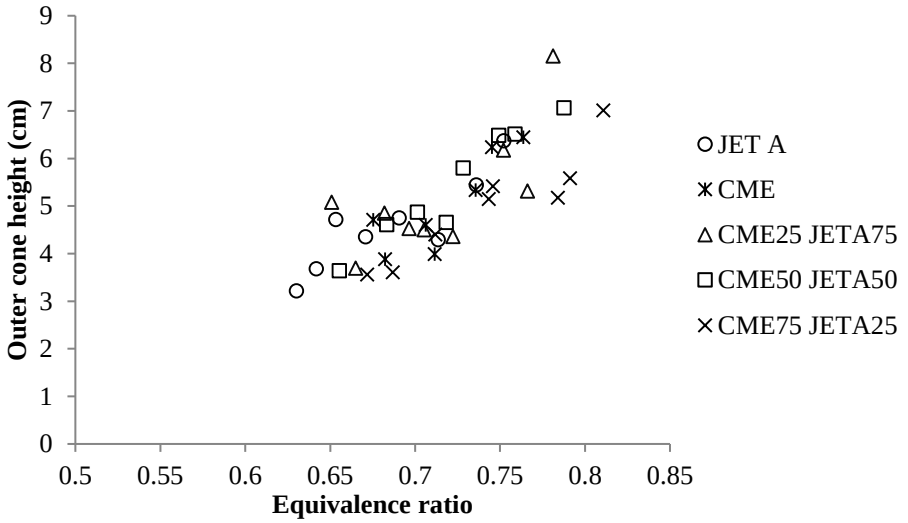


c) coflow velocity of 2.3 m/s

Figure 4.20: Change in outer cone height with equivalence ratio for flames of CME blends at different coflow velocities

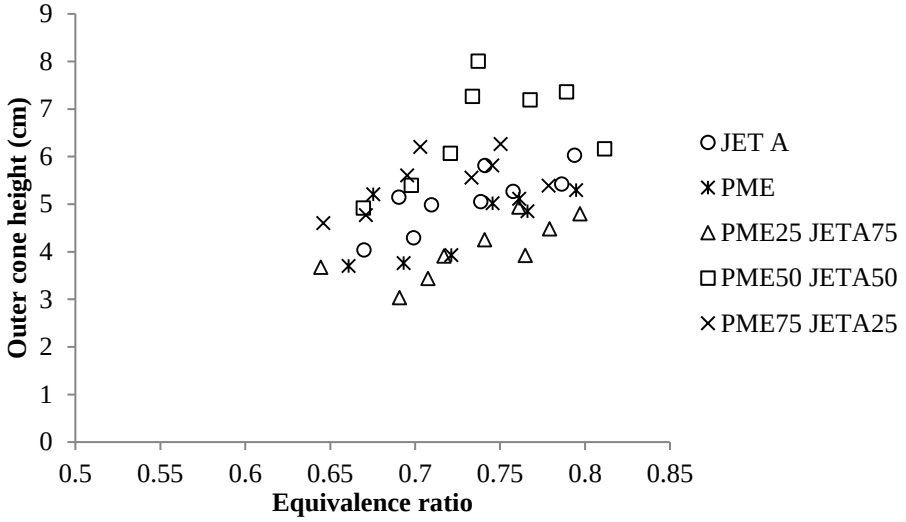


a) no coflow

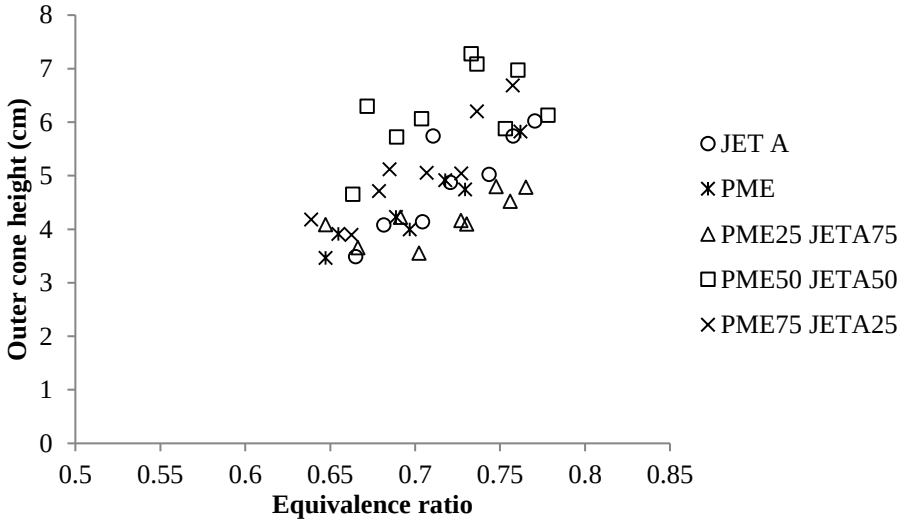


b) coflow velocity of 1.1 m/s

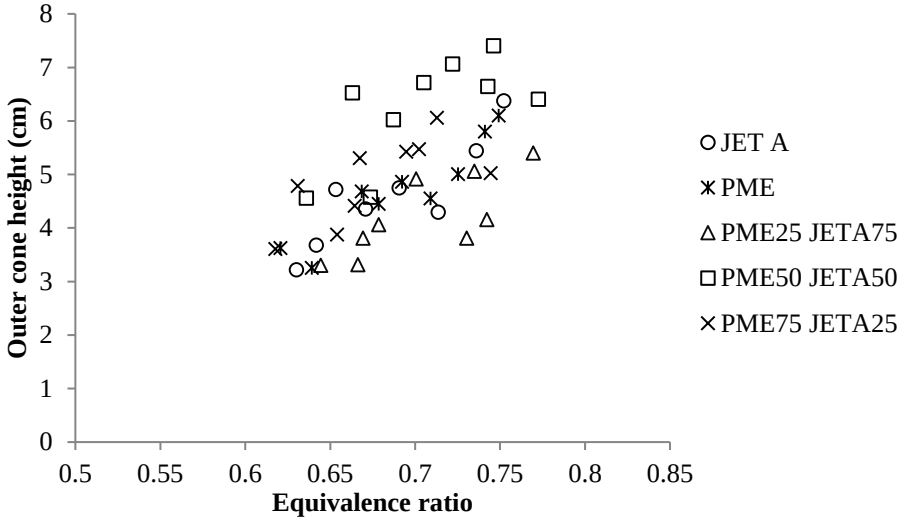


c) coflow velocity of 2.3 m/s

Figure 4.21: Change in outer cone height with equivalence ratio for flames of PME blends at different coflow velocities

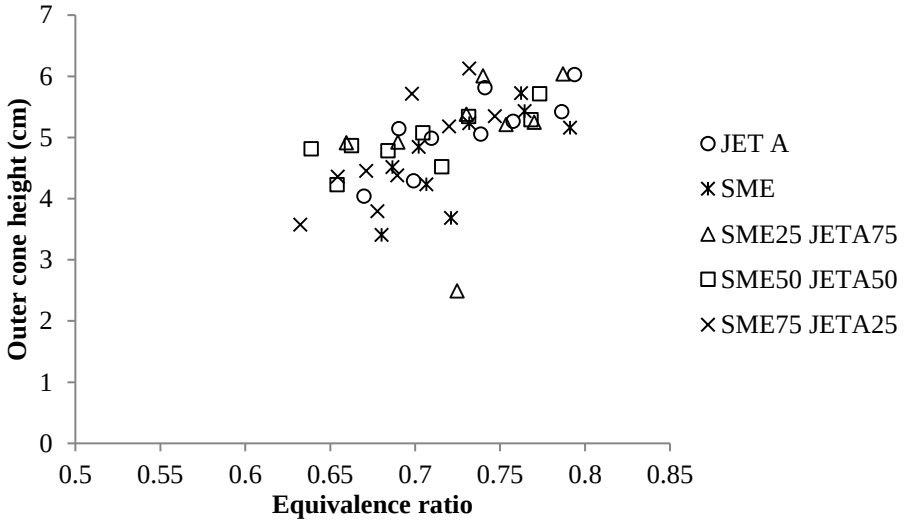


a) no coflow

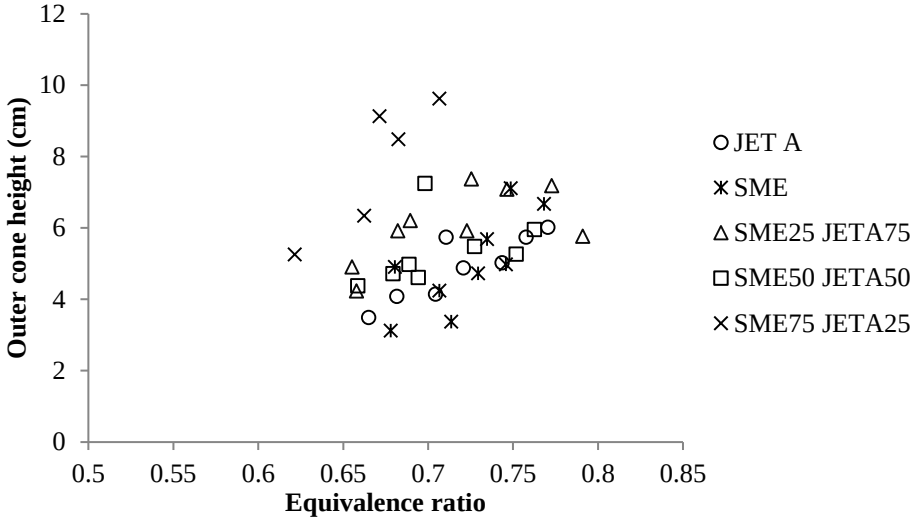


b) coflow velocity of 1.1 m/s

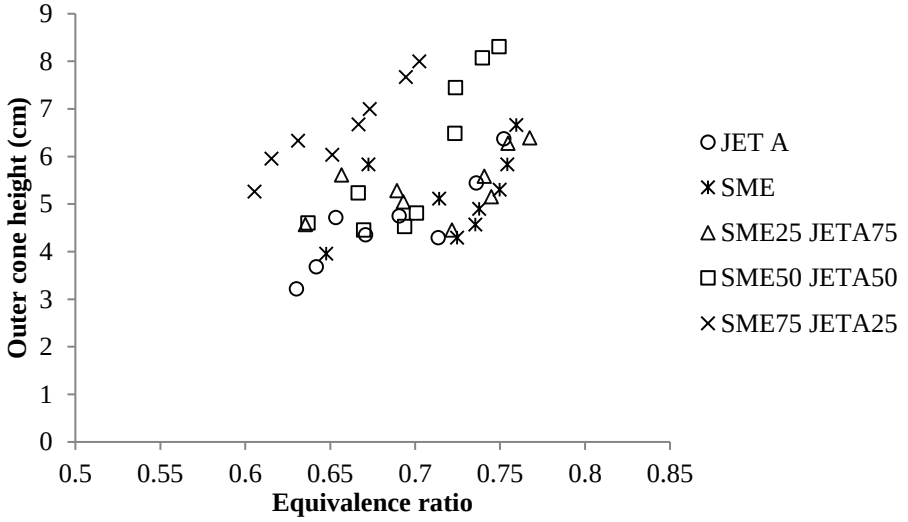


c) coflow velocity of 2.3 m/s

Figure 4.22: Change in outer cone height with equivalence ratio for flames of SME blends at different coflow velocities

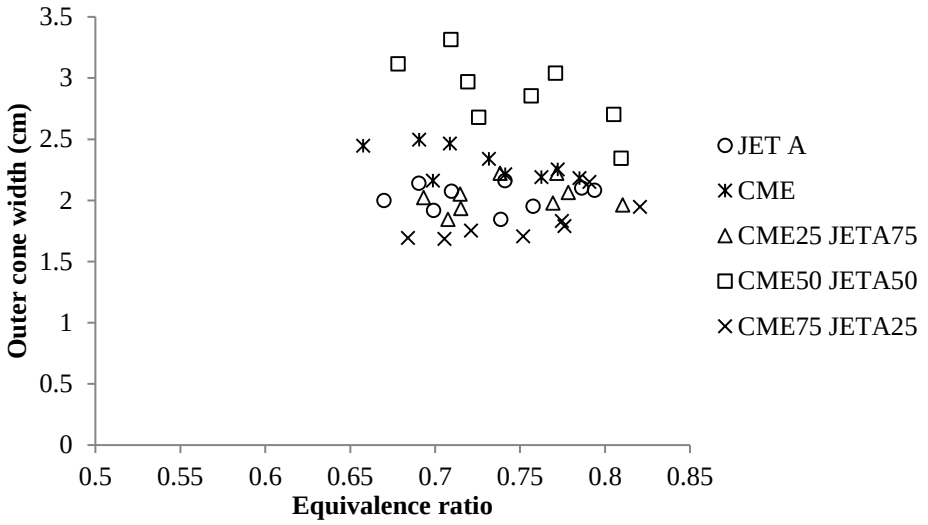


a) no coflow

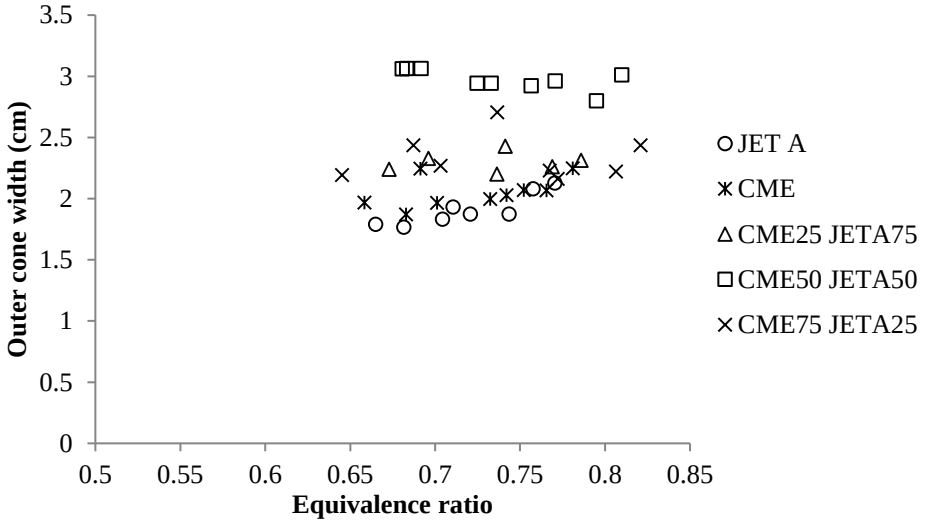


b) coflow velocity of 1.1 m/s

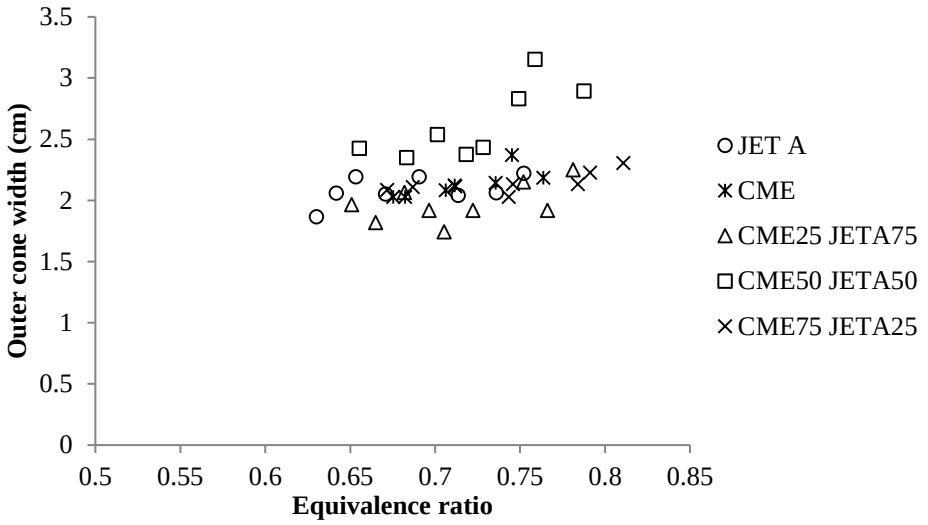


c) coflow velocity of 2.3 m/s

Figure 4.23: Change in outer cone width with equivalence ratio for flames of CME blends at different coflow velocities

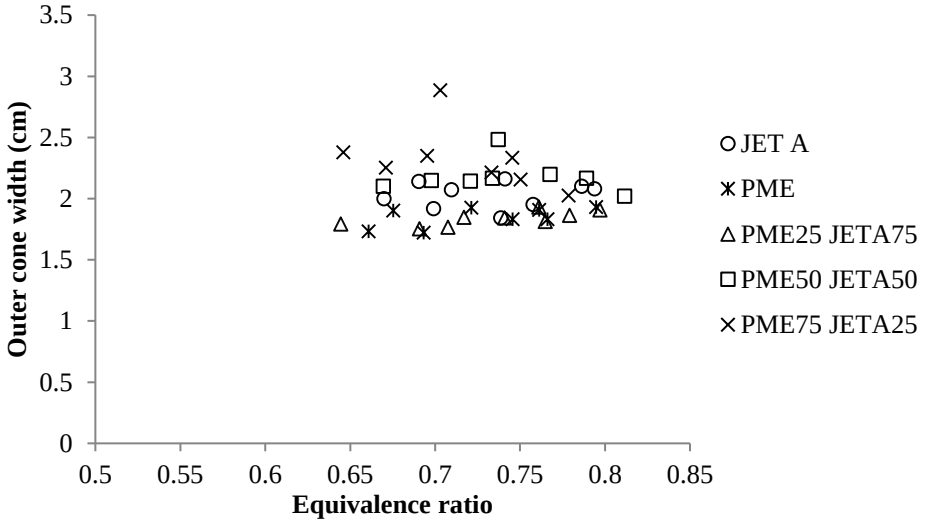


a) no coflow

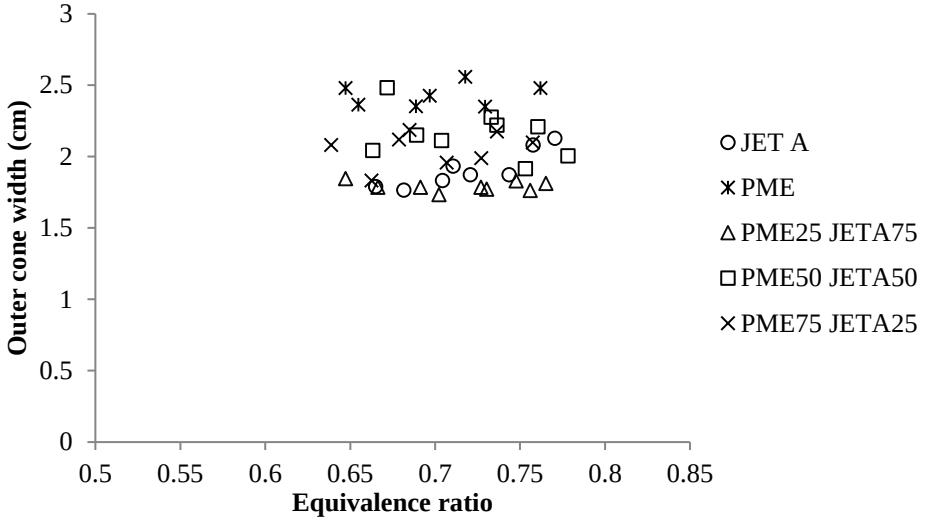


b) coflow velocity of 1.1 m/s

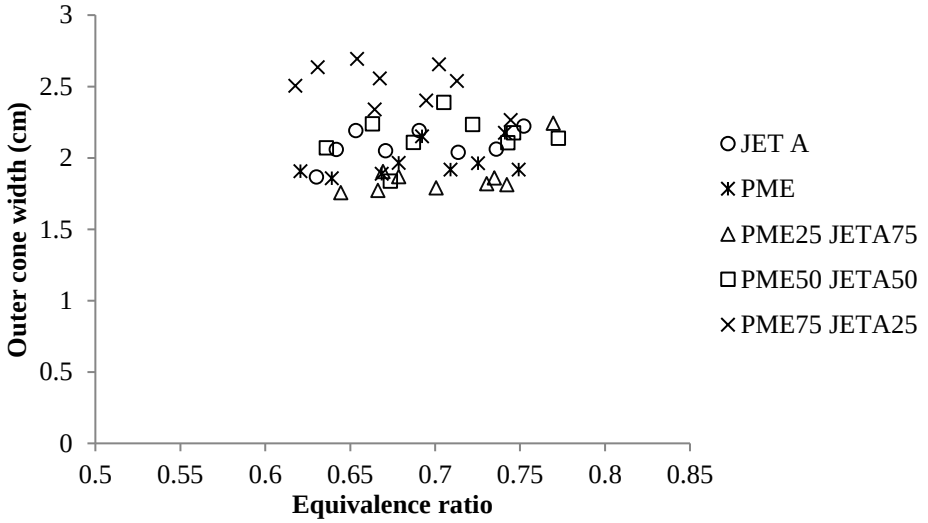


c) coflow velocity of 2.3 m/s

Figure 4.24: Change in outer cone width with equivalence ratio for flames of PME blends at different coflow velocities

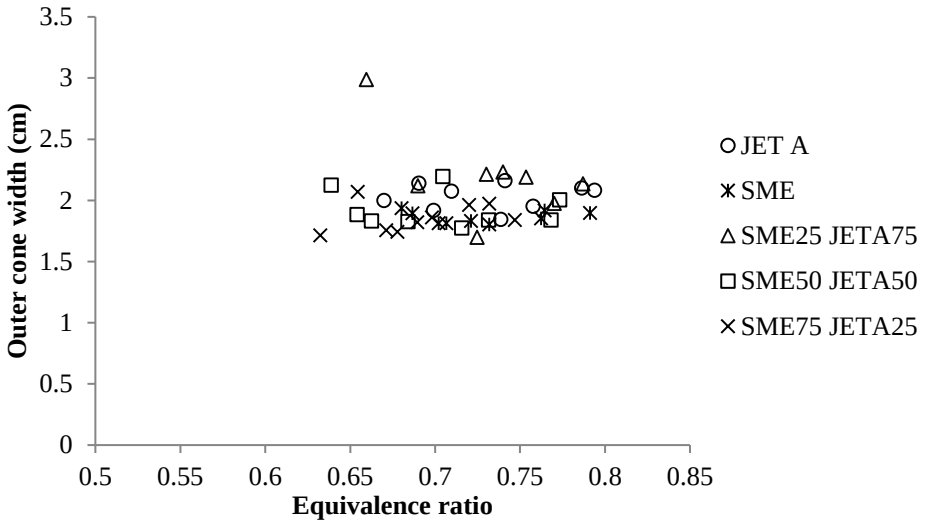


a) no coflow

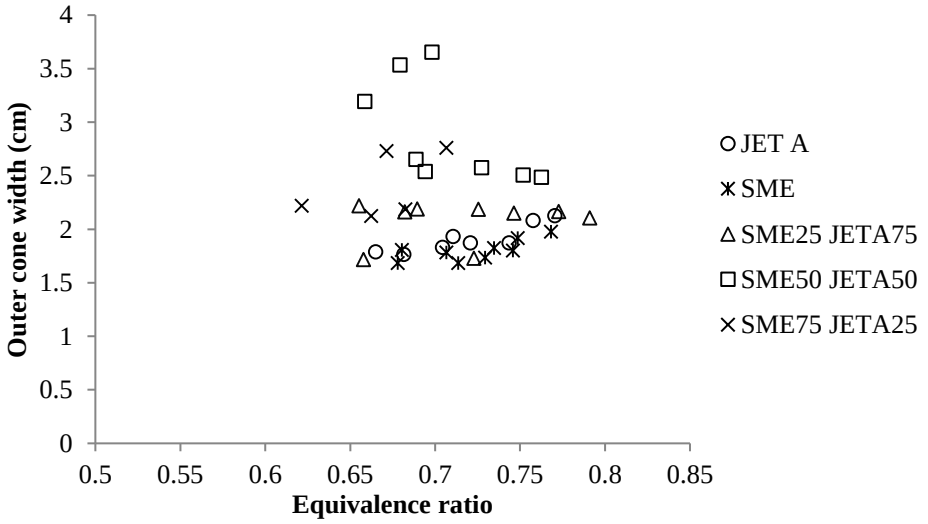


b) coflow velocity of 1.1 m/s

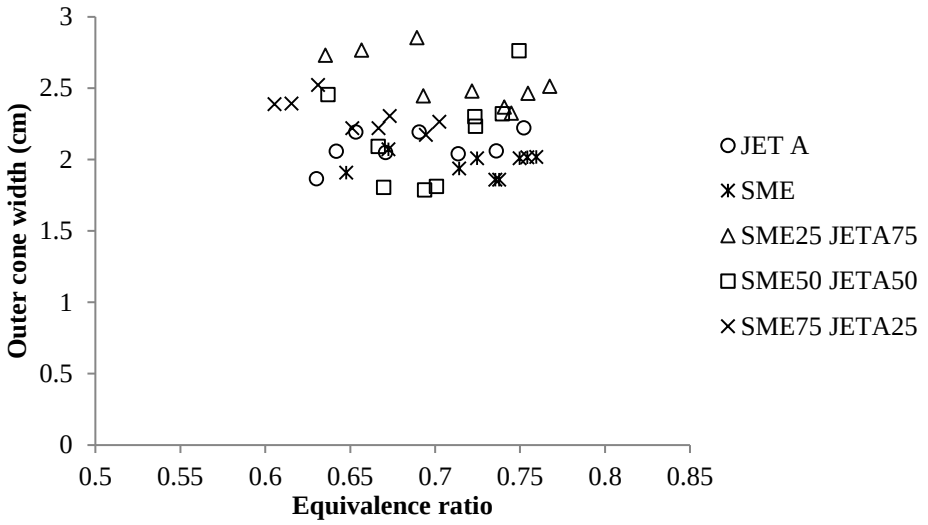


c) coflow velocity of 2.3 m/s

Figure 4.25: Change in outer cone width with equivalence ratio for flames of SME blends at different coflow velocities

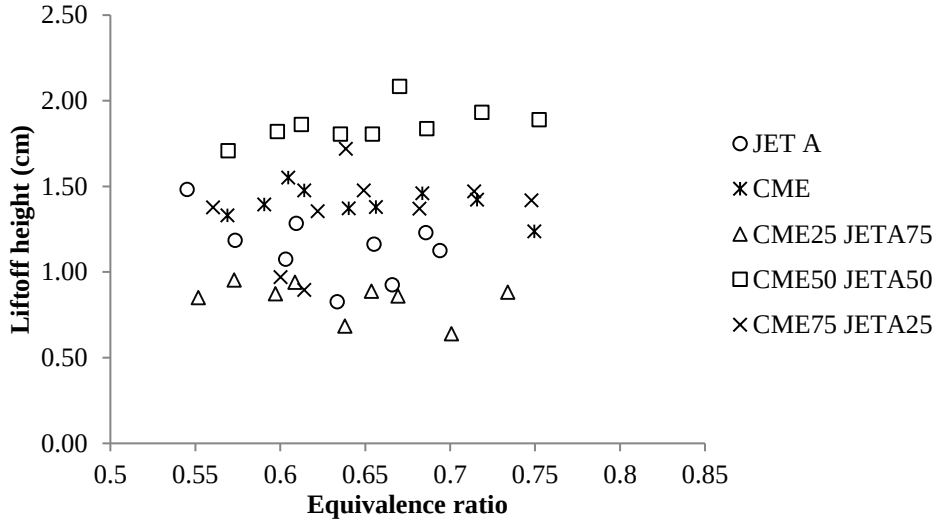


a) CME blends

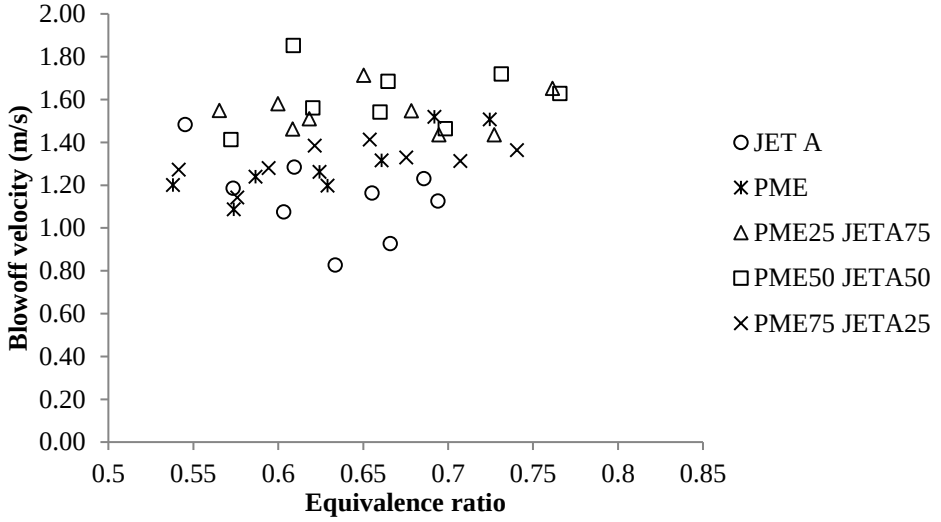


b) PME blends

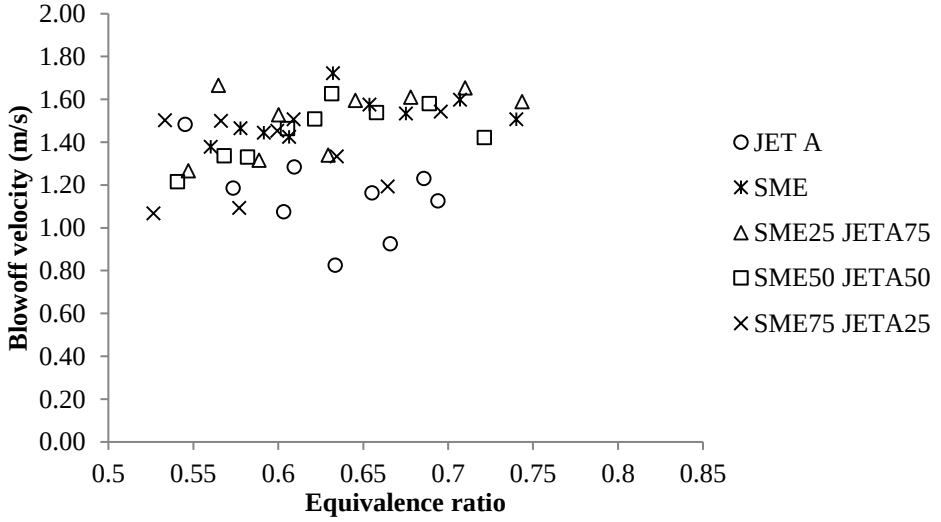


c) SME blends

Figure 4.26: Change in liftoff height with equivalence ratio for flames of blends

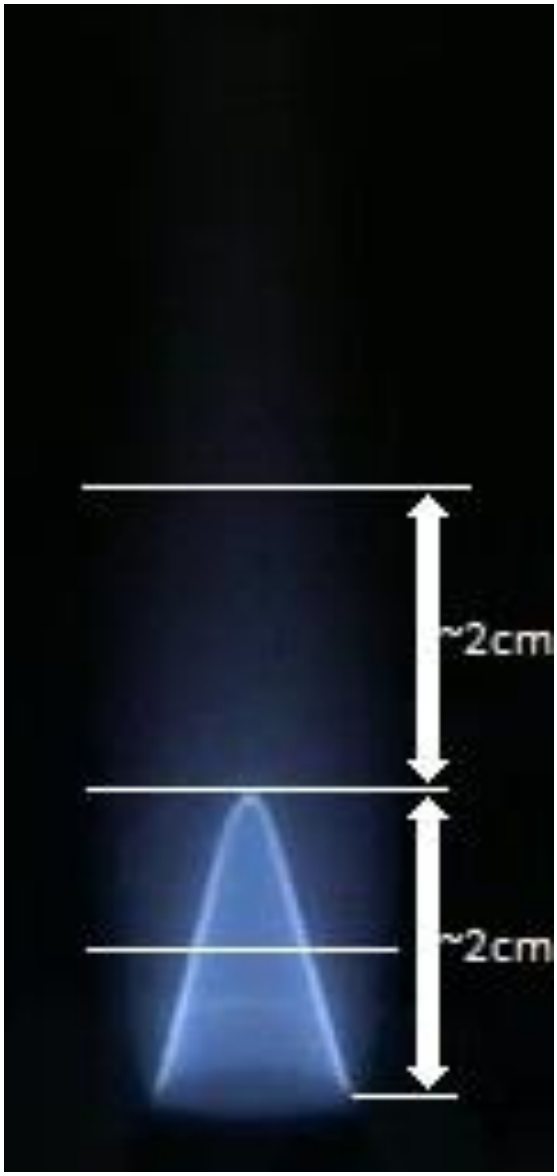


Figure 4.27: Example of heights at which the temperature profiles were measured (Jet A flame)

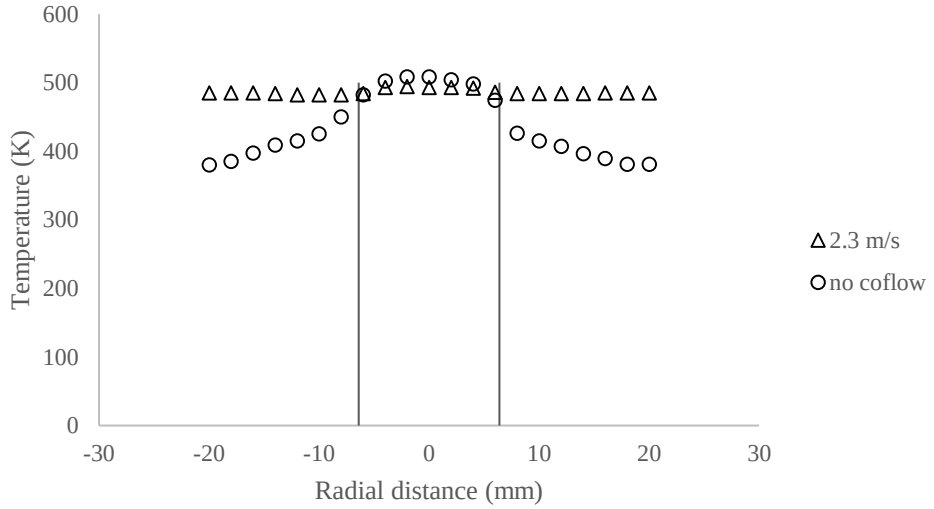


Figure 4.28: Temperature profile across the burner in absence of flame measured at 3 mm above the burner for two different conditions: without coflow and at coflow velocity of 2.3 m/s; temperature was set to 493 K and primary airflow velocity of 4.3 m/s

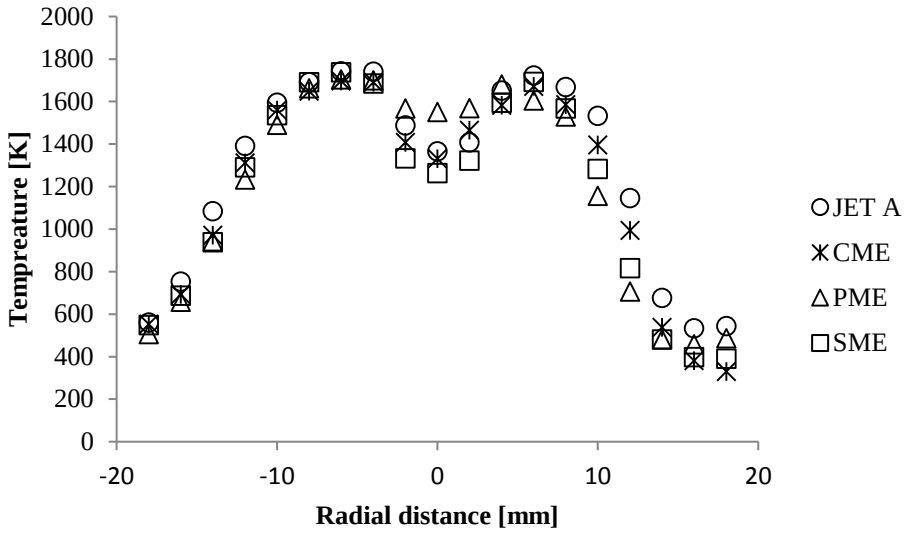


a) at half inner cone height

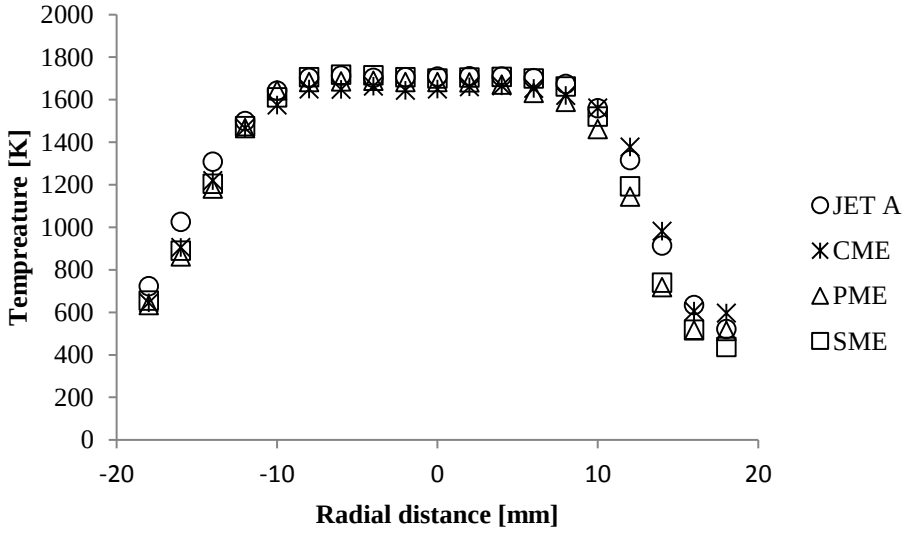


b) at tip of inner cone

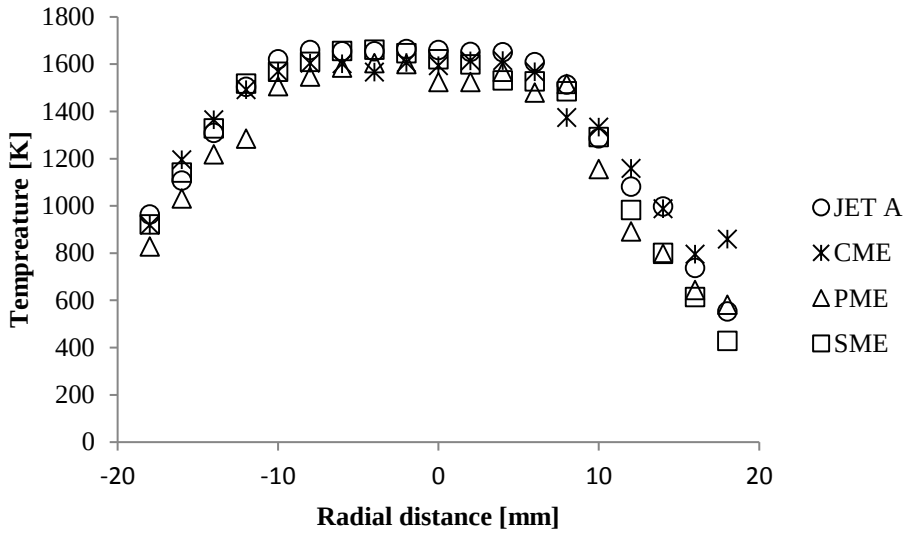


c) at twice the inner cone height

Figure 4.29: Inflame temperature profiles of pure fuels at no coflow, Re ~ 2,500, Φ ~ 0.9

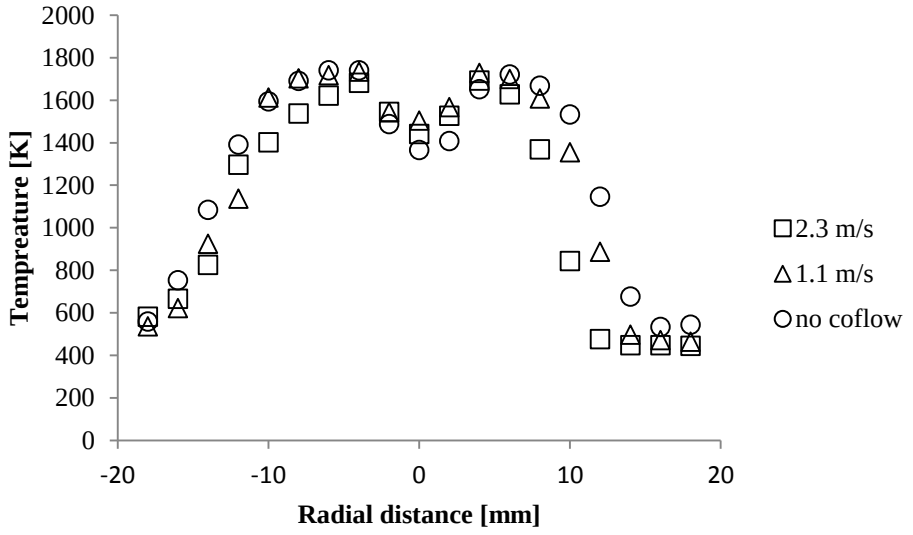


a) at half inner cone height

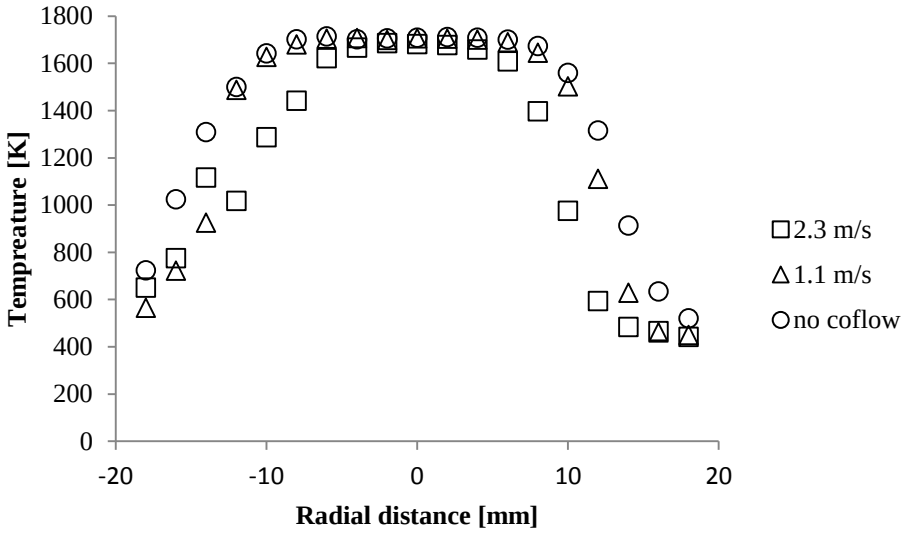


b) at tip of inner cone

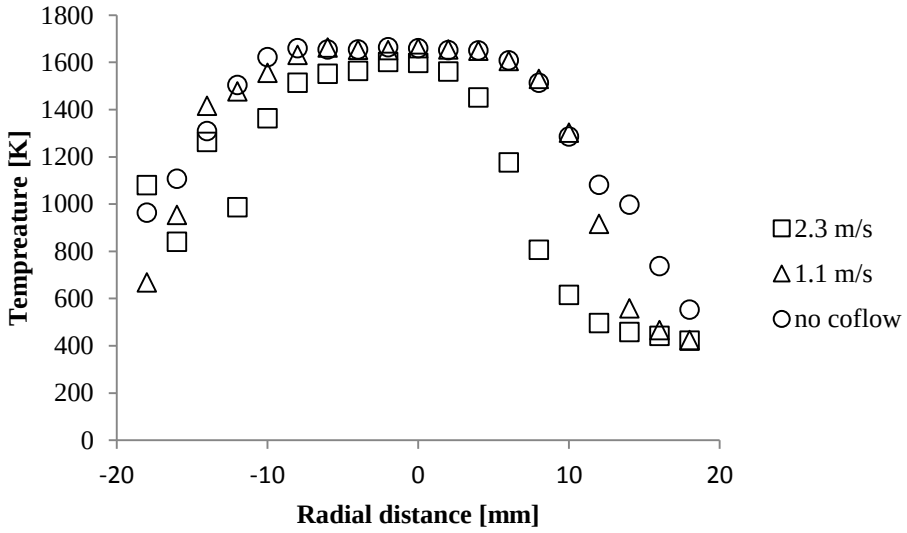


c) at twice the inner cone height

Figure 4.30: Jet A inflame temperature profiles at different coflow rates, Re ~ 2,500, $\Phi \sim 0.9$

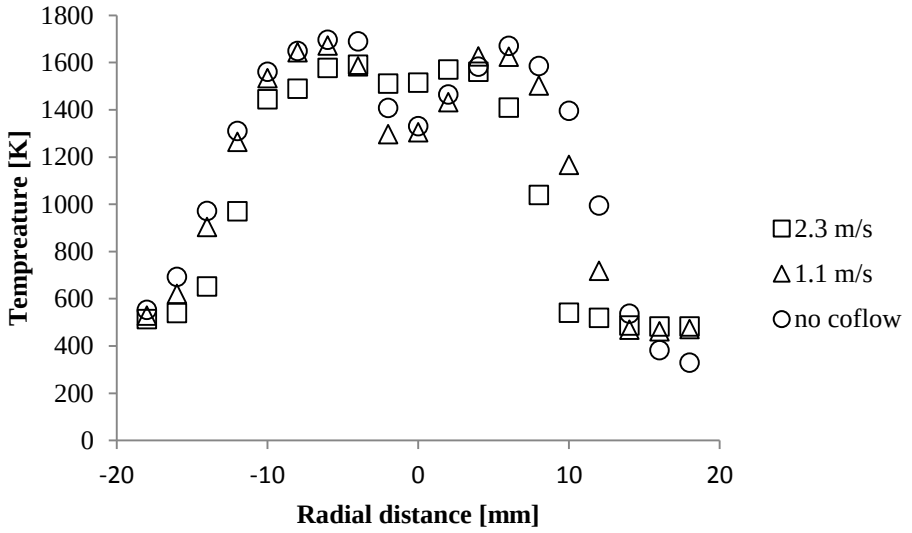


a) at half inner cone height

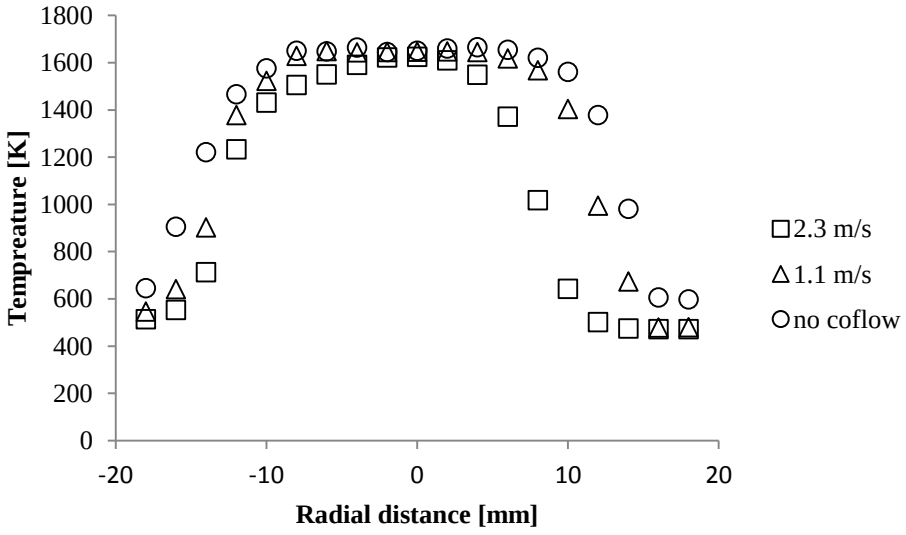


b) at tip of inner cone

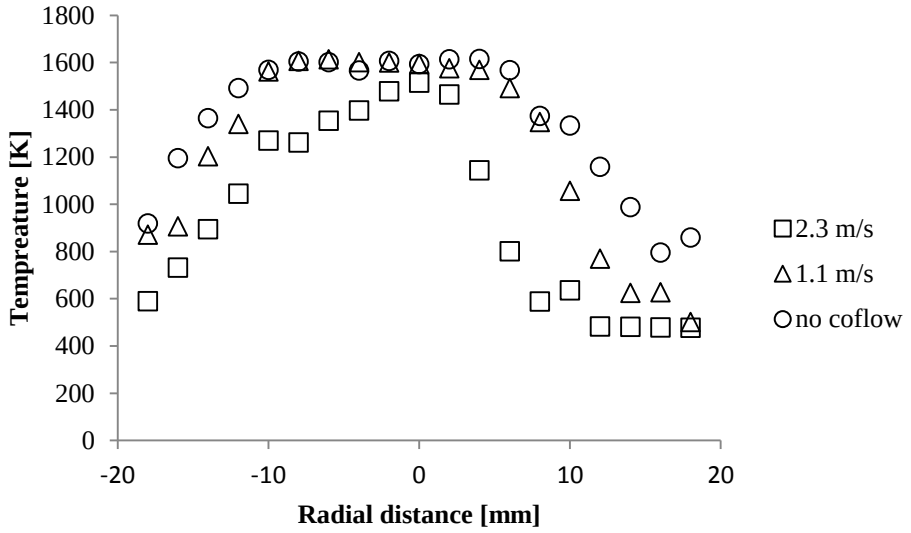


c) at twice the inner cone height

Figure 4.31: CME inflame temperature profiles at different coflow rates, Re ~ 2,500, Φ ~ 0.9

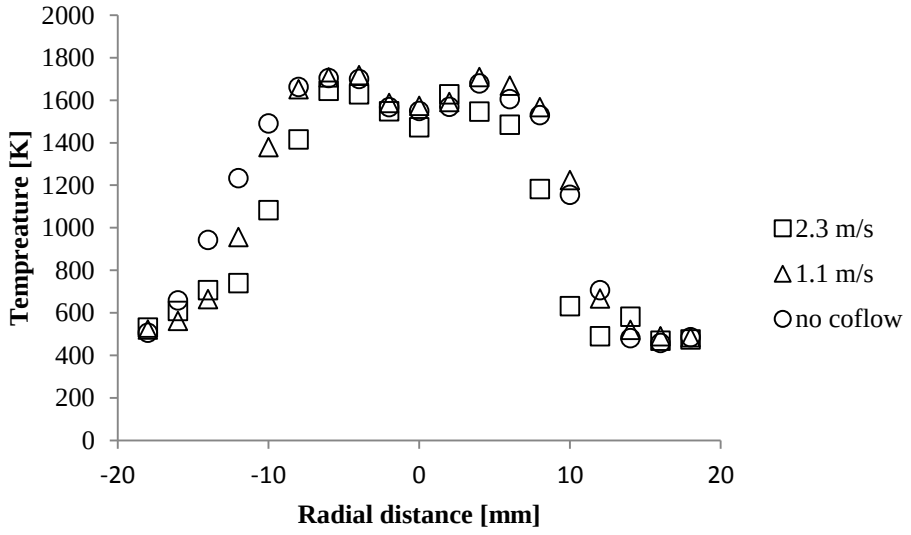


a) at half inner cone height

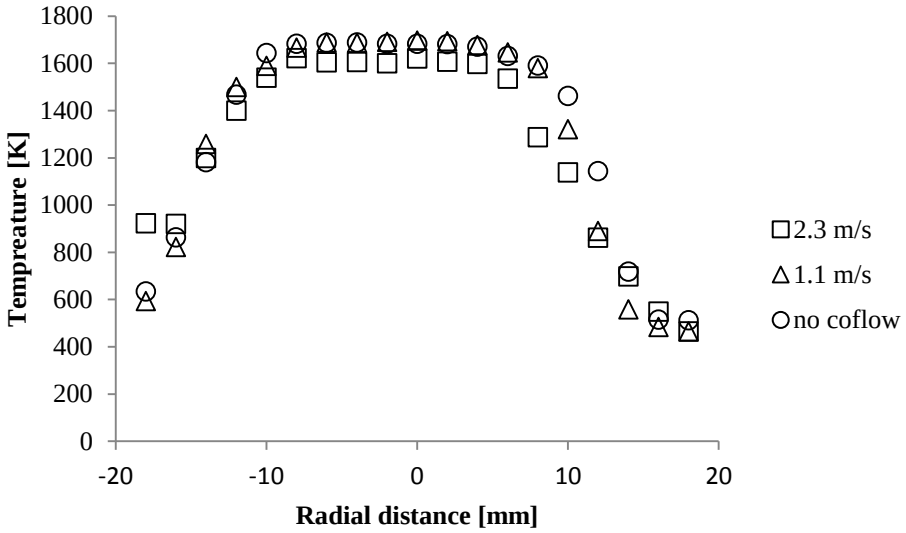


b) at tip of inner cone

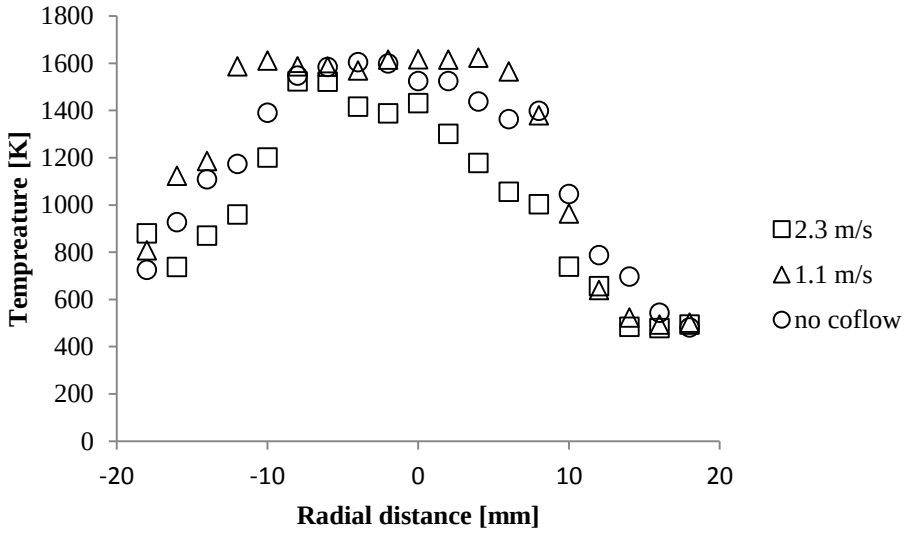


c) at twice the inner cone height

Figure 4.32: PME inflame temperature profiles at different coflow rates, Re ~ 2,500, $\Phi \sim 0.9$

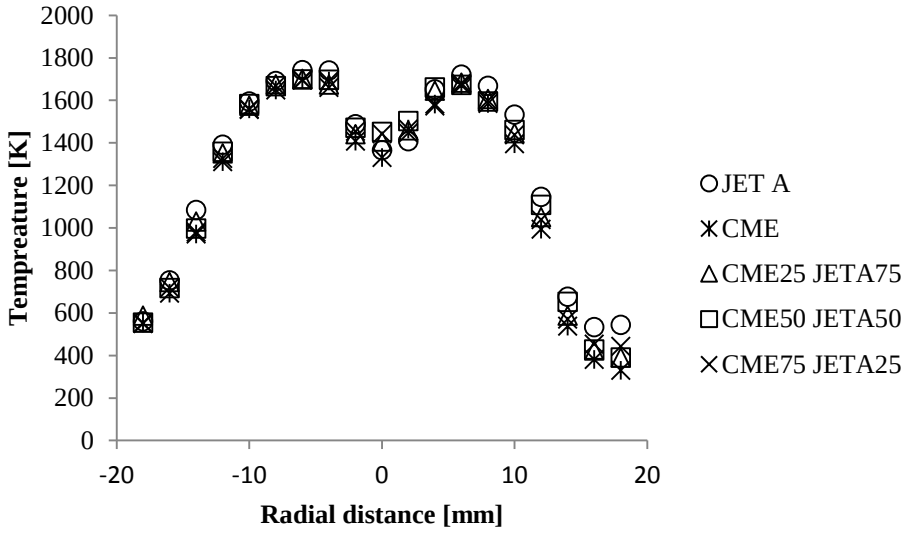


a) at half inner cone height

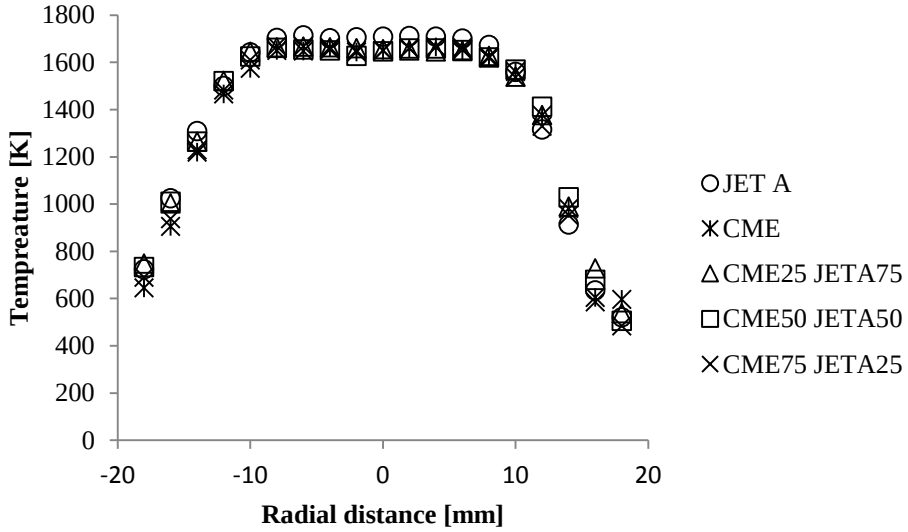


b) at tip of inner cone

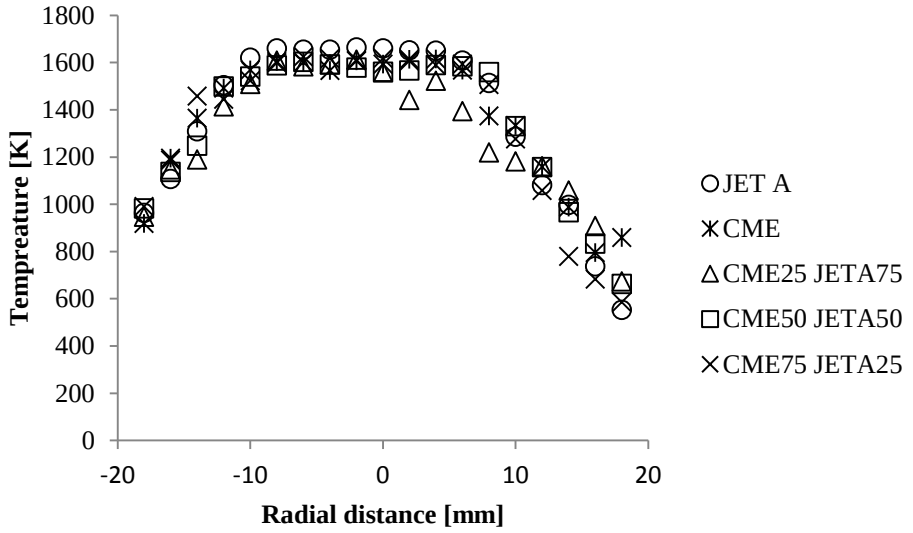


c) at twice the inner cone height

Figure 4.33: CME blends inflame temperature profiles at no coflow, Re ~ 2,500, Φ ~ 0.9

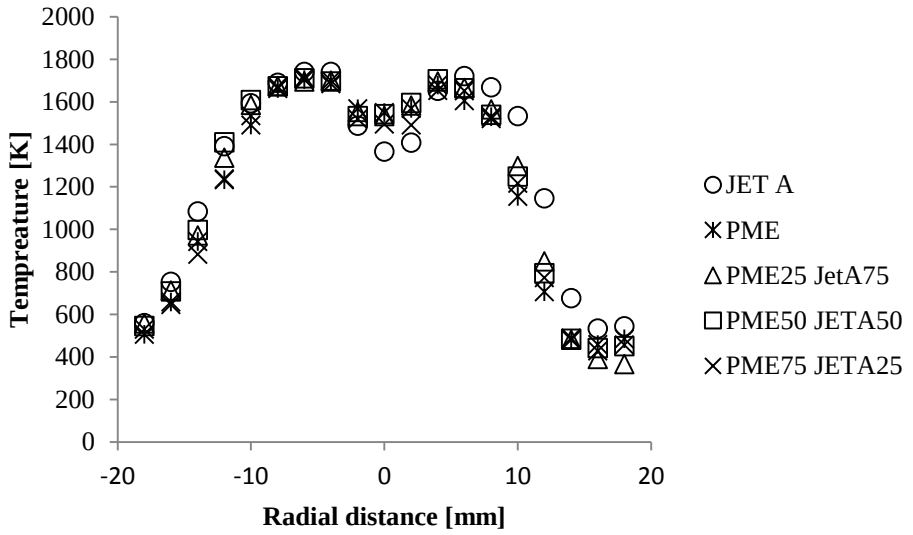


a) at half inner cone height

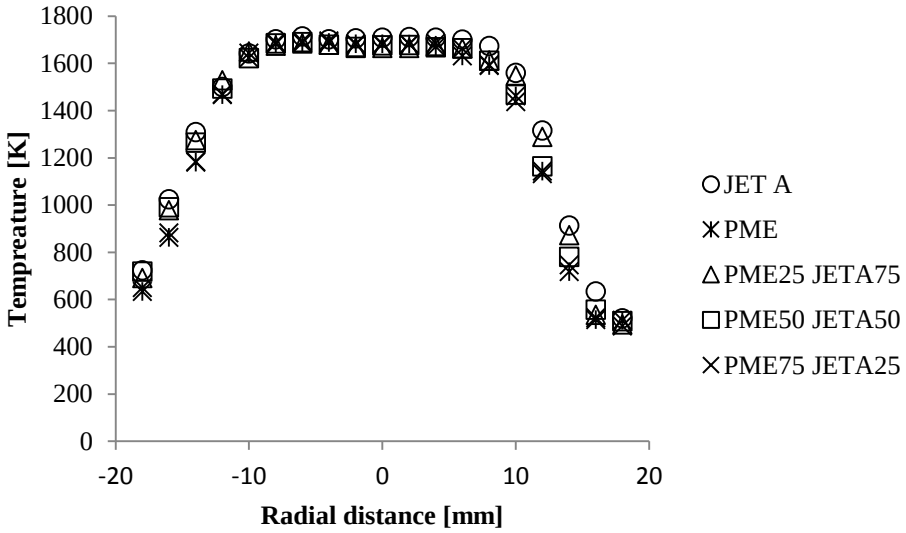


b) at tip of inner cone

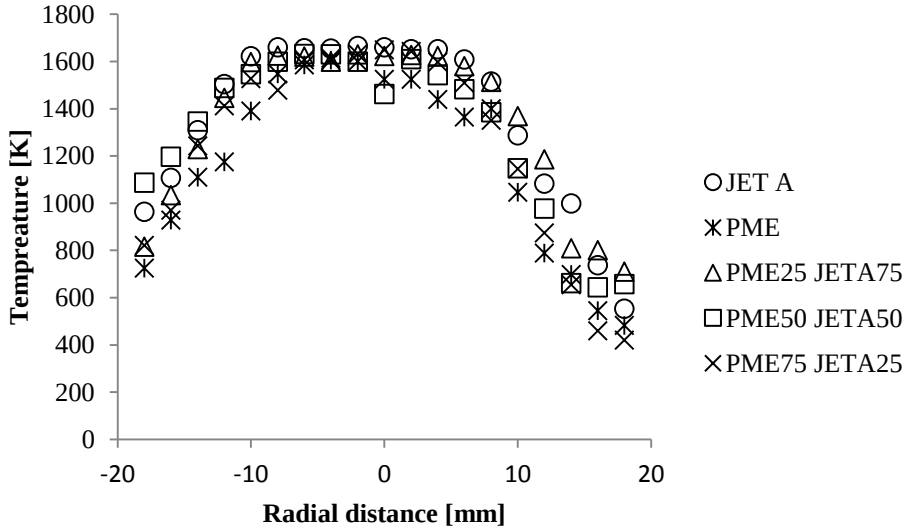


c) at twice the inner cone height

Figure 4.34: PME blends inflame temperature profiles at no coflow, Re ~ 2,500, $\Phi \sim 0.9$

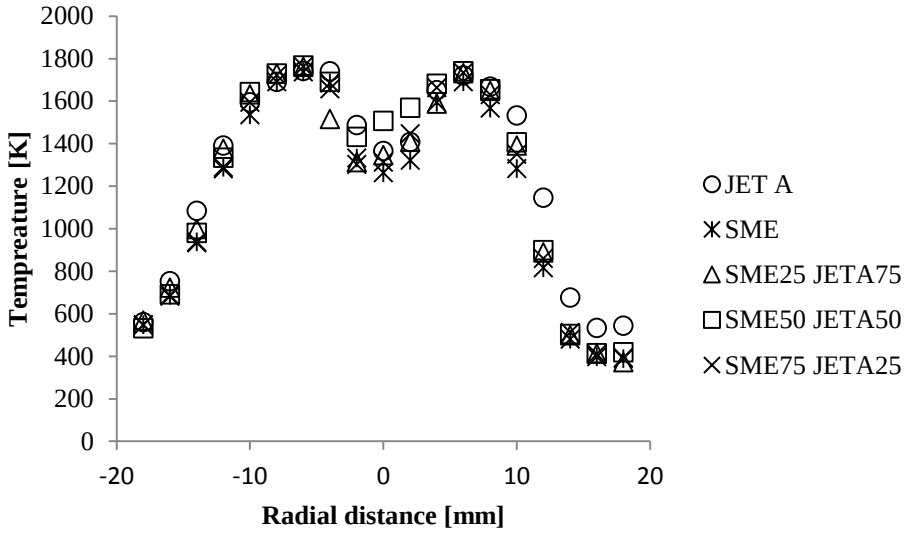


a) at half inner cone height

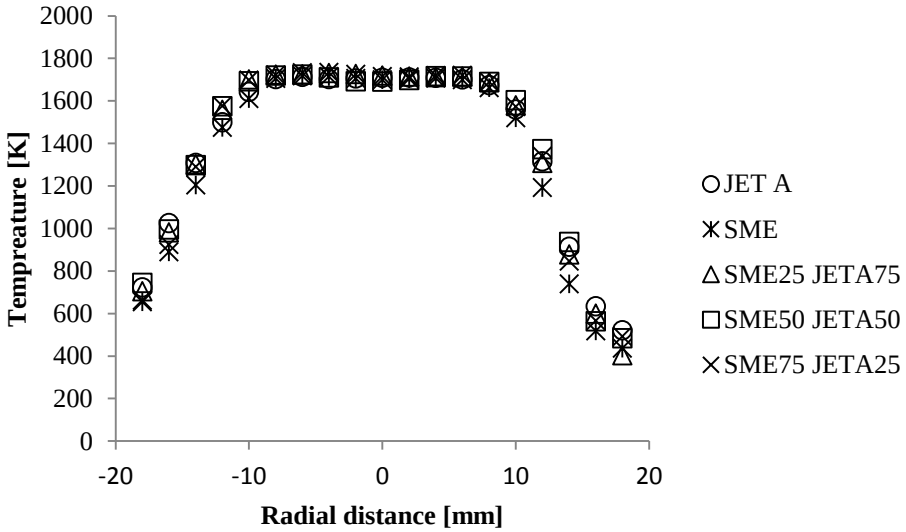


b) at tip of inner cone

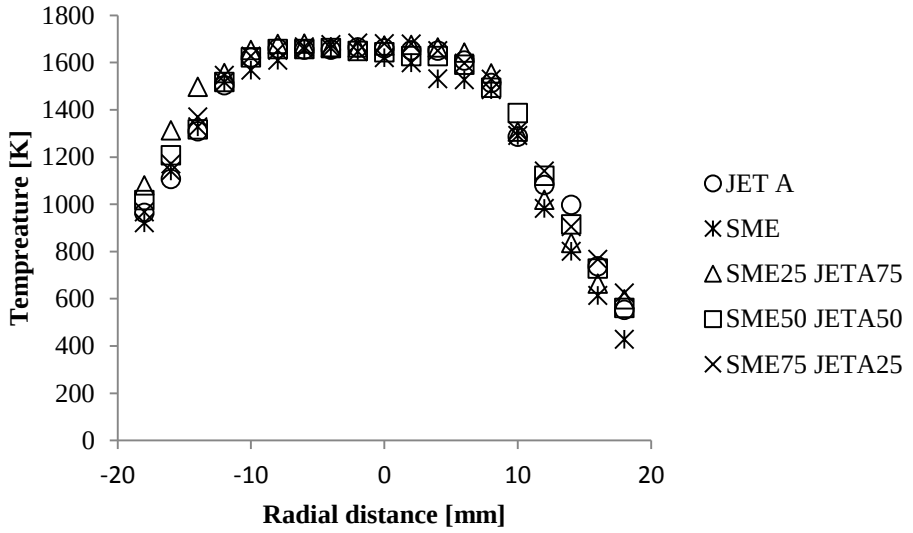


c) at twice the inner cone height

Figure 4.35: SME blends inflame temperature profiles at no coflow, Re ~ 2,500, Φ ~ 0.9

# Chapter 5 Summary and Conclusions

The blowoff velocities of partially-premixed prevaporized laminar flames of Jet A, CME, PME, SME and their blends were studied with and without coflow. Three different coflow velocities were used: 1.1 m/s, 2.3 m/s, and 3.5 m/s (corresponding to volumetric flow rates of 2 L/s, 4 L/s, and 6 L/s, respectively). The injector-exit equivalence ratio was in the range 0.54-0.84. Jet A flames were studied as a baseline for petroleum fuel comparison. Fuel blends were made with Jet A and each of the biofuels. Flames of three blends per biofuel with 25%, 50% and 75% concentration by volume of biofuel were studied. Liquid fuel was injected using a syringe and a syringe pump into a stream of hot air far enough upstream to ensure complete vaporization of the fuel by the time it reached burner exit where it was ignited. The blowoff velocity was determined by increasing the primary airflow rate until the flame blew off while the fuel flow rate and coflow rate were kept constant. All flames at coflow velocity of 3.5 m/s were lifted prior to blowout. On very rare occasions a flame would shortly lift off even at coflow velocity of 2.3 m/s. Most flames were fully attached to the burner rim prior to blowoff. All lifted flames were unstable with constant changes in shape and size. The blowoff velocity increased linearly with equivalence ratio. Other studies have shown that the flame velocity increased as the equivalence ratio was increased in the lean regime, causing an increase in blowoff velocity. There was no significant difference in blowoff velocity of the flames of pure fuels; the blowoff velocities of the blend flames were around the values of the pure fuel flames.

A video of each blowoff was recorded and thereafter images were extracted from the video in order to analyze the flame dimensions. Flame inner cone height, outer cone height, outer cone width (measured at the widest point), and liftoff height were calculated. The results indicate that flames became taller with increase in equivalence ratio. More precisely, flame inner and outer cone height increased in a roughly linear fashion with increase in equivalence ratio. Flames of higher equivalence ratio are more fuel-rich flames which needed to entrain more air to achieve full combustion. Thus, the higher equivalence ratio flames were taller. The liftoff height of various flames did not change significantly with equivalence ratio; it varied around constant value within 1.0 cm to 1.5 cm. Liftoff height of some flames varied more than of the other flames, but it was not possible to discern any pattern. Coflow did not affect the flame dimensions significantly apart from causing the liftoff when coflow velocity was 3.5 m/s (maximum coflow velocity in this study).

Temperature measurements were made within the flames. The measurements were taken at the coflow velocities of 1.1 m/s, 2.3 m/s, and at no coflow. The temperature was measured at three different heights – at the half of the inner cone, at the tip of the inner cone, and at the twice the height of the inner cone (which was approximately slightly higher than half of the outer cone height). The temperature profiles in the various flames were similar, with peak temperatures of around 1740 K. The adiabatic flame temperatures at stoichiometric conditions were comparable for all the fuels. Coflow did not have a significant effect on the peak temperature.

The injector was designed to provide a uniform flow with a sharp gradient at the edge. The Damköhler number has been used to characterize the blowoff of flames.

Blowoff occured when the gas velocity gradient at the jet edge became higher than the flame velocity near the jet edge. Thus, the blowoff-limit was reached when the gas velocity near the edge was tangential to the flame velocity variation with distance from the boundary. Thus, the gradient of velocity near the edge was an important factor determining the flow time scale. The velocity profiles of the jet were measured using a pitot-static probe. Velocity gradients at the jet edge were calculated for different primary airflow velocities and different coflow velocities. As the coflow velocity was increased, the blowoff velocities were increased due to the reduction in the velocity gradient at the edge. The differences in the values of blowoff velocities for the blend flames became smaller as the coflow velocity was increased. A Damköhler number (based on the velocity gradient at the jet edge and the laminar flame speed and thermal diffusivity) value of 2-8 characterized the blowoff velocity. The laminar flame velocity of the fuels at low equivalence ratio was estimated assuming a parabolic correlation between laminar flame velocity and equivalence ratio. The laminar flame velocity was estimated to vary with temperature as $T^{1.5}$.

The inflame temperature profiles showed some asymmetry. Temperature profiles indicate that the left side of the flame was slightly at a higher temperature. This is probably due to the flame swaying towards one side more than the other due to the lack of complete uniformity in coflow velocity. Future experiments should ensure that coflow is more uniform. It was not possible to control the temperature at the burner exit directly since the presence of the thermocouple would disrupt the flow. Future work could find a way to control the temperature directly without interrupting the flow.

# References


Aggarwal, S. K., 2009: Extinction of laminar partially premixed flames, *Progress in Energy and Combustion Science,* **35**, pp. 528-570.

Ask Different, How long is the duration of exposure on an iPhone 6 in iOS 8?, https://apple.stackexchange.com/questions/194601/how-long-is-the-duration-of-exposure-on-an-iphone-6-in-ios-8, *StackExchange*, retrieved November 28, 2017.

Aung, K. T., Hassan, M. I., and Faeth, G. M., 1997: Flame stretch interactions of laminar premixed hydrogen/air flames at normal temperature and pressure, *Combustion and Flame*, **109**, pp. 1-24.

Azzoni, R., Ratti, S., Aggarwal S. K., and Puri, I. K., 1999: The structure of triple flames stabilized on a slot burner, *Combustion and Flame*, **119**, pp. 23-40.

Balakrishnan, A., Parthasarathy, R. N., and Gollahalli, S. R., 2016: A review on the effects of biodiesel blends on compression ignition engine NOx emissions, *Journal of Energy an Environmental Sustainability*, **1**, 67-76.

Boulanger, J., Vervisch, L., Reveillon, J., and Ghosal, S., 2003: Effects of heat release in laminar diffusion flames lifted on round jets, *Combustion and Flame*, **134**, pp. 355-368.

Briones, A. M., Aggarwal, S. K., and Katta, V. R., 2006: A numerical investigation of flame liftoff stabilization, and blowout, *Physics of Fluids*, **18**, pp. 570-588.

Broadwell, J. E., Dahm W. J. A., and Mungal, M. G., 1985: *Twentieth Symposium (International) on Combustion, The Combustion Institute*, pp. 303.

Brown, C. D., Watson, K. A., and Lyons, K. M., 1999: Studies on lifted jet flames in coflow: The stabilization mechanism in the near- and far- fields, *Flow Turbulence and Combustion*, **62**, pp. 249-273.

Burgess, C. P., and Lawn, C. J., 1999: The premixuture model of turbulent burning to describe lifted jet flames, *Combustion and Flame*, **119**, pp. 95-108.

Chen Y. C., and Bilger, R. W., 2000: Stabilization mechanisms of lifted laminar flames in axisymmetric jet flows, *Combustion and Flame*, **122**, pp. 377-399.

Chinthamony, S., 2005: Strucutre of gas jet diffusion flames from an elliptic burner in an elliptic coflow, *Master's Thesis,* School of Aerospace and Mechanical Engineering, University of Oklahoma, Norman, OK.

Choi, B. C., and Chung, S. H., 2013: An experimental study on turbulent lifted flames of methane in coflow jets at elevated temperatures, *Fuel*, **103**, pp. 956-962.

Choi C. W., and Puri, I. K., 2003: Response of flame speed to positively and negatively curved premixed flames, *Combustion Theory and Modelling*¸ **7**, pp. 205-220.

Chong, C. T., and Hochgreb, S., 2011: Measurements of Laminar Flame Speeds of Liquid Fuels: Jet –A1, Diesel and Palm Methyl Esters and Blends Using Particle Imaging Velocimetry, *Proceedings of the Combustion Institute*, **33**, 979-986.

Chung, S. H., and Lee, B. J., 1991: On the characteristics of laminar lifted flames in a non-premixed jet, *Combustion and Flame*, **86**, pp. 62-72.

Cole-Parmer, 2017: Rotameter – Variable Area Flowmeter Technical Information, General Correction Equations, https://www.coleparmer.com/tech-article/rotameters-variable-area-flowmeters-tech-info, retrieved November 13, 2017.

Durbin, T., Collins, J., Norbeck, J., and Smith, M., 2000: Effects of Biofuel, Biofuel Blends, and a Synthetic Diesel on Emissions from Light Heavy-Duty Diesel Vehicles, *Environmental Science and Technology*, **34**, pp. 349-355.

Eickhot, H., Lenze, B., and Leuckel, W., 1984: Experimental investigation of the stabilization mechanism of jet diffusion flames, *Twentieth Symposium (International) on Combustion, The Combustion Institute*, pp. 311-8.

Glassman, I., and Yetter, R. A., 1996: *Combustion*, Fourth Edition, Academic Press, New York.

Gomez-Meyer, J., Gollahalli, S. R., Parthasarathy, R. N., and Quiroga, J., 2012: Laminar flame speed of soy and canola biofuels, *Ciencia Tecno Futuro*, **4**, pp. 76-83.

Gore, J. P., and Zhan, N. J., 1996: NOx emission and jamor species concentrations in partially premixed laminar methane/air co-flow jet flames, *Combustion and Flame*, **105**, pp. 414-427.

Hariharan, P., 2004: An experimental study on elliptic turbulent partially premixed propane/hydrogen/air flames with and without coflow air, *Master's Thesis*, School of Aerospace and Mechanical Engineering, University of Oklahoma, Norman, OK.

Hasper, A., Schmitz, J., Holleman, F., and Verwey, F., 1992: Heat transport in cold-wall single-wafer low pressure chemical vapor deposition reactors. *Journal of Vacuum Science and Technology*, **10**, pp. 3193-3202.

Hertzberg, J. R., Shepherd, I. G., and Talbot, L., 1991: Vortex Shedding Behind Rod Stabilized Flames, *Combustion and Flame*, **86**, pp. 1-11.

Higgins, B., and Siebers, D., 2001: Measurement of the flame life-off location on DI diesel sprays using OH chemiluminescence, *SAE Paper 2001-01-0918*, https://doi.org/10.4271/2001-01-0918.

Jarosinki, J., 1986: A survey of recent studies on flame extinction, *Progress on Energy and Combustion Science*, **12**, pp. 81-116.

Jha, S., Fernando, S., and Filipto, S., 2008: Flame temperature analysis of biodiesel blends and components, *Fuel*, **87**, pp. 1982-1988.

Kanury, A., 1975: *Introduction to Combustion Phenomena: Combustion Science and Technology Book Series* (Volume 2), Langhorne, PA, Gordon and Breach Science Publishers.

Kalghathi, G. T., 1984: Lift-off heights and visible lengths of vertical turbulent jet diffusion flames in still air, *Combustion Sci. and Tech.*, **41**, pp. 17-29.

Kedia, K. S., and Ghoniem, A. F., 2015: The blow-off mechanism of a bluff-body stabilized laminar premixed flame, *Combustion and Flame*, **162**, pp. 1304-1315.

Kim, N. I., Seo, J. I., Oh, K. C., and Shin, H. D., 2005: Lift off characteristics of triple flame with concentration gradient, *Thirtieth Symposium (International) on Combustion, The Combustion Institute*, Pittsburg, PA, pp. 367-374.

Kioni, P. N., Bray, K. N. C., Greenhalgh D. A., and Rogg, B., 1999: Experimental and numerical studies of a triple flame, *Combustion and Flame*, **116**, pp. 192-206.

Ko, Y. S., and Chung, S. H., 1999: Propagation of unsteady tribrachial flames in laminar non-premixed jets, *Combustion and Flame*, **118**, pp. 151-163.

Kumar, K., Sung, C. J., and Hui, X., 2009: Laminar Flame Speeds and Extinction Limits of Conventional and Alternative Jet Fuels, *47th AIAA Aerospace Sciences Meeting*, AIAA 2009-991, Orlando.

Labeckas, G., and Slavinskas, S., 2006: The Effect of Rapeseed Oil Methyl Ester on Direct Injection Diesel Engine Performance and Exhaust Emissions, *Energy Conversion & Management*, **47**, pp. 1954-1967.

Lawn, C. J., 2009: Lifted flames on fuel jets in co-flowing air, *Progress in Energy and Combustion Science*, **35**, pp. 1-30.

Lim, W., Ooi, T., and Hong, H., 2009: Study on low temperature properties of palm oil methyl esters-petrodiesel blends, *Journal of Oil Palm Research*, **21**, pp. 683-692.

Liu, W., Kelley, A. P., and Law, C. K., 2011: Non-premixed ignition, laminar flame propagation, and mechanism reduction of n-butanol, iso-butanol, and methyl butanoate, *The Combustion Institute*, **33**, pp. 995-1002.

Lee, B. J., and Chung, S. H., 1997: Stabilization of lifted tribrachial flames in laminar non-premixed jet, *Combustion and Flame*, **109**, pp. 163-172.

Lee, B. J., Cha, M. S., and Chung, S. H., 1997: Characteristics of laminar lifted flames in a partially premixed jet, *Combustion Science and Technology*, **127**, pp. 55-70.

Lee, J., and Chung, S. H., 2001: Characteristics of reattachment and blowout of laminar lifted flames in partially premixed propane jets, *Combustion and Flame*, **127**, pp. 2194-2204.

Lee, J., Jin, S. H., and Chung, S. H., 2003: Lifted flames in laminar jets of propane in coflow air, *Combustion and Flame*, **135**, pp. 449-462.

Lewis, B., and von Elbe, G., 1987: *Combustion, Flames and Explosions of Gases*, Third edition, Academic Press, New York.

Lima, J. A. P., Marín, E., da Silva, M. G., Sthel, M. S., Cardoso, S. L., Takeuti, D. F., Gatts, C., Vargas, H., Rezende, C. E., and Miranda, L. C. M., 2000: On the use of the thermal wave resonator cavity sensor for monitoring hydrocarbon vapors, *American Institute of Physics*, **71**, S0034-6748(00)03107-5.

Liu, W., Kelley, A. P., and Law, C. K., 2011: Non-premixed ignition, laminar flame propagation, and mechanism reduction of n-butanol, iso-butanol, and methyl butanoate, *The Combustion Institute*, **33**, pp. 995-1002.

Lock, A. J., Briones, A. M., Qin, X., Aggarwal, S. K., Puri, I. K., and Hegde, U., 2005: Liftoff characteristics of partially premixed flames in normal and microgravity, *Combustion and Flame*, **143**, pp. 159-173.

Love, N., 2009: Effects of equivalence ratio and iodine number on NOx emissions from the flames of biofuels and hydrocarbons, *Dissertation*, School of Aerospace and Mechanical Engineering, University of Oklahoma, Norman, OK.

Love, N., Parthasarathy, R. N., and Gollahalli, S. R., 2009: Rapid characterization of radiation and pollutant emissions of biofuel and hydrocarbon liquid fuels, *Journal of Energy Resources*, **131**, pp. 1-9.

Maleta, T., Parthasarathy, R. N., and Gollahalli, S. R., 2017: Blowout characteristics of partially premixed flames of prevaporized blends of biofuels and petroleum fuels, *International Mechanical Engineering Congress and Exposition*, ASME, IMECE2017-70612, Tampa, FL.

Maxwell, J., 1950: *Data Book on Hydrocarbons Application to Process Engineering*, Rober E. Krieger Publishing Co., Malabar, FL.

Merchan-Merchan, W., Sanmiguel, S. G., and McCollam, S., 2012: Analysis of soot particles derived from biodiesels and diesel fuel air-flames, *Fuel*, **102**, pp. 525-535.

Montgomery, C. J., Kaplan, C. R., and Oran, E. S., 1998: The effect of coflow velocity on a lifted methane-air jet diffusion flame, *Twenty-Seventh Symposium (International) on Combustion, The Combustion Institute*, pp. 1175–1182.

Mongia, H. C., 2004: Perspective of gas turbine combustion modeling, *42nd AIAA Aerospace Sciences Meeting and Exhibit, AIAA Paper 2004-0156,* Reno, NV.

Muralidharan, K., Vasudevan, D., and Sheeba, K., 2001: Performance, Emission and Combustion Characteristics of Biodiesel Fuelled Variable Compression Ratio Engine, *Energy*, **36**, pp. 5385-5393.

Navarro-Martinez, S., and Kronenberg, A., 2008: Analysis of stabilization mechanisms in lifted flames, *LES and DNS of Ignition Processes and Complex-Structure Flames with Local Extinction, AIP Conf. Proceedings*, **1190**, pp. 13-38.

Nicholson, H., and Field, J., 1951: Some Experimental Techniques for the Investigation of the Mechanism of Flame Stabilization in the Wake of Bluff Bodies, *Proc. Comb. Inst*., **3**, pp. 44-68.

Nilsson, E. J., and Konnov, A. A., 2015: Trends in Laminar Burning Velocities of C2-C7 Esters, *European Combustion Meeting*, ECM 2015, Budapest, Hungary.

Peters, N., and Williams, F. A., 1983: Liftoff Characteristics of Turbulent Jet Diffusion Flames, *AIAA Journal*, **21**, pp. 423-429.

Pitts, W. M., 1988: Assessment of theories for the behavior and blowout of lifted turbulent jet diffusion flames, *Twenty-Second Symposium (International) on Combustion, The Combustion Institute*, **22**, pp. 809-816.

Plessing, T., Terhoeven, P., Peters, N., and Mansour, M. S., 1998: An experimental and numerical study of a laminar triple flame, *Combustion and Flame*, **115**, pp. 335-353.

Puri, I. K., Aggarwal, S. K., Ratti, S., and Azzoni, R., 2001: On the similitude between lifted and burner stabilized triple flames: A numerical and experimental investigation, *Combustion and Flame*, **124**, pp. 311-325.

Rokke, N. A., Hustad, J. E., and Sonju, O. K., 1994: A study of partially premixed unconfined propane flames, *Combustion and Flame*, **97**, pp. 88-106.

Ruetsch, G.R., Vervisch, L., and Linan, A., 1995: Effects of heat release on triple flame, *Physics of Fluids*, **6**, pp. 1147-1454.

Savas, O., and Gollahalli, S. R., 1986: Stability of lifted laminar round gas-jet flame, *Journal of Fluid Mechanics*, **165**, pp. 297-318.

Shu, Z., Choi, C. W., Aggarwal, S. K., Katta, V. R., and Puri, I. K., 1999: Gravitational effects on the structure of steady two-dimensional partially premixed methane-air flames, *Combustion and Flame*, **118**, pp. 91-107.

Singh, V. N., 2013: Effects of equivalence ratio on combustion characteristics of laminar partially premixed flames of petroleum-biofuel blends, *Dissertation*, School of Aerospace and Mechanical Engineering, University of Oklahoma, Norman, OK.

Scholl, K., and Sorenson, S., 1993: Combustion of Soybean Oil Methyl Ester in a Direct Injection Diesel Engine, SAE Technical Paper 930934, *International Congress and Exposition*, pp. 211–223.

Sulmon, M., Van Geem, K., and De Bruycker, R., 2016: Experimental & kinetic modeling study of the thermal decomposition and laminar flame speeds of esters, *Master's dissertation*, Department of Chemical Engineering and Technical Chemistry, University of Gent

Takahashi, F., and Schmoll, W. J., 1990: Lifting criteria of jet diffusion flames, *Twenty-Third Symposium (International) on Combustion, The Combustion Institute*, Pittsburg, PA, pp. 677-683.

Terry, S. D., and Lyons, K. M., 2006: Turbulent lifted flames in the hysteresis regime and effects of coflow, *Journal of Energy Resource Technology*, **128**, pp. 319-324.

Tieszen, S. R., Stamps, D. W., and O'Hern, T. J., 1996: A heuristic model of turbulent mixing applies to blowout of turbulent jet diffusion flames, *Combustion and Flame*, **106**, pp. 442-466.

Turns, S. R., 2011: *An Introduction to Combustion*, Third Edition, McGraw-Hill, New York

Vanquickenbourne, L., and van Tiggelen, A., 1966: The stabilization mechanism of lifted diffusion flames, *Combustion and Flame*, **10**, pp. 59-69.

Wang, Y. L., Feng, Q., Egolfoupolos, F. N., and Tostsis, T.T., 2011: Studies of C4 and C10 methyl ester flames, *Combustion and Flame*, **158**, pp. 1507-1519.

Wang, W. G., Lyons, D. W., Clark, N. N., Gautam, M., and Norton, P. M., 2000: Emissions from nine heavy trucks fueled by diesel and biodiesel blend without engine odification, *Environmental Science and Technology*, **34**, pp. 933–939.

Wheeler, A. J., and Ganji, A. R., 1996: *Introduction to Engineering Experimentation*, Prentice Hall, Upper Saddle River, New Jersey, pp. 160-178.

White, F. M., 2006: *Viscous Fluid Flow*, Third Edition, McGraw Hill, New York.

Williams, F. A., 2000: Progress in knowledge of flamelet structure and extinction, *Progress in Energy and Combustion Science*, **26**, pp. 657-682.

Willingham, K., 2014: Blowout characteristics of vaporized methyl ester biofuel flames, *Master Thesis*, School of Aerospace and Mechanical Engineering, University of Oklahoma, Norman, OK.

Willingham, K., Parthasarathy, R. N. and Gollahalli, S. R., 2015: Blowout limits of partially premixed methyl ester and Jet-A flames, *International Energy Conversion Engineering Conference*, AIAA, IECEC2015-2194549, New York.

Wilson, D. A., and Lyons, K. M., 2008: Effects of dilution and co-flow on the stability of lifted non-premixed biogas-like flames, *Fuel*, **87**, pp. 405-413.

Wohl, K., Kapp, N. M., and Gazley, C., 1949: The stability of open flames, *Third Symp. On Combustion and Flame and Explosion Phenomena*, pp. 3-21.

Won, S. H., Kim, J., Hong, K. J., Cha, M. S., and Chung, S. H., 2005: Stabilization of lifted flame edge in the near field of coflow jets for dilute methane, *Thirtieth Symposium (International) on Combustion, The Combustion Institute*, Pittsburg, PA, pp. 339-347.

Wu, Y., Lu, Y., Al-Rahbi, I.S., and Kalghatgi, G.T., 2007: Prediction of the liftoff, blowout and blowoff stability limits of pure hydrogen and hydrogen/hydrocarbon mixture jet flames, *International Journal of Hydrogen Energy*, **34**, pp. 5940-5945.

Zhang, Q., 2008: Lean Blowoff Characteristics of Swirling H2/CO/CH4 Flames, *PhD Dissertation*, Department of Aerospace Engineering, Georgia Institute of Technology, Atlanta, GA.

# Appendix A: Blowoff Velocities

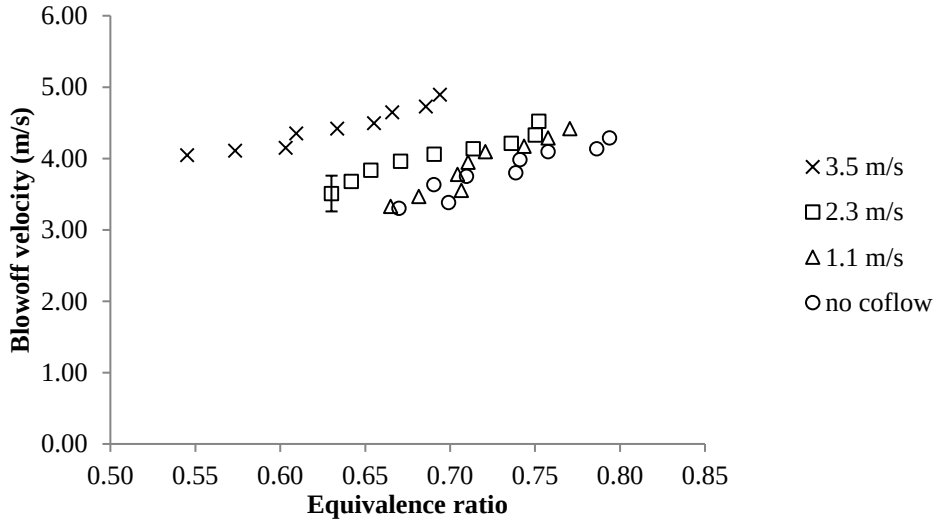


Figure 6.1: Change in blowoff velocity of Jet A with equivalence ratio for different coflow velocities

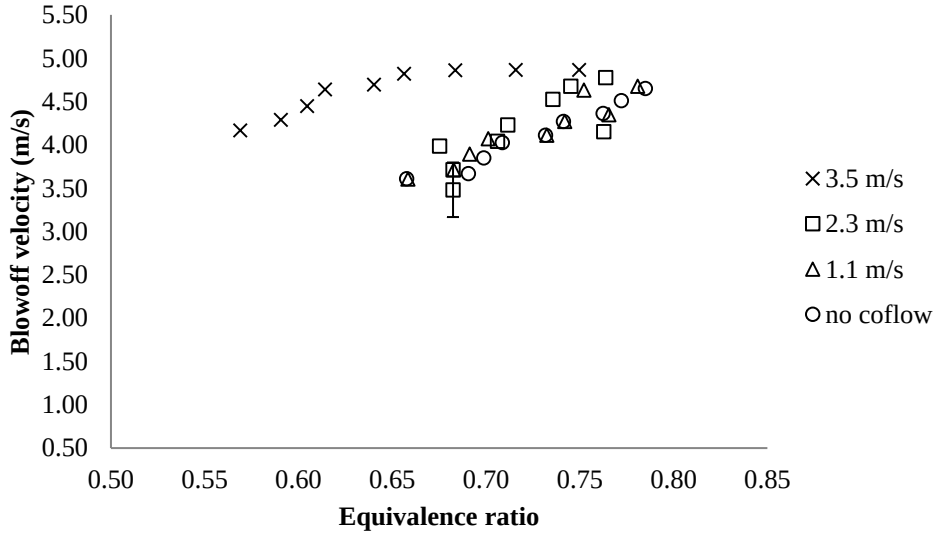


Figure 6.2: Change in blowoff velocity of CME with equivalence ratio for different coflow velocities

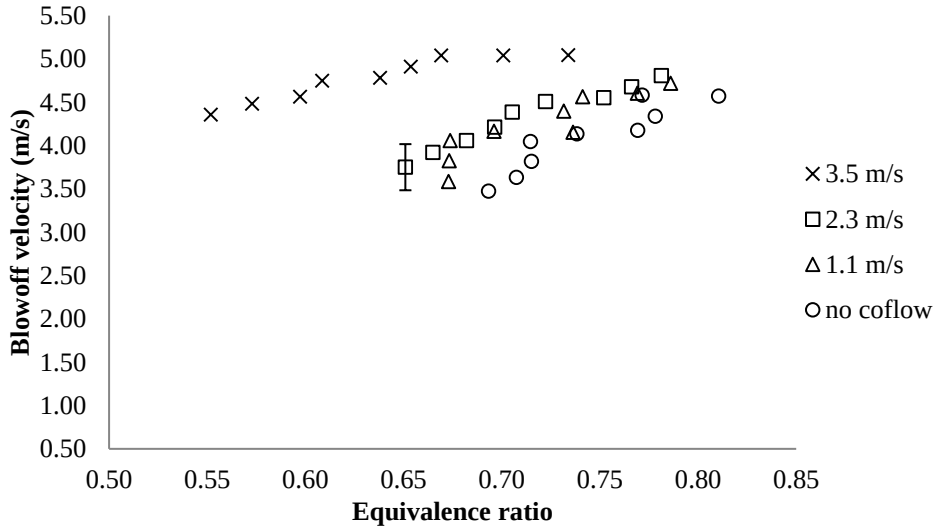


Figure 6.3: Change in blowoff velocity of CME25 JETA75 with equivalence ratio for different coflow velocities

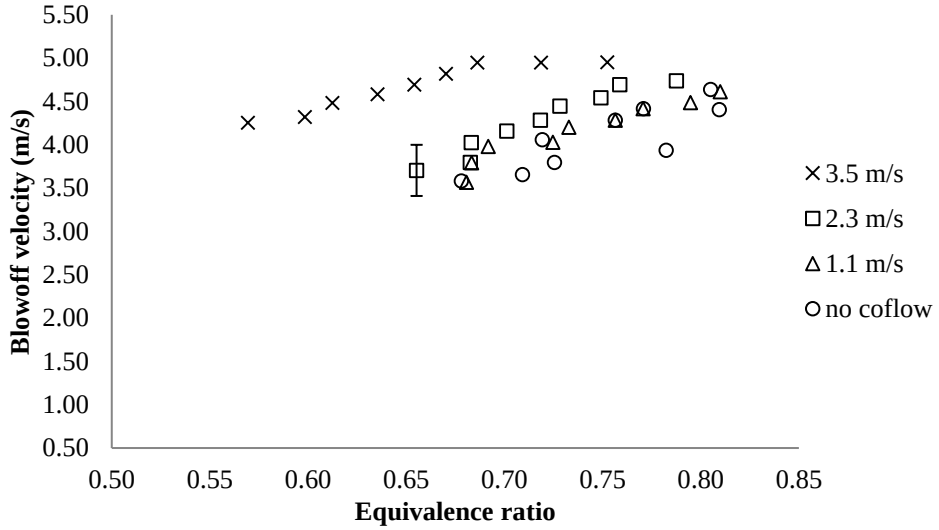


Figure 6.4: Change in blowoff velocity of CME50 JETA50 with equivalence ratio for different coflow velocities

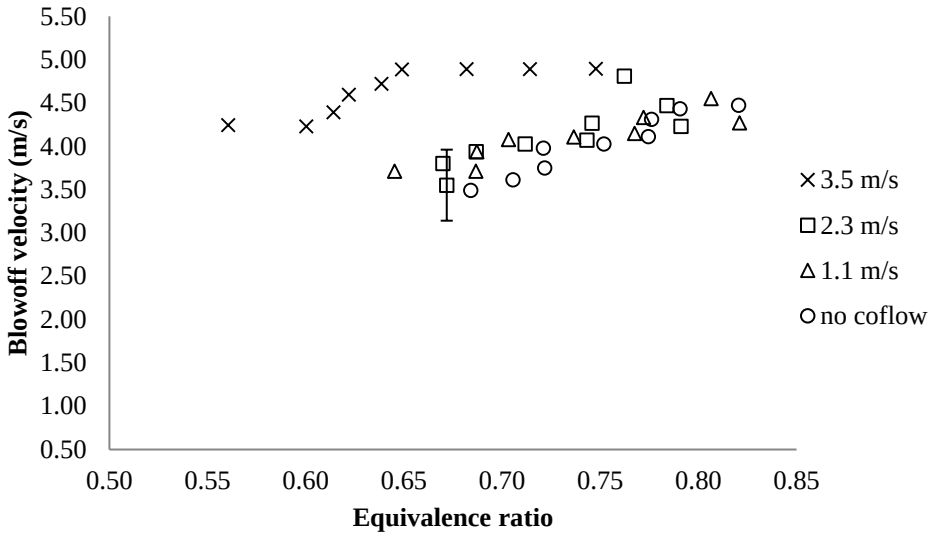


Figure 6.5: Change in blowoff velocity of CME75 JETA25 with equivalence ratio for different coflow velocities

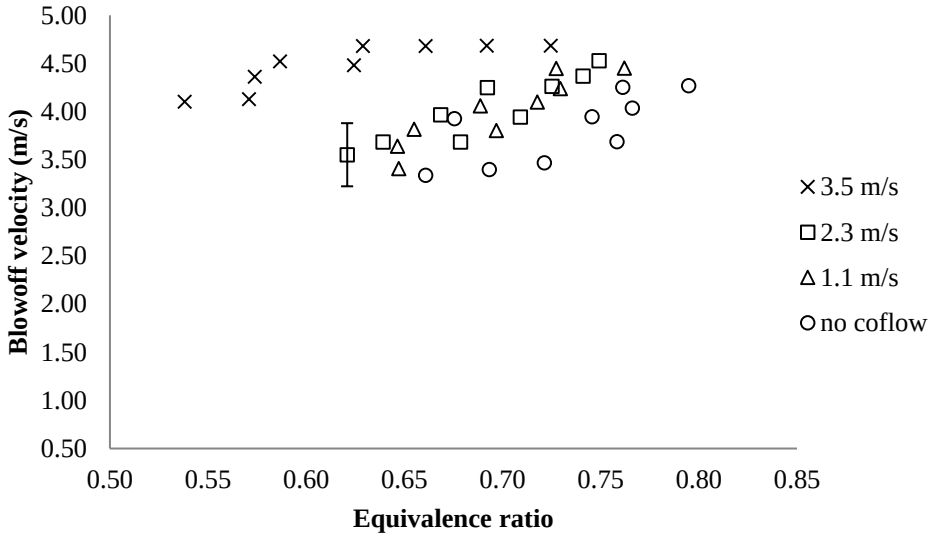


Figure 6.6: Change in blowoff velocity of PME with equivalence ratio for different coflow velocities

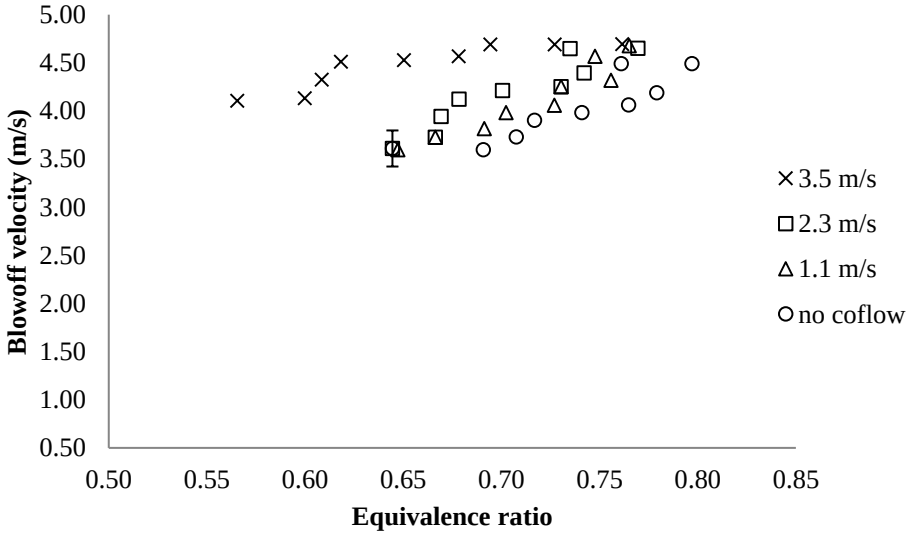


Figure 6.7: Change in blowoff velocity of PME25 JETA75 with equivalence ratio for different coflow velocities

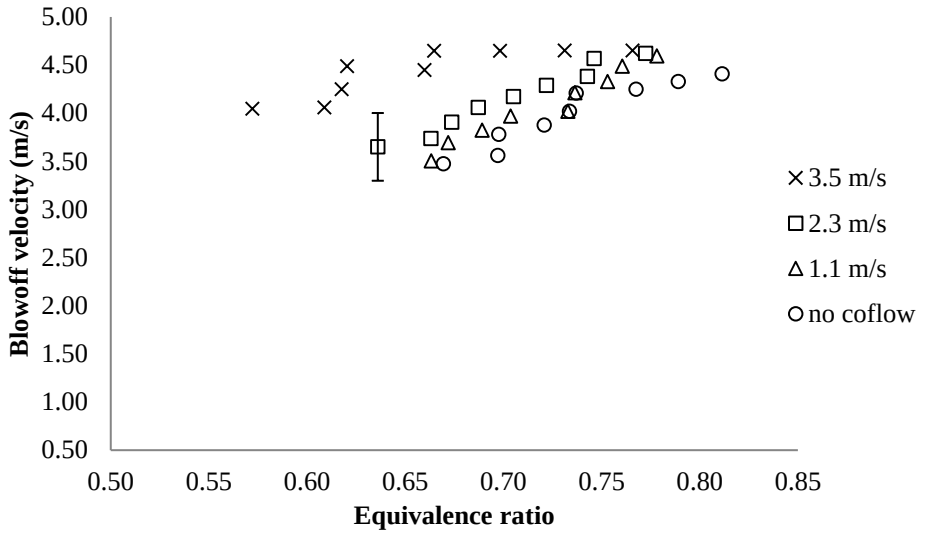


Figure 6.8: Change in blowoff velocity of PME50 JETA50 with equivalence ratio for different coflow velocities

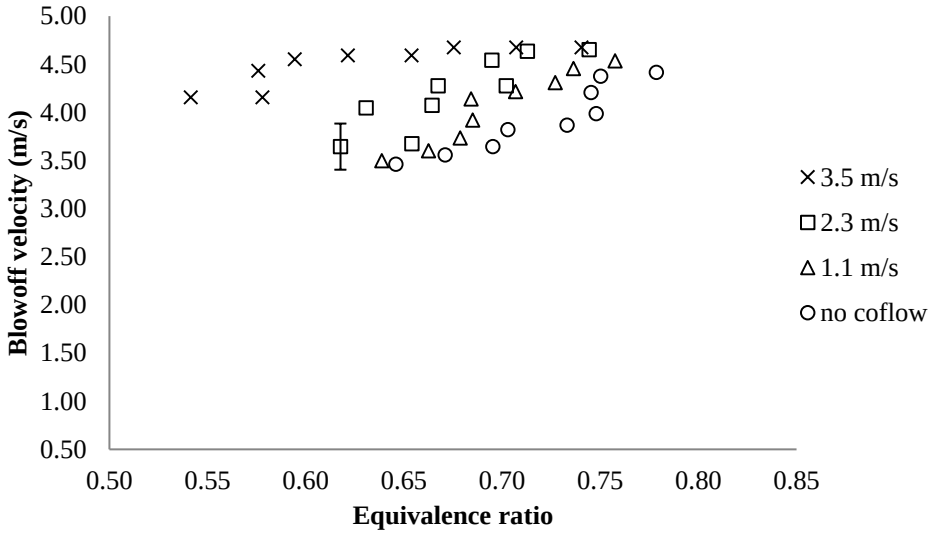


Figure 6.9: Change in blowoff velocity of PME75 JETA25 with equivalence ratio for different coflow velocities

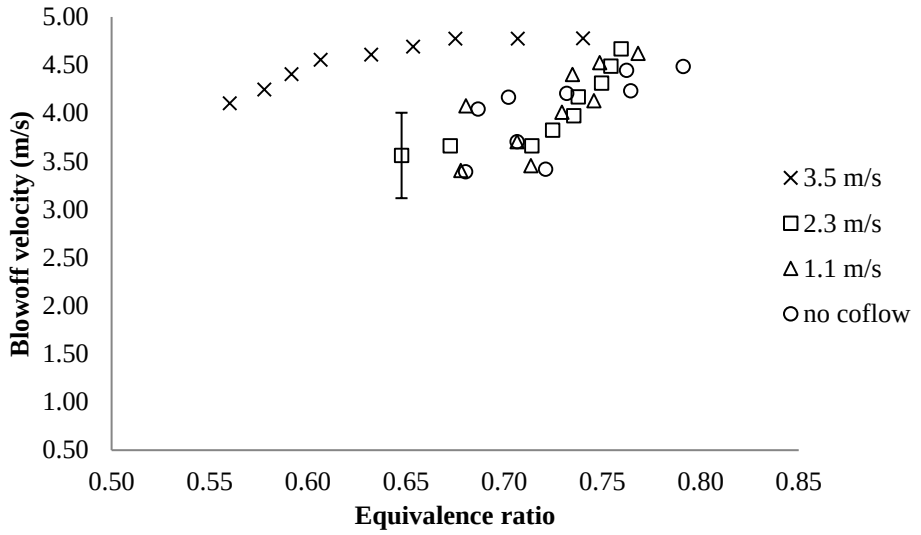


Figure 6.10: Change in blowoff velocity of SME with equivalence ratio for different coflow velocities

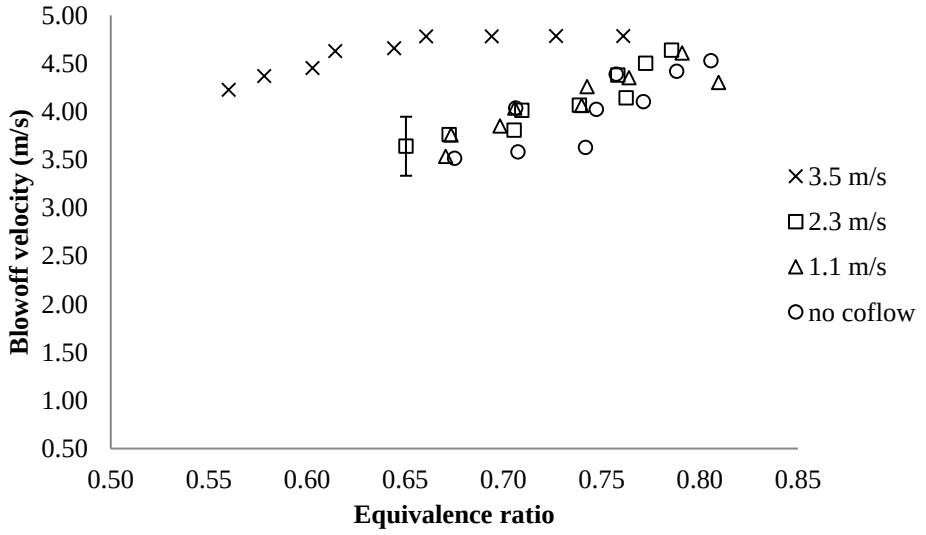


Figure 6.11: Change in blowoff velocity of SME25 JETA75 with equivalence ratio for different coflow velocities

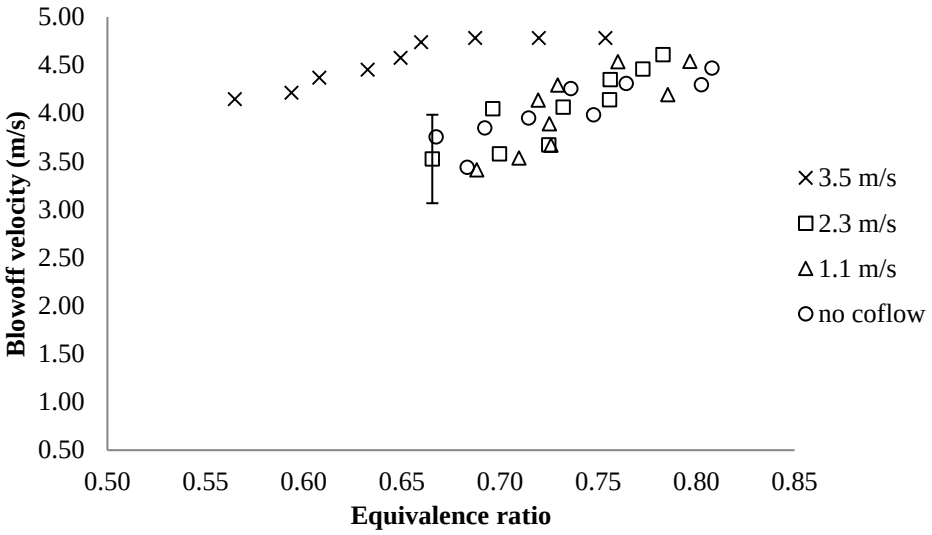


Figure 6.12: Change in blowoff velocity of SME50 JETA50 with equivalence ratio for different coflow velocities

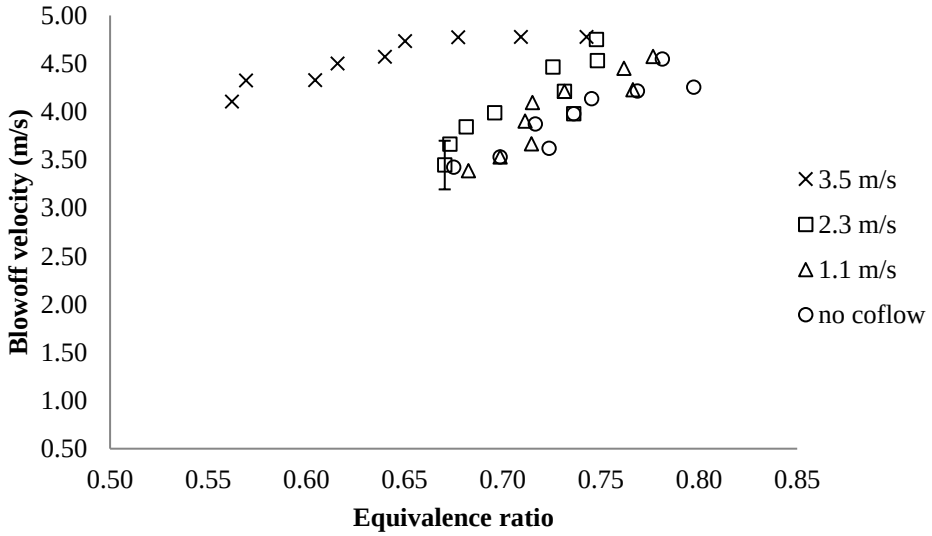


Figure 6.13: Change in blowoff velocity of SME75 JETA25 with equivalence ratio for different coflow velocities

# Appendix B: Flame Dimensions

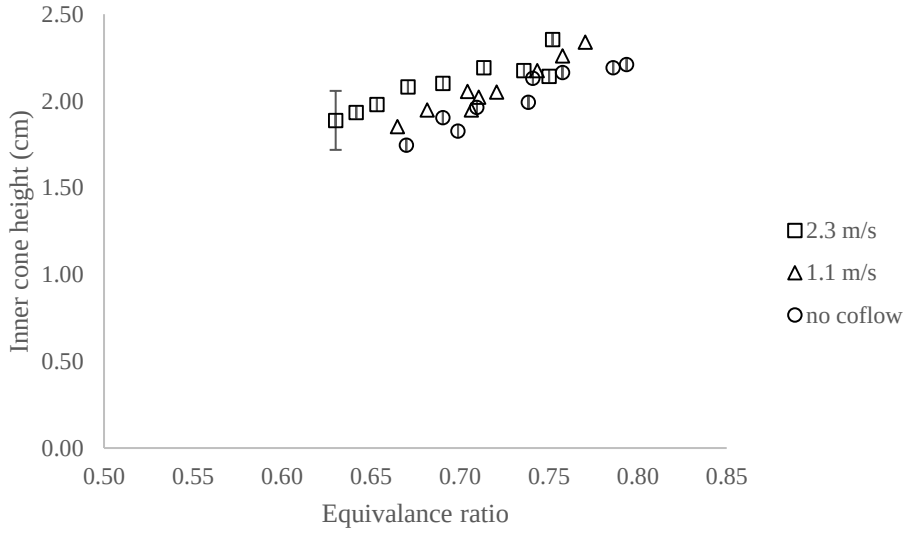


Figure 6.14: Change in inner cone height with equivalence ratio for Jet A flames at different coflow velocities

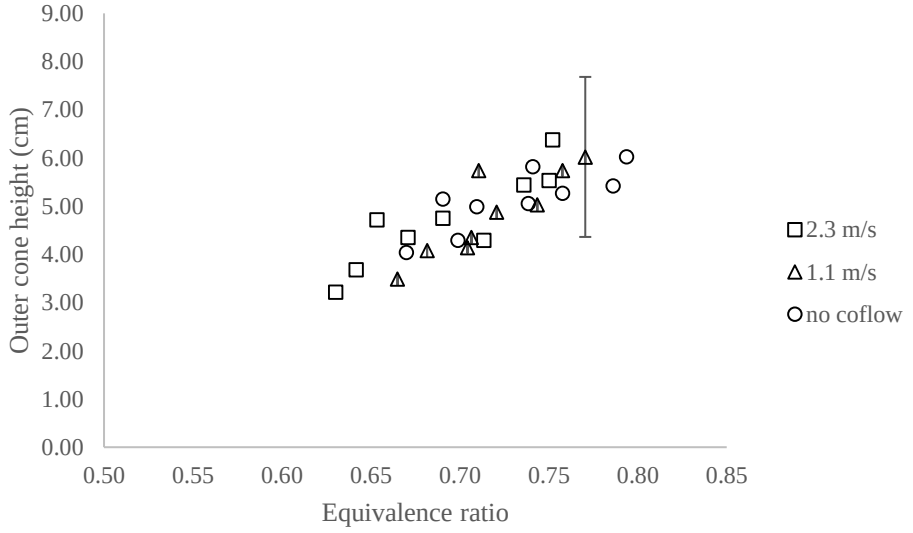


Figure 6.15: Change in outer cone height with equivalence ratio for Jet A flames at different coflow velocities

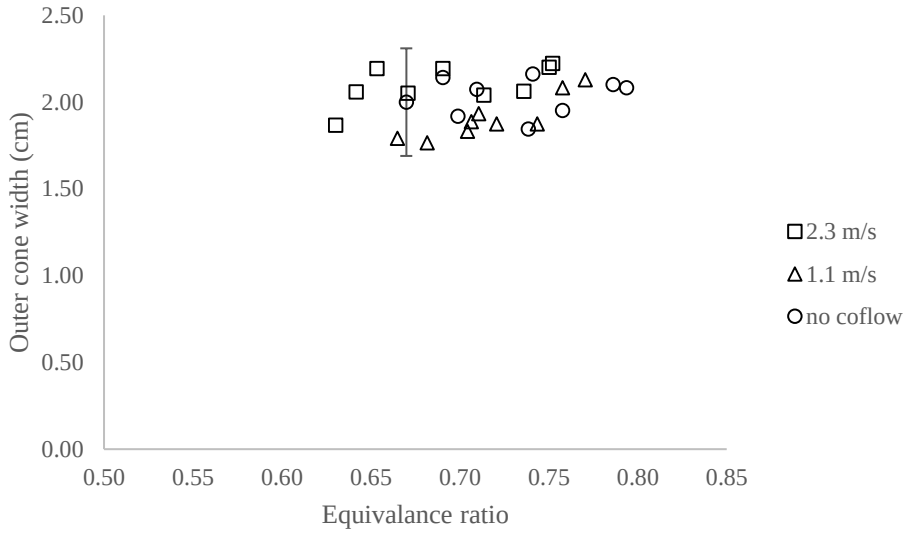


Figure 6.16: Change in outer cone width with equivalence ratio for Jet A flames at different coflow velocities

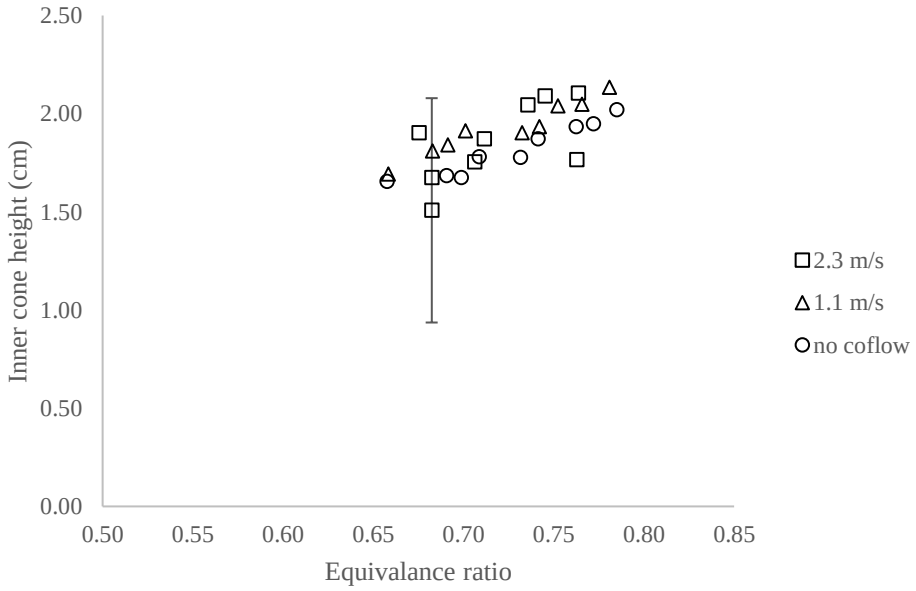


Figure 6.17: Change in inner cone height with equivalence ratio for CME flames at different coflow velocities

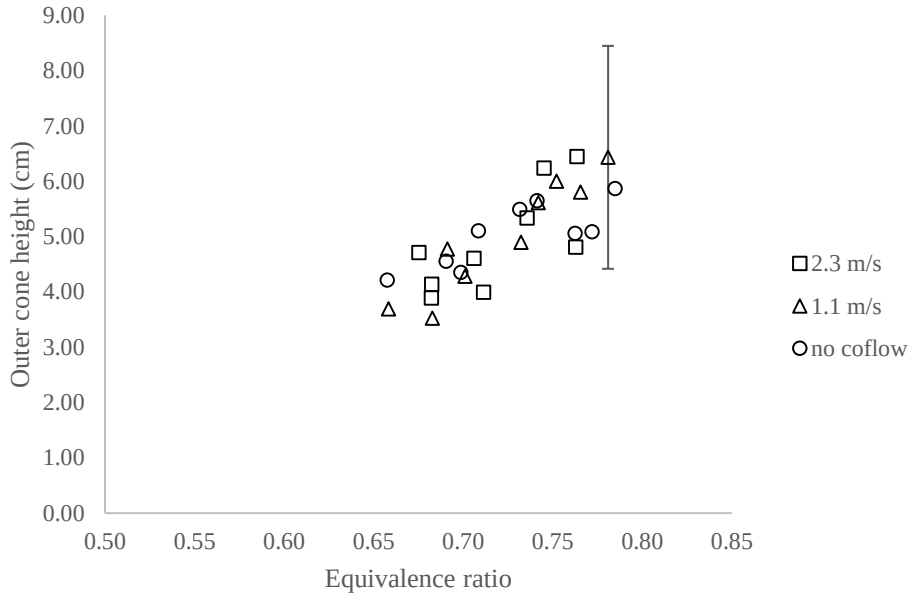


Figure 6.18: Change in outer cone height with equivalence ratio for CME flames at different coflow velocities

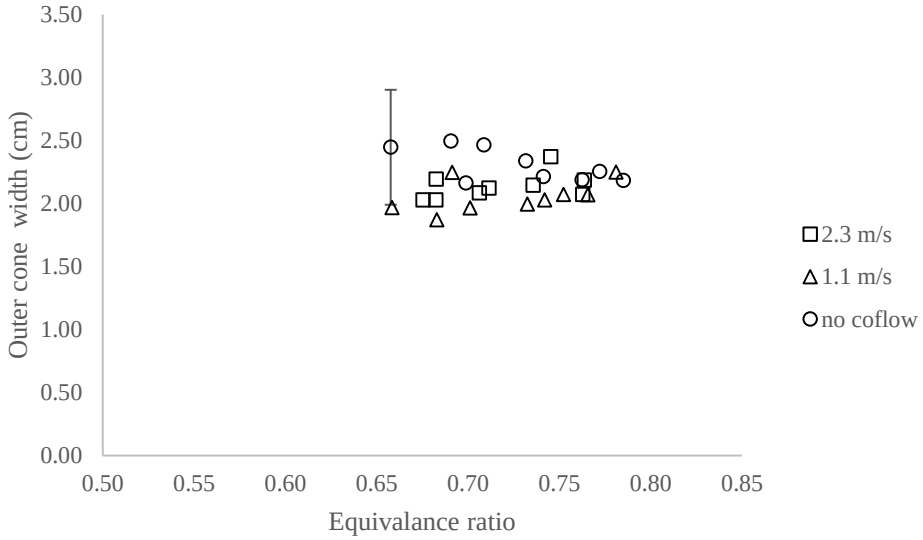


Figure 6.19: Change in outer cone width with equivalence ratio for CME flames at different coflow velocities

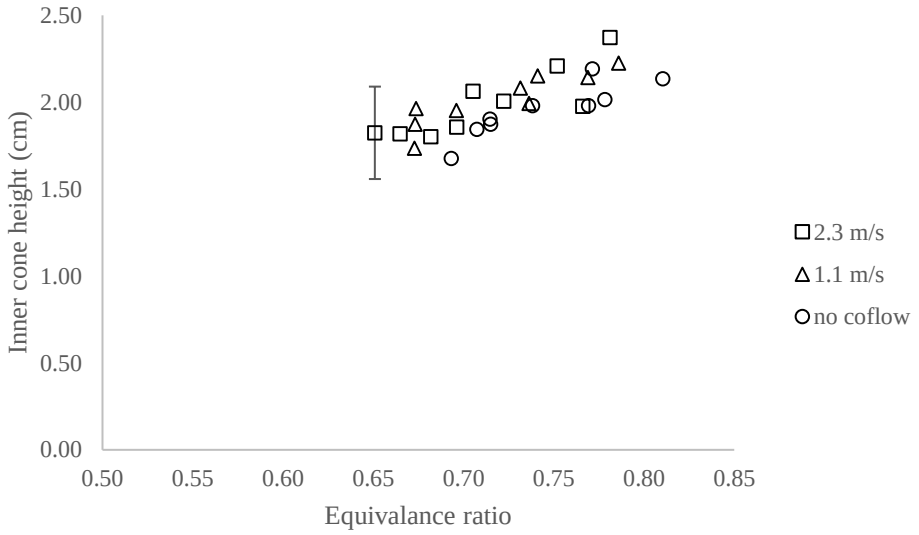


Figure 6.20: Change in inner cone height with equivalence ratio for CME25 JETA75 flames at different coflow velocities

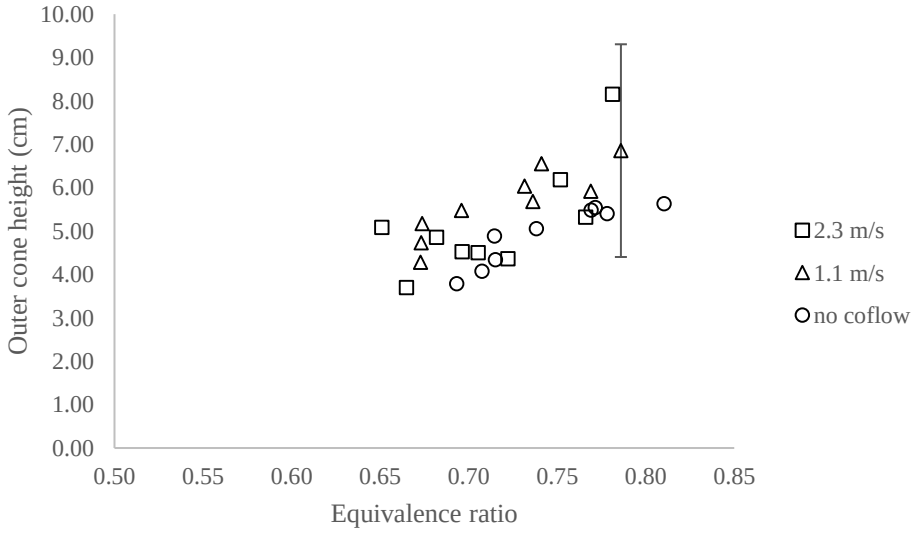


Figure 6.21: Change in outer cone height with equivalence ratio for CME25 JETA75 flames at different coflow velocities

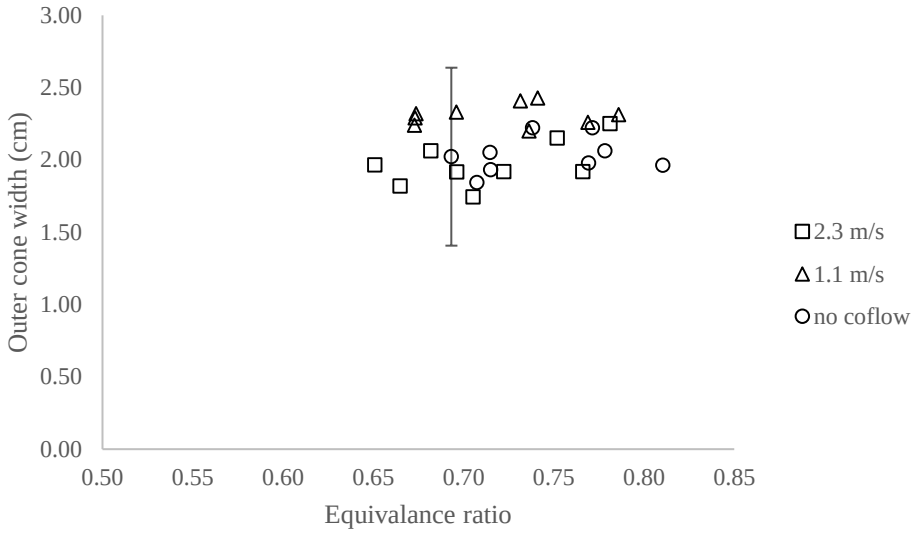


Figure 6.22: Change in outer cone width with equivalence ratio for CME25 JETA75 flames at different coflow velocities

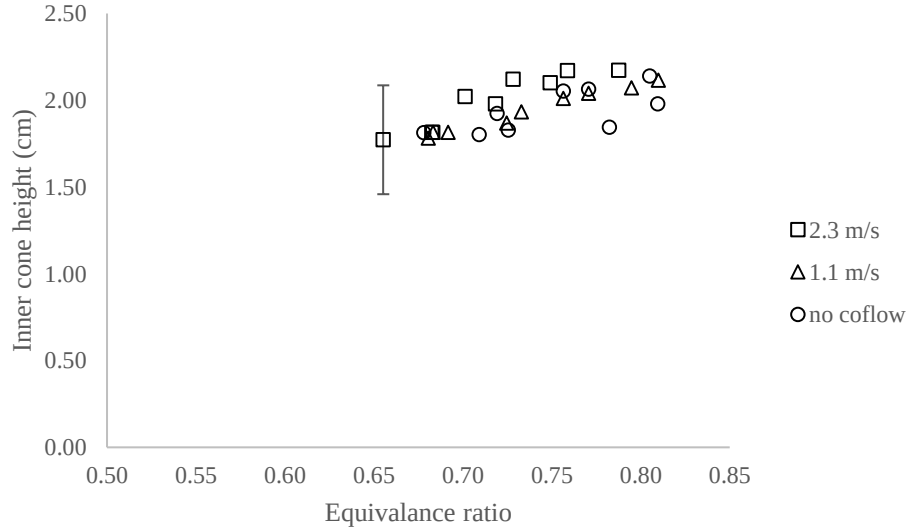


Figure 6.23: Change in inner cone height with equivalence ratio for CME50 JETA50 flames at different coflow velocities

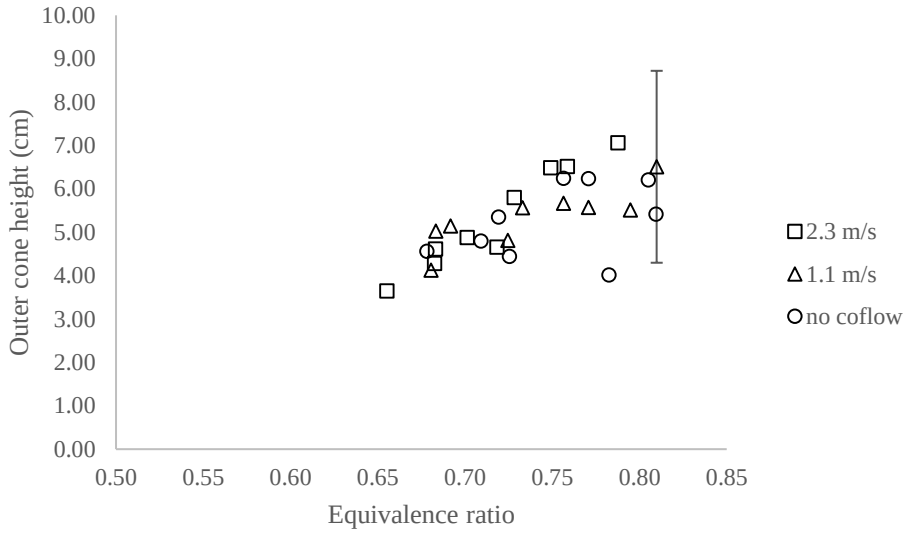


Figure 6.24: Change in outer cone height with equivalence ratio for CME50 JETA50 flames at different coflow velocities

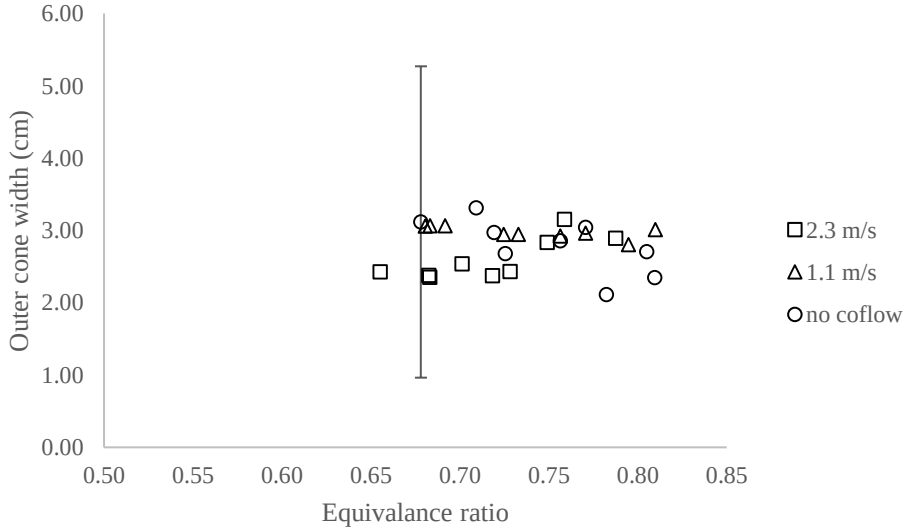


Figure 6.25: Change in outer cone width with equivalence ratio for CME50 JETA50 flames at different coflow velocities

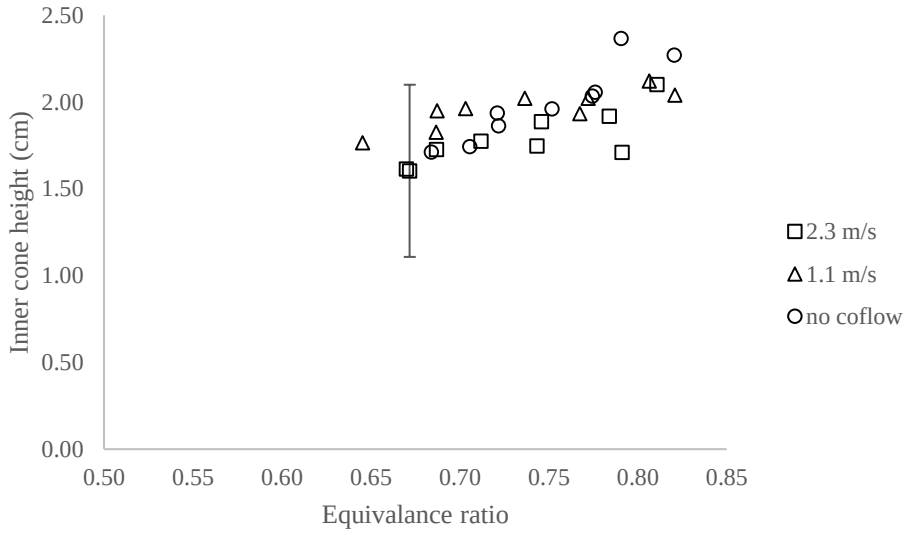


Figure 6.26: Change in inner cone height with equivalence ratio for CME75 JETA25 flames at different coflow velocities

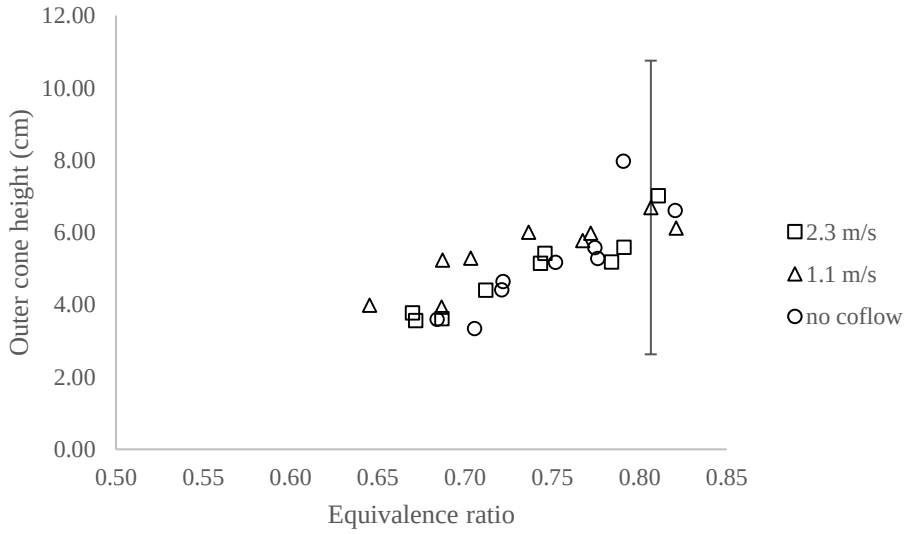


Figure 6.27: Change in outer cone height with equivalence ratio for CME75 JETA25 flames at different coflow velocities

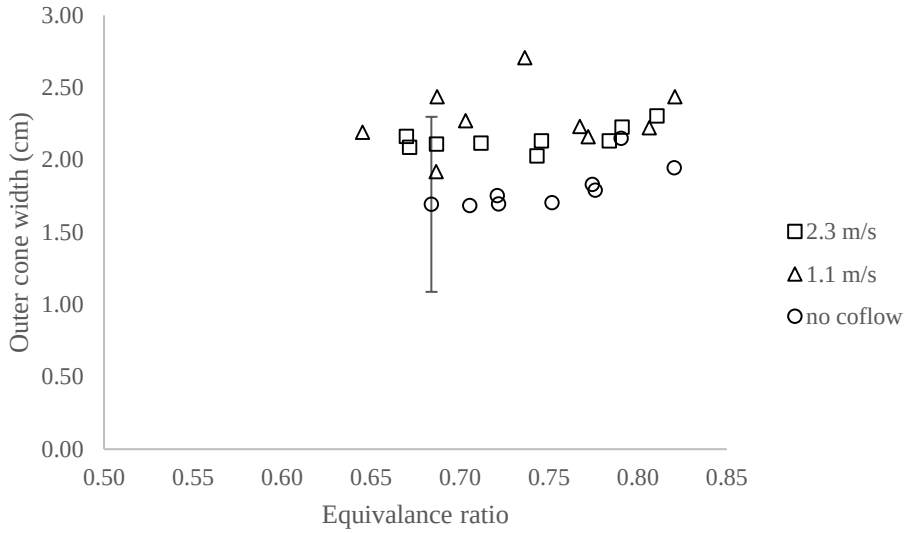


Figure 6.28: Change in outer cone width with equivalence ratio for CME75 JETA25 flames at different coflow velocities

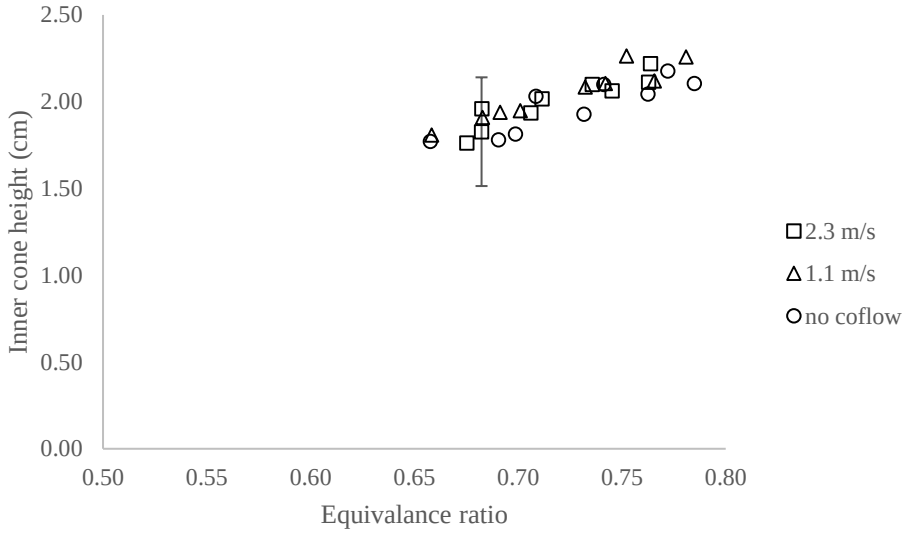


Figure 6.29: Change in inner cone height with equivalence ratio for PME flames at different coflow velocities

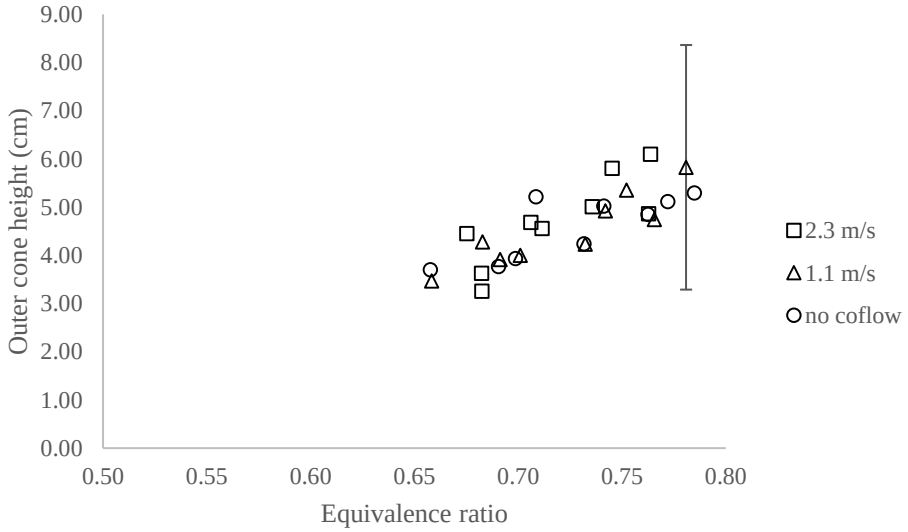


Figure 6.30: Change in outer cone height with equivalence ratio for PME flames at different coflow velocities

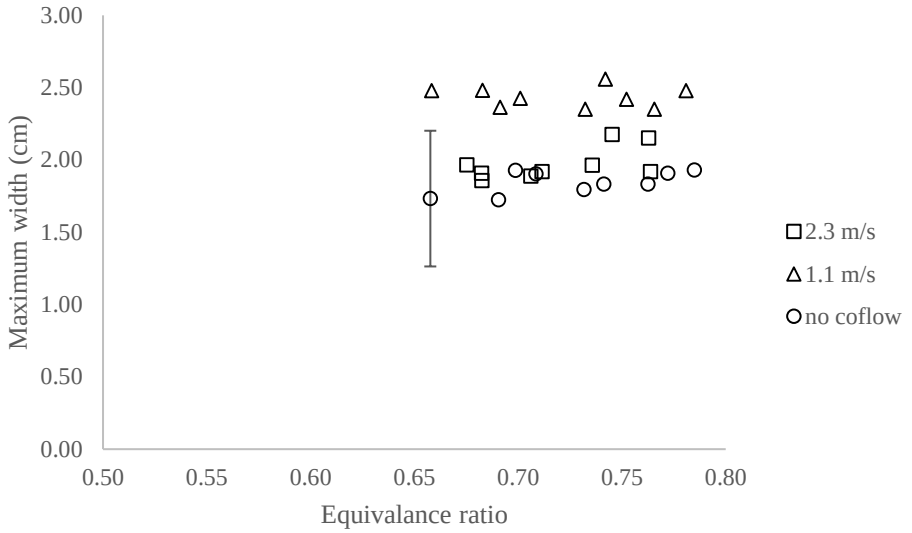


Figure 6.31: Change in outer cone width with equivalence ratio for PME flames at different coflow velocities

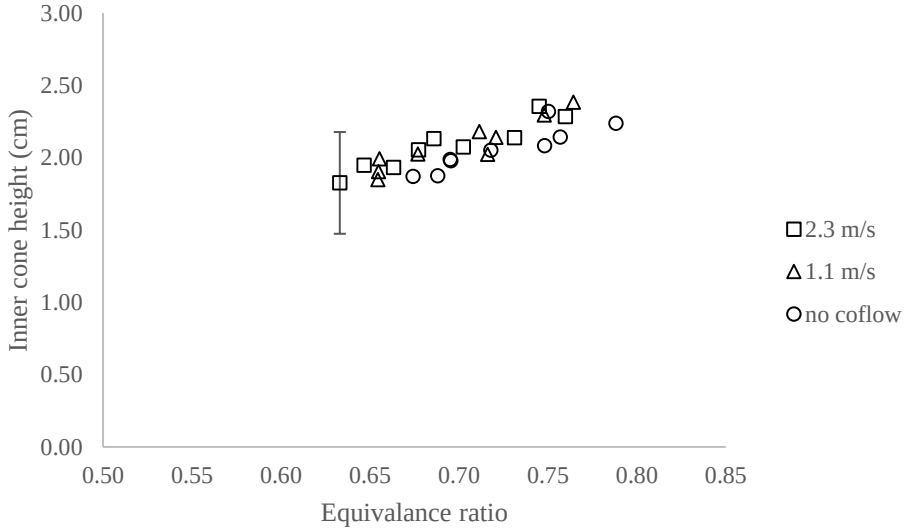


Figure 6.32: Change in inner cone height with equivalence ratio for PME25 JETA75 flames at different coflow velocities

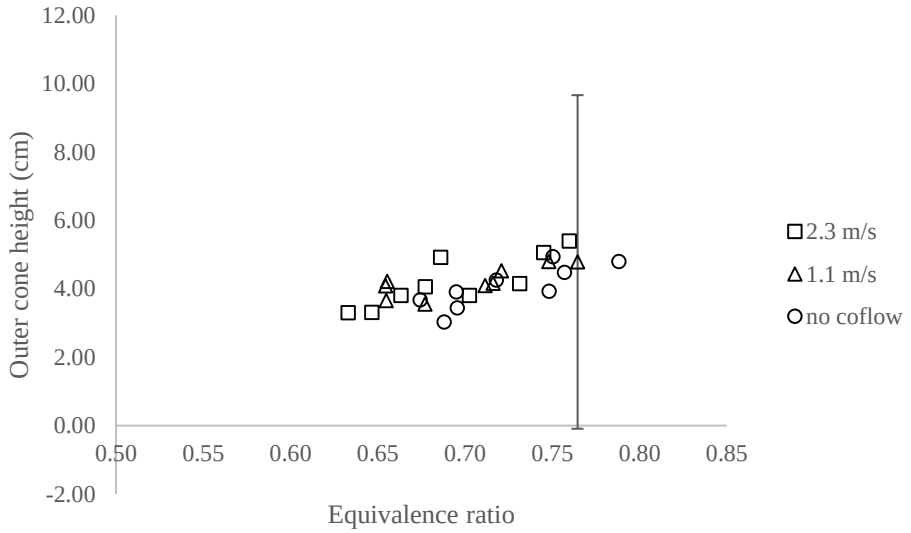


Figure 6.33: Change in outer cone height with equivalence ratio for PME25 JETA75 flames at different coflow velocities

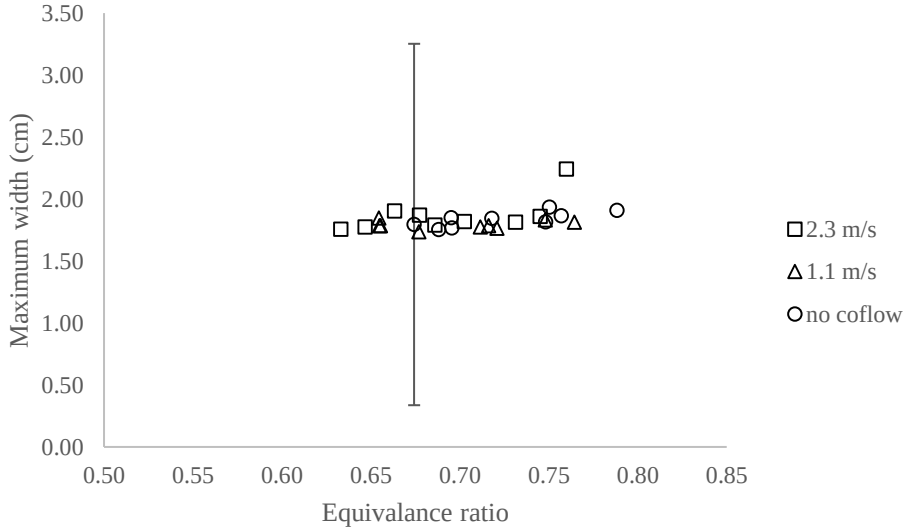


Figure 6.34: Change in outer cone width with equivalence ratio for PME25 JETA75 flames at different coflow velocities

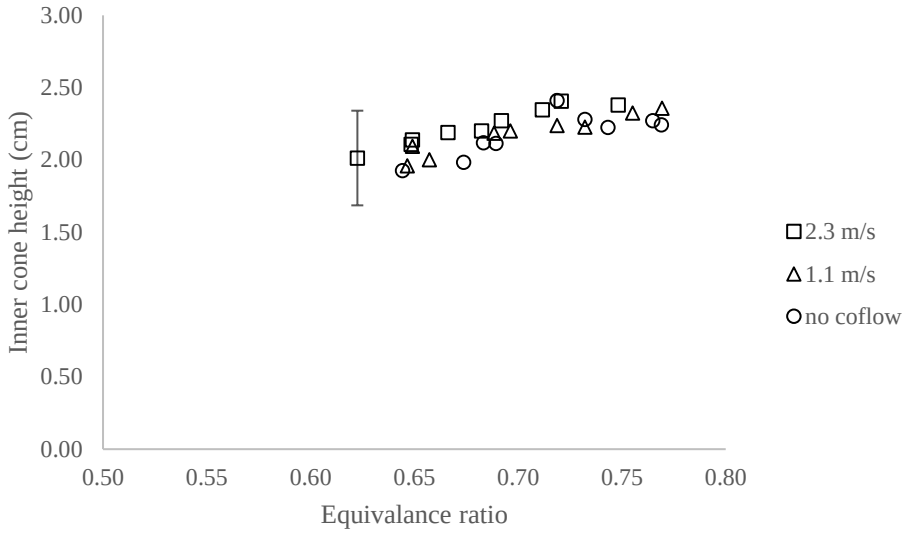


Figure 6.35: Change in inner cone height with equivalence ratio for PME50 JETA50 flames at different coflow velocities

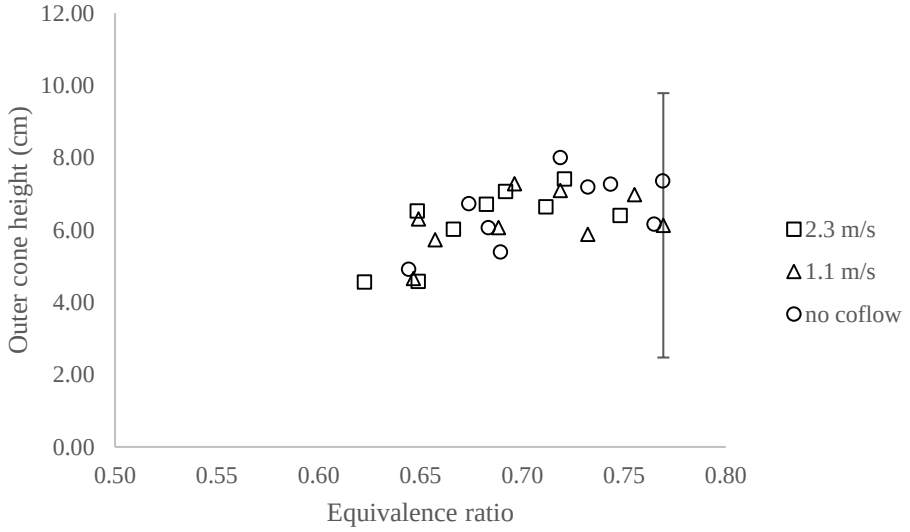


Figure 6.36: Change in outer cone height with equivalence ratio for PME50 JETA50 flames at different coflow velocities

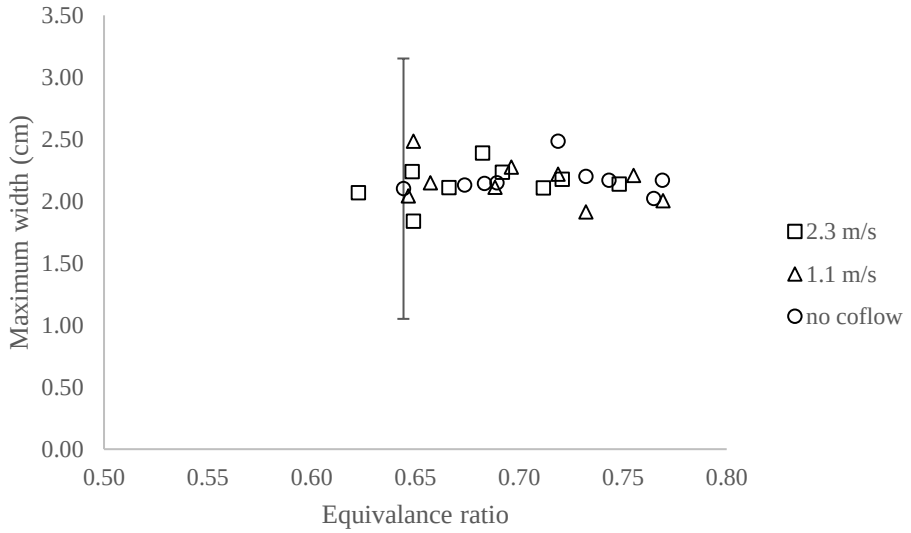


Figure 6.37: Change in outer cone width with equivalence ratio for PME50 JETA50 flames at different coflow velocities

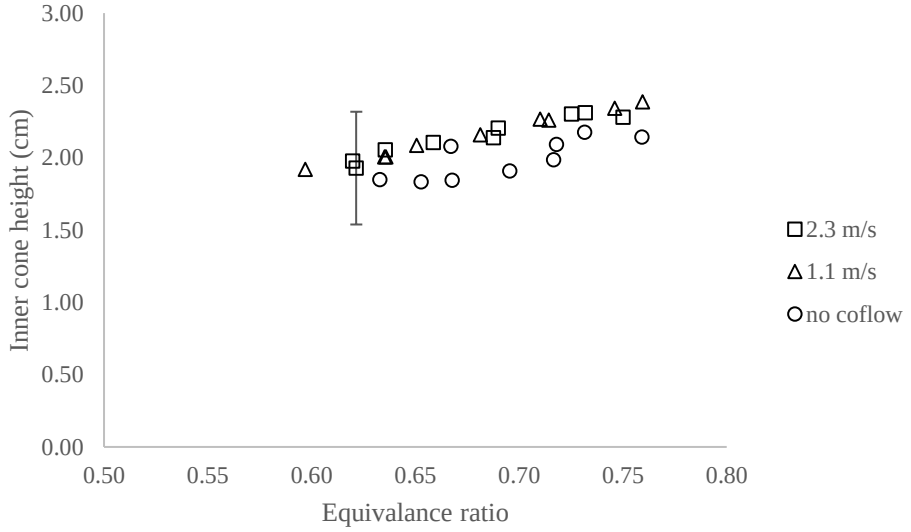


Figure 6.38: Change in inner cone height with equivalence ratio for PME75 JETA25 flames at different coflow velocities

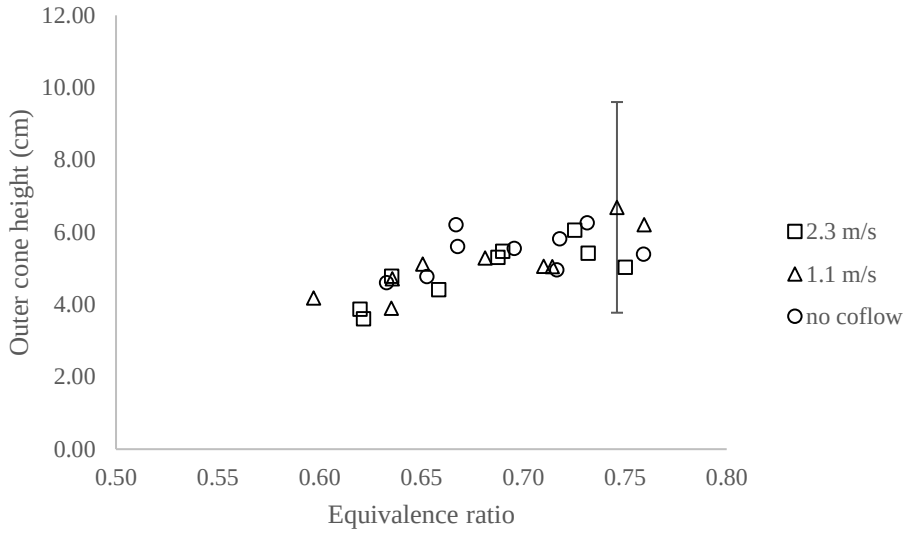


Figure 6.39: Change in outer cone height with equivalence ratio for PME75 JETA25 flames at different coflow velocities

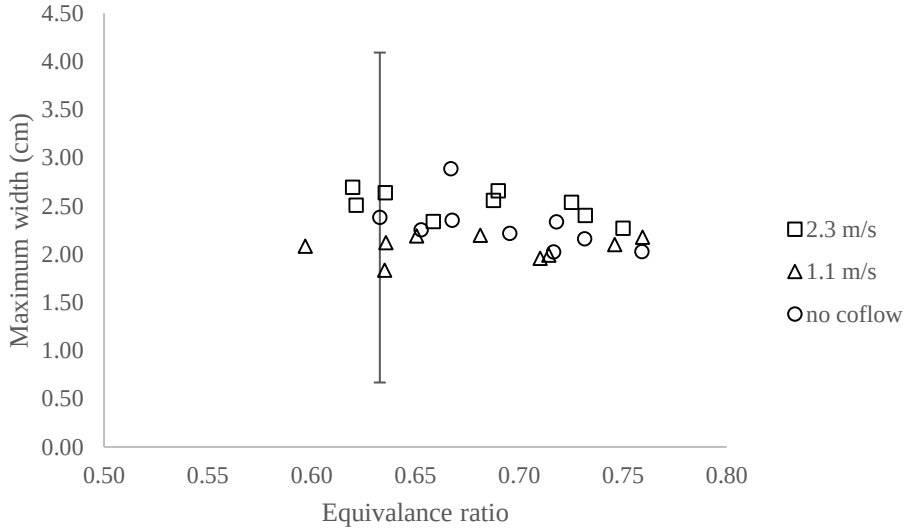


Figure 6.40: Change in outer cone width with equivalence ratio for PME75 JETA25 flames at different coflow velocities

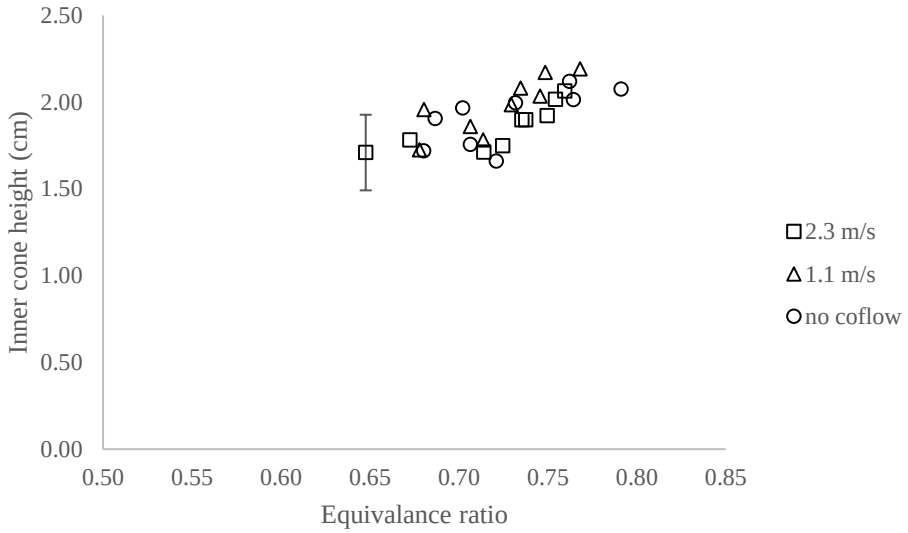


Figure 6.41: Change in inner cone height with equivalence ratio for SME flames at different coflow velocities

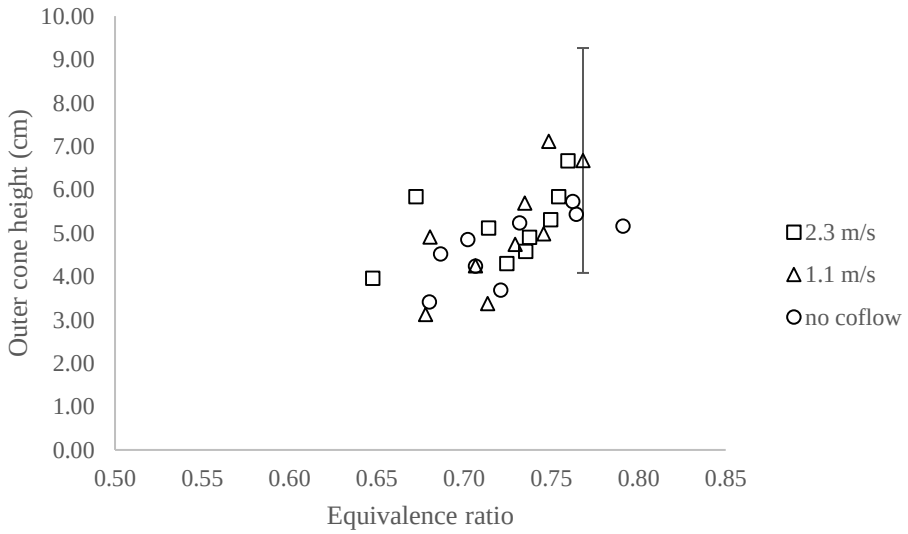


Figure 6.42: Change in outer cone height with equivalence ratio for SME flames at different coflow velocities

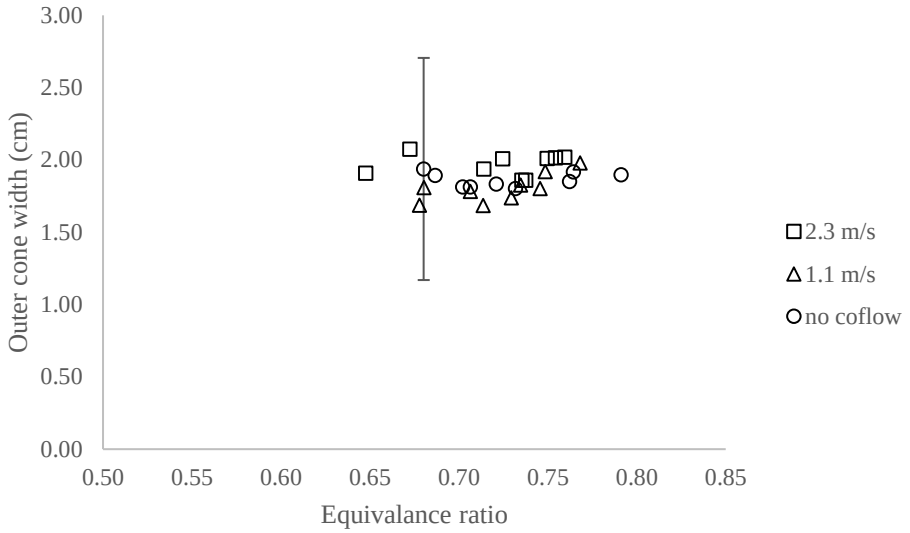


Figure 6.43: Change in outer cone width with equivalence ratio for SME flames at different coflow velocities

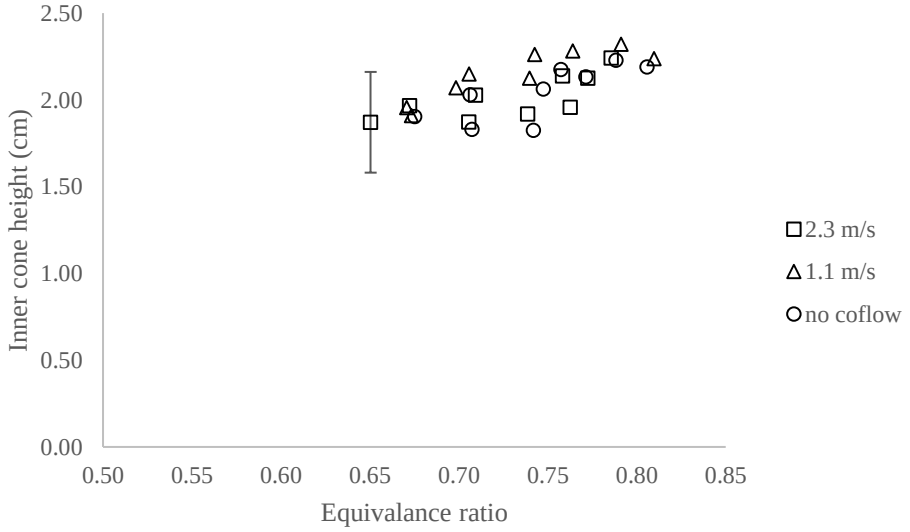


Figure 6.44: Change in inner cone height with equivalence ratio for SME25 JETA75 flames at different coflow velocities

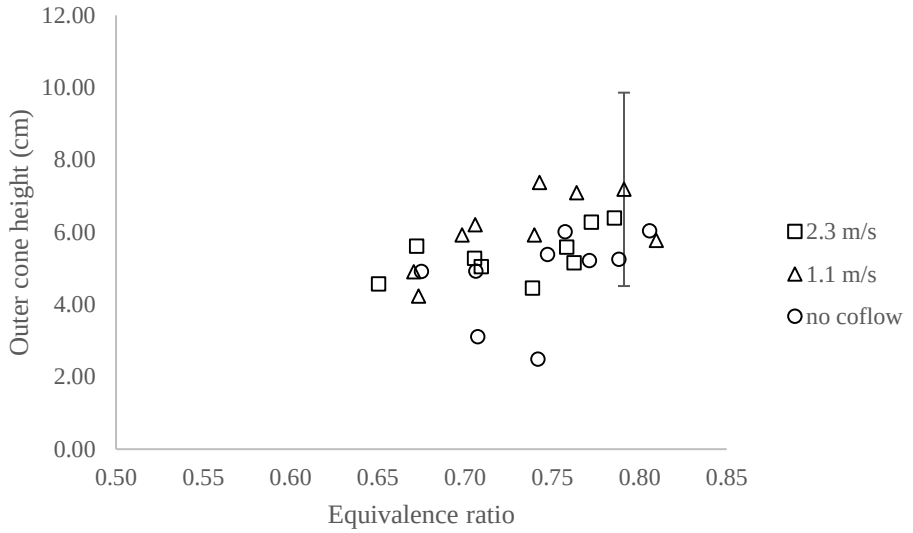


Figure 6.45: Change in outer cone height with equivalence ratio for SME25 JETA75 flames at different coflow velocities

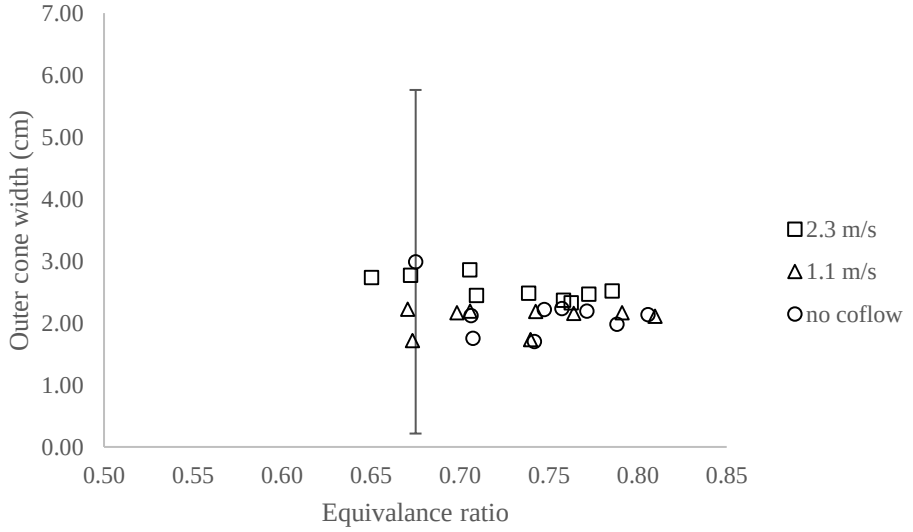


Figure 6.46: Change in outer cone width with equivalence ratio for SME25 JETA75 flames at different coflow velocities

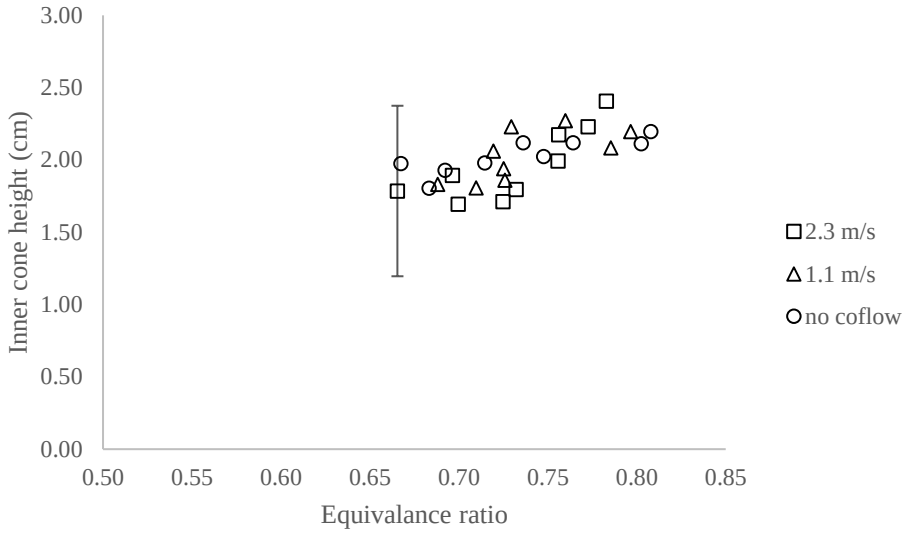


Figure 6.47: Change in inner cone height with equivalence ratio for SME50 JETA50 flames at different coflow velocities

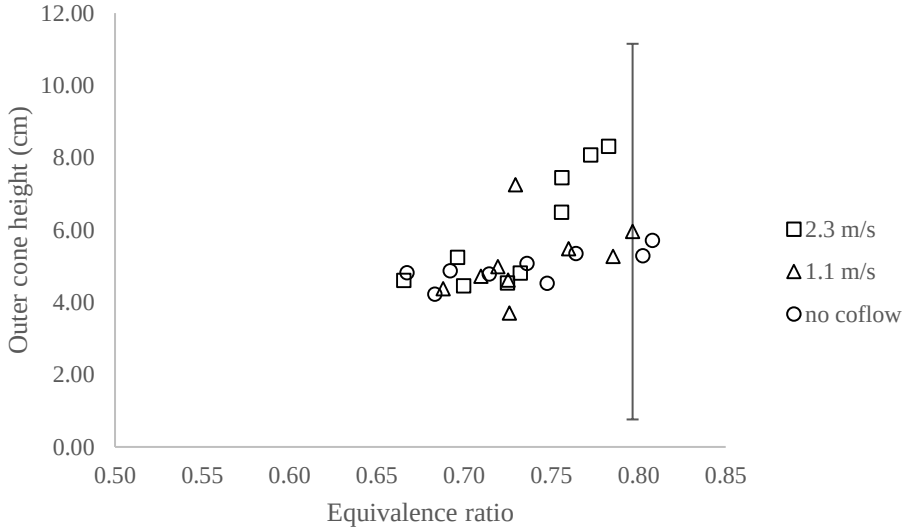


Figure 6.48: Change in outer cone height with equivalence ratio for SME50 JETA50 flames at different coflow velocities

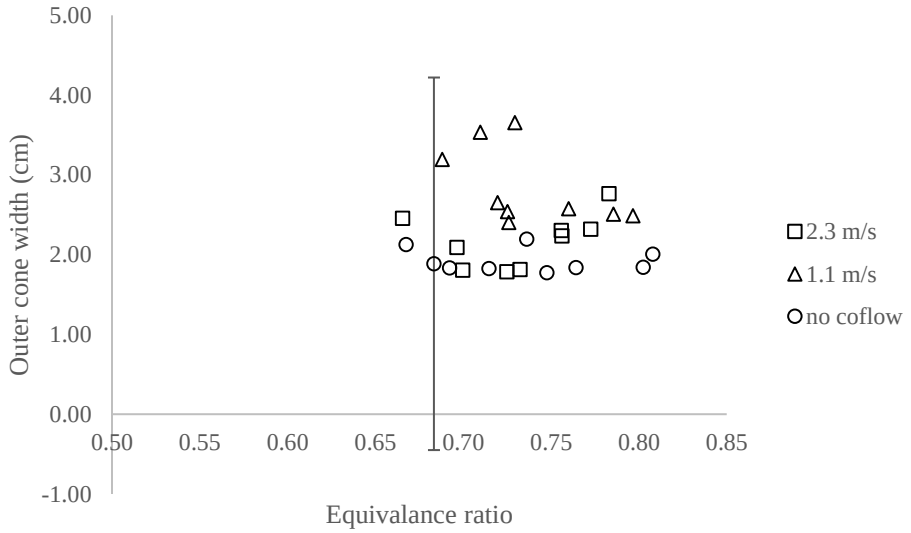


Figure 6.49: Change in outer cone width with equivalence ratio for SME50 JETA50 flames at different coflow velocities

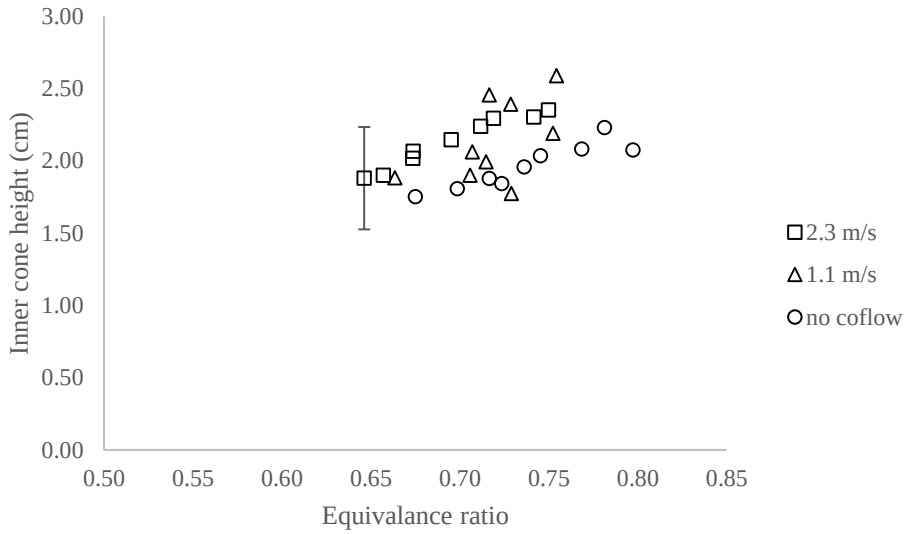


Figure 6.50: Change in inner cone height with equivalence ratio for SME75 JETA25 flames at different coflow velocities

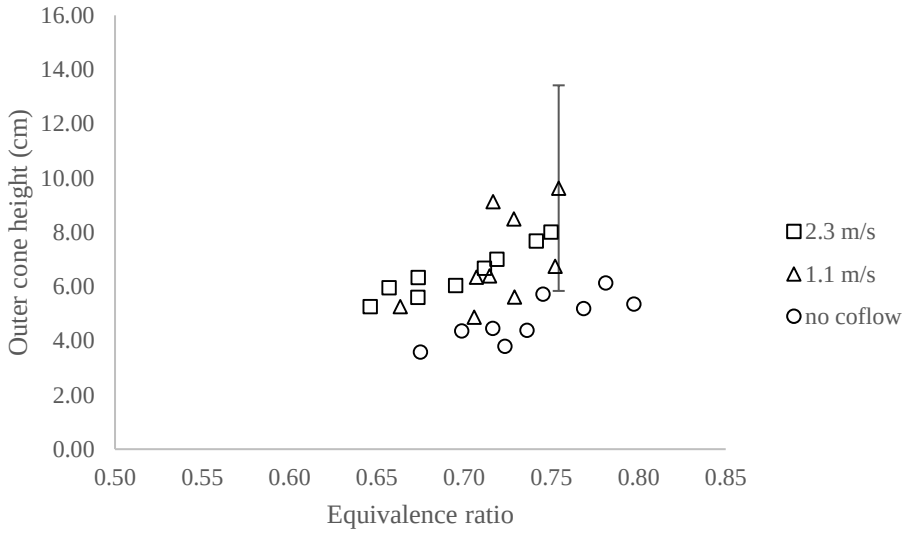


Figure 6.51: Change in outer cone height with equivalence ratio for SME75 JETA25 flames at different coflow velocities

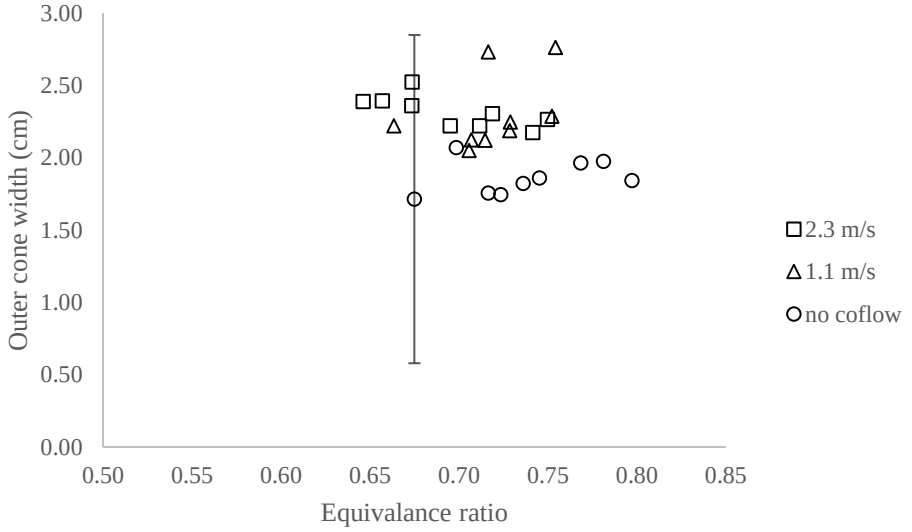


Figure 6.52: Change in outer cone width with equivalence ratio for SME75 JETA25 flames at different coflow velocities

# Appendix C: Temperature Profiles

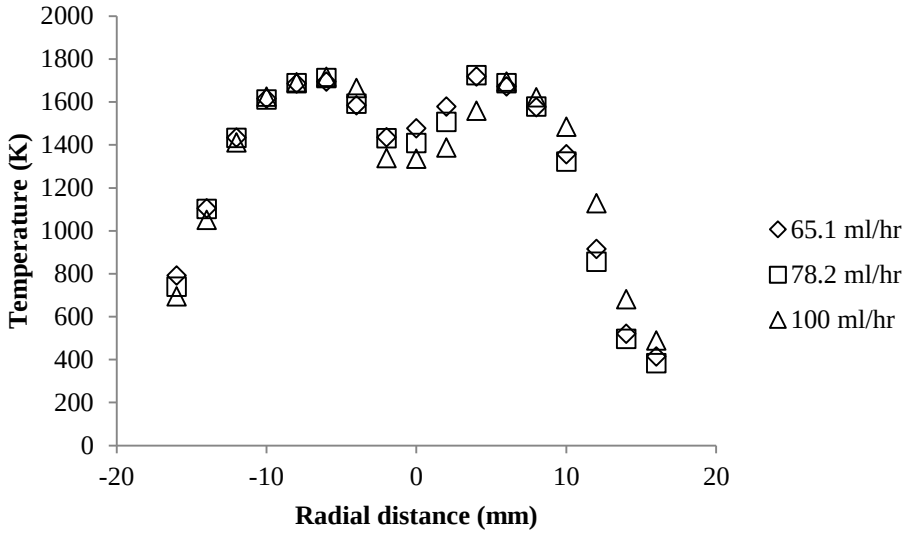


a) at half inner cone height

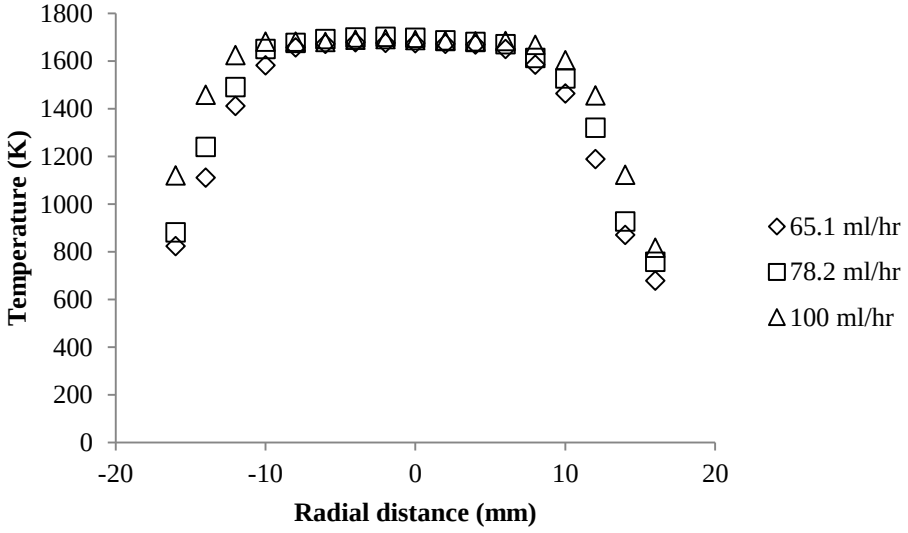


b) at inner cone tip

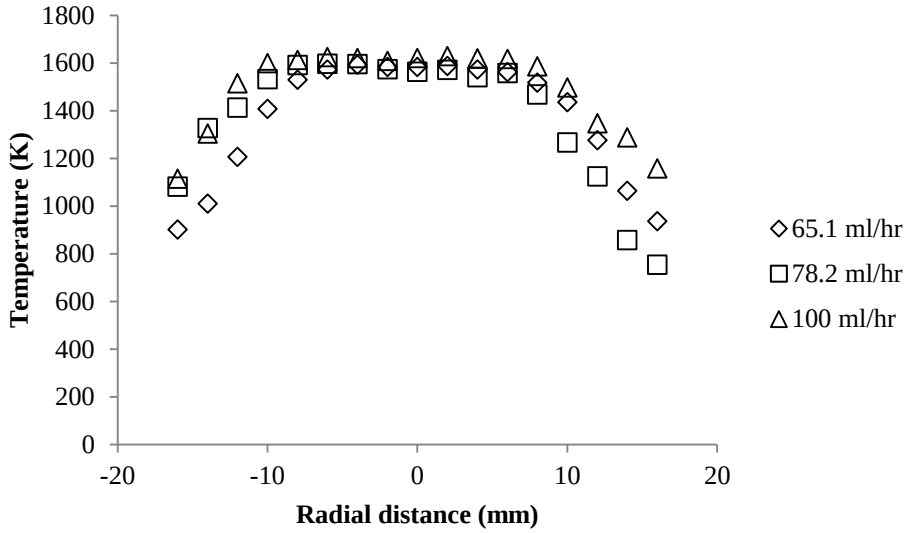


c) at twice the inner cone height

Figure 6.53: Temperature independence of fuel flow rate

The inflame temperature measurements were corrected using the equations 6.1, 6.2, and 6.3. This correction procedure is explained in more detail by Jha et al. (2008).

$$Re = (ud_{bead})/v_{air} \tag{6.1}$$

$$Nu = \left(\frac{h_c d_{bead}}{k_{air}}\right) = 2 + (0.4Re^{0.5} + 0.06Re^{0.667})Pr^{0.4} \tag{6.2}$$

$$T_{corrected} = \left(\frac{\sigma\varepsilon}{h_c}\right)(T_{Recorded}^4 - T_\infty^4) + T_{recorded} \tag{6.3}$$

T is the temperature, u is the velocity of the plume, $d_{bead}$ is the diameter of the thermocouple bead, $v_{air}$ is kinematic viscosity of air, $h_c$ is determined by the heat transfer equations, $k_{air}$ is the thermal conductivity of air, Nu is nusslet number, Pr is Prandtl number, Re is Reynolds number, σ is Stefan Boltzman constant, and ε is emissivity factor (depends on the thermocouple material).

# Appendix D: Laminar Flame Speed Estimation

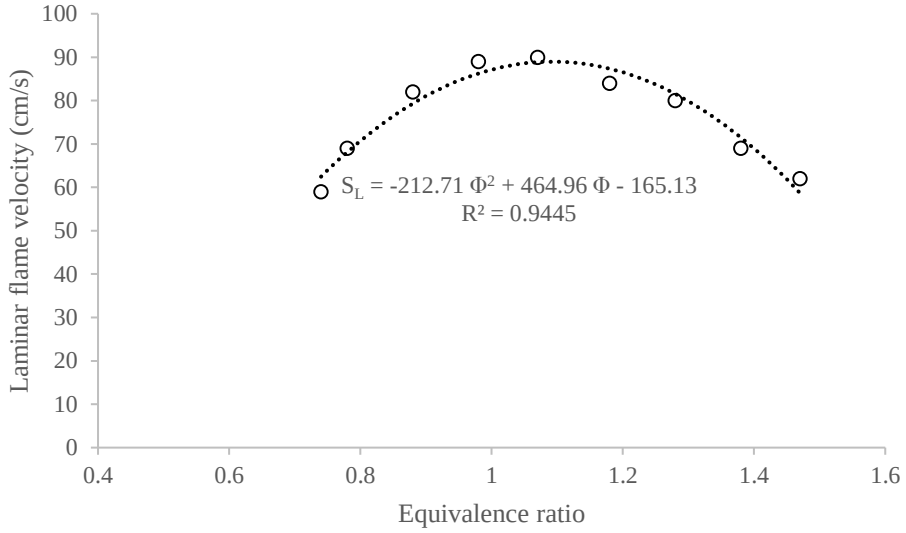


Figure 6.54: Change in laminar flame velocity with equivalence ratio; Fuel: Jet A, Temperature = 470 K

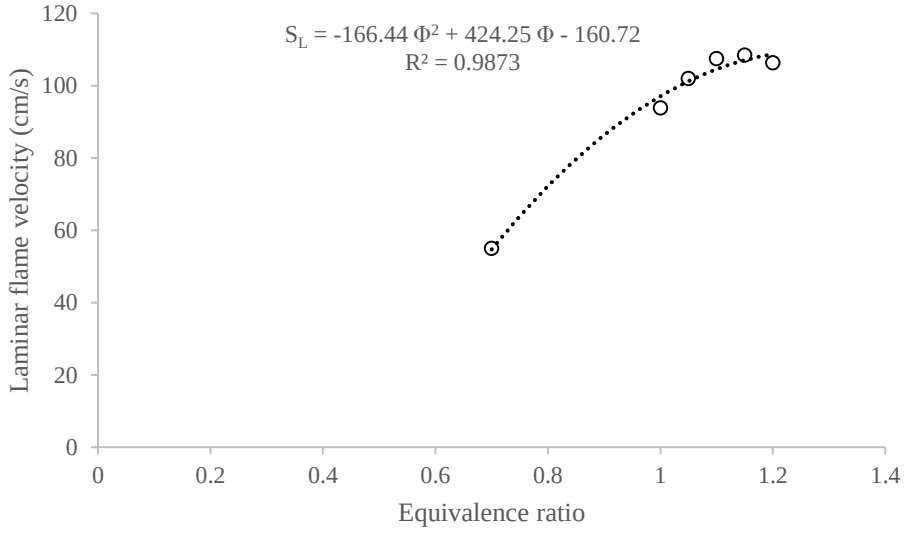


Figure 6.55: Change in laminar flame velocity with equivalence ratio; Fuel: CME, Temperature = 623 K

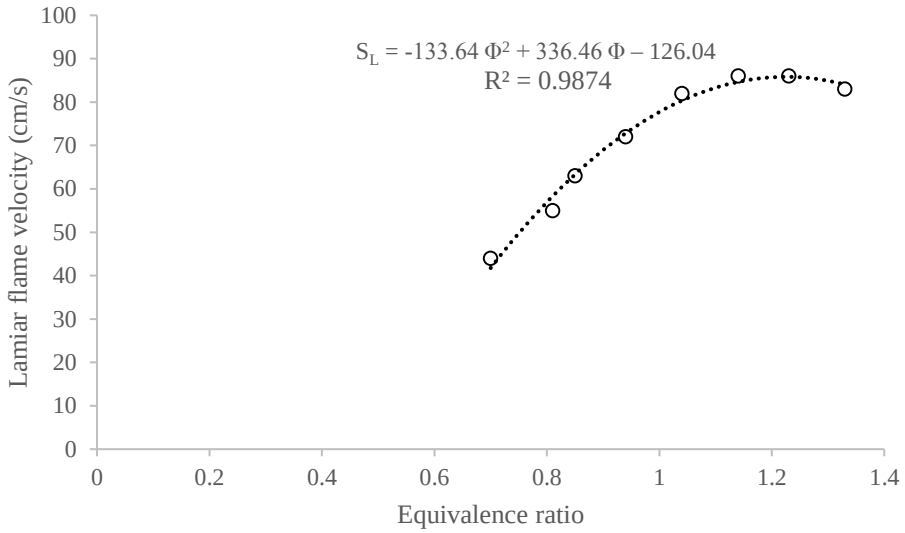


Figure 6.56: Change in laminar flame velocity with equivalence ratio; Fuel: PME, Temperature = 470 K

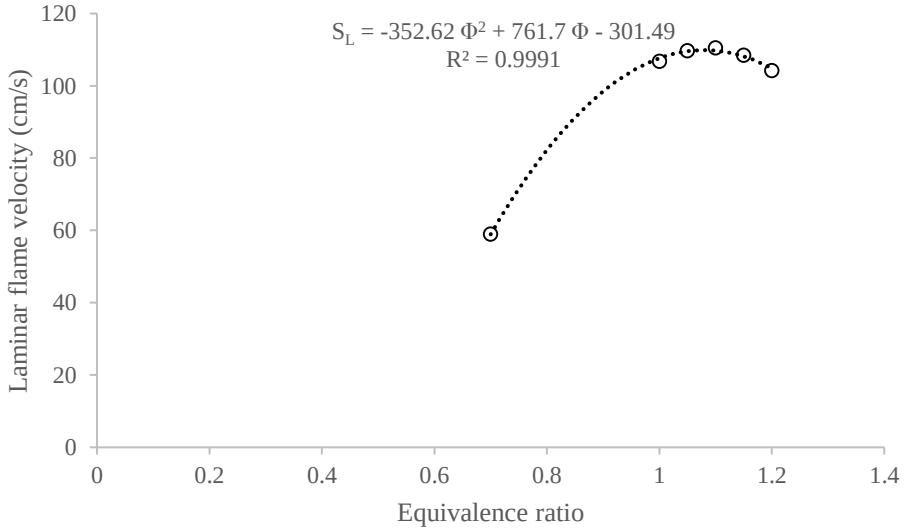


Figure 6.57: Change in laminar flame velocity with equivalence ratio; Fuel: SME, Temperature = 623 K

## Appendix E: MATLAB code

MATLAB code for calculating flame dimensions:

```
k=1;
burner_inner_diameter = 1.279; %centimeter
A=zeros(10,6); %sets metrix to size 9x6
B=zeros(10,6); %sets metrix to size 9x6
coflow = 0; %only for no coflow, and 25% and 50% coflow
A(1,:)=coflow;
B(1,:)=coflow;
inner_height_initial_array = zeros(1,5);
outer_height_initial_array = zeros(1,5);
angle_initial_array = zeros(1,5);
max_Width_initial_array = zeros(1,5);
ref_length_initial_array = zeros(1,5);
threshold_inner = 0.4;
threshold_outer=0.07;
ref_length_thickness = 10;
folder_name = 'SME blowouts\SME 75 JETA 25\'
for i=45:3:69
images = strcat('C:\Users\malet_000\Google Drive\Combustion lab\',folder_name,
num2str(coflow), '% coflow\Frames\zeros\c_', num2str(i), 'g0000.jpg');
image1 = imread (images);
```

```
%image1 = imread('C:\Users\malet_000\Desktop\testing batch\c_45g0000.jpg');
I = rgb2gray(image1);
pure = imbinarize(I,threshold_inner);%turns image into binary image with given
threshold (0.0-1.0)
BW = edge(pure); %detects edges in the grayscale image (only in gray scale)
[r1,c1] = find(BW);
x2 = max(c1);
x1 = min(c1);
y2 = max(r1);
y1 = min(r1);
bottom = y2; %where burner ends, flame attached
% loop through all elements of pure
for( s = (floor(bottom)):length(pure) )
   % set each element to 0
   pure(s,:) = 0;
end
for( s = 1:(floor(bottom)- ref_length_thickness))
   % set each element to 0
   pure(s,:) = 0;
end
BW = edge(pure); %detects edges in the grayscale image (only in gray scale)
[r1,c1] = find(BW);
x2 = max(c1);
```

```
x1 = min(c1);
ref_length = (x2 - x1);

pure = imbinarize(I,threshold_inner);%turns image into binary image with given
threshold (0.0-1.0)
BW = edge(pure); %detects edges in the grayscale image (only in gray scale)
[r1,c1] = find(BW);
x2 = max(c1);
x1 = min(c1);
y2 = max(r1);
y1 = min(r1);
bottom = y2; %where burner ends, flame attached
inner_height = burner_inner_diameter*(bottom - y1)/ref_length;
angle = atan(0.5*burner_inner_diameter/inner_height)*180/pi;


A(k+1,:,:,:,:,:) = [ i inner_height ref_length i i angle];
%{
figure(1)
title_image = num2str(i);
figtitle='blowout';
set(gcf,'numbertitle','off','name',figtitle)
subplot(3,3,k), imshowpair(image1,pure,'montage')
```

```
title(title_image);
%print('C:\Users\malet_000\Documents\MATLAB','-djpeg')
%}


pure = imbinarize(I,threshold_outer);%turns image into binary image with given
threshold (0.0-1.0)
BW = edge(pure); %detects edges in the grayscale image (only in gray scale)
[r1,c1] = find(BW);
x2 = max(c1);
x1 = min(c1);
max_Width=x2-x1;
y1 = min(r1);

if i==57
figure(1)
title_image = num2str(i);
figtitle='blowout';
set(gcf,'numbertitle','off','name',figtitle)
imshowpair(image1,pure,'montage')
title(title_image);
end
```

```
outer_height=(bottom - y1);


A(k+1,4)=[outer_height*burner_inner_diameter/ref_length];
A(k+1,5)=[max_Width*burner_inner_diameter/ref_length];
%{
figure(2)
title_image = num2str(i);
figtitle='blowout';
set(gcf,'numbertitle','off','name',figtitle)
subplot(3,3,k), imshowpair(image1,pure,'montage')
title(title_image);
%print('C:\Users\malet_000\Documents\MATLAB','-djpeg')
%}
%INITIAL
for j=0:4
images = strcat('C:\Users\malet_000\Google Drive\Combustion lab\',folder_name,
num2str(coflow),'% coflow\Initial frames\c_', num2str(i), 'i000', num2str(j),'.jpg');
image1 = imread (images);
%image1 = imread('C:\Users\malet_000\Desktop\testing batch\c_45g0000.jpg');
I = rgb2gray(image1);
pure = imbinarize(I,threshold_inner);%turns image into binary image with given
threshold (0.0-1.0)
BW = edge(pure); %detects edges in the grayscale image (only in gray scale)
```

```
[r1,c1] = find(BW);
x2 = max(c1);
x1 = min(c1);
y2 = max(r1);
y1 = min(r1);
bottom = y2;%where burner ends, flame attached

% loop through all elements of pure
for( s = (floor(bottom)):length(pure) )
   % set each element to 0
   pure(s,:) = 0;
end
for( s = 1:(floor(bottom)- ref_length_thickness))
   % set each element to 0
   pure(s,:) = 0;
end
BW = edge(pure); %detects edges in the grayscale image (only in gray scale)
[r1,c1] = find(BW);
x2 = max(c1);
x1 = min(c1);
ref_length = (x2 - x1);
```

```
pure = imbinarize(I,threshold_inner);%turns image into binary image with given
threshold (0.0-1.0)
BW = edge(pure); %detects edges in the grayscale image (only in gray scale)
[r1,c1] = find(BW);
x2 = max(c1);
x1 = min(c1);
y2 = max(r1);
y1 = min(r1);
bottom = y2;%where burner ends, flame attached

inner_height = burner_inner_diameter*(bottom - y1)/ref_length;
angle = atan(0.5*burner_inner_diameter/inner_height)*180/pi;
%{
if j==0
figure(3)
title_image = num2str(i);
figtitle='initial';
set(gcf,'numbertitle','off','name',figtitle)
subplot(3,3,k), imshowpair(image1,pure,'montage')
title(title_image);
%print('C:\Users\malet_000\Documents\MATLAB','-djpeg')
end
%}
```

```
pure = imbinarize(I,threshold_outer);%turns image into binary image with given
threshold (0.0-1.0)
BW = edge(pure); %detects edges in the grayscale image (only in gray scale)
[r1,c1] = find(BW);
x2 = max(c1);
x1 = min(c1);
max_Width=x2-x1;
y1 = min(r1);

outer_height=(bottom - y1);

inner_height_initial_array(1,(j+1)) = inner_height;
outer_height_initial_array (1,(j+1))= outer_height;
angle_initial_array (1,(j+1))= angle;
max_Width_initial_array(1,(j+1)) = max_Width;
ref_length_initial_array (1,(j+1))= ref_length;
end
inner_height=mean(inner_height_initial_array);
outer_height=mean(outer_height_initial_array);
angle=mean(angle_initial_array);
max_Width=mean(max_Width_initial_array);
ref_length=mean(ref_length_initial_array);
```

```
B(k+1,:,:,:,:,:) = [ i inner_height ref_length i i angle];

B(k+1,4)=[outer_height*burner_inner_diameter/ref_length];

B(k+1,5)=[max_Width*burner_inner_diameter/ref_length];


k=k+1;

end


%REPETITION starts HERE

k=1;

c=1;

R_first=zeros(4,6); %sets metrix to siza 4x6

R_second=zeros(4,6); %sets metrix to siza 4x6

R_first_initial=zeros(4,6); %sets metrix to siza 4x6

R_second_initial=zeros(4,6); %sets metrix to siza 4x6

f=1;

g=1;

for j=2:3

   for i=45:3:69

   if i==45 || i==54 || i==63 || i==69


title_image = num2str(i);

images = strcat('C:\Users\malet_000\Google Drive\Combustion lab\',folder_name,

num2str(coflow), '% coflow\Frames\zeros\c_', num2str(i), 'g0000 (', num2str(j), ').jpg');
```

```
image1 = imread (images);
I = rgb2gray(image1);
pure = imbinarize(I,threshold_inner);%turns image into binary image with given
threshold (0.0-1.0)
BW = edge(pure); %detects edges in the grayscale image (only in gray scale)
[r1,c1] = find(BW);
x2 = max(c1);
x1 = min(c1);
y2 = max(r1);
y1 = min(r1);
bottom = y2;%where burner ends, flame attached

% loop through all elements of pure
for( s = (floor(bottom)):length(pure) )
   % set each element to 0
   pure(s,:) = 0;
end
for( s = 1:(floor(bottom)- ref_length_thickness))
   % set each element to 0
   pure(s,:) = 0;
end
BW = edge(pure); %detects edges in the grayscale image (only in gray scale)
[r1,c1] = find(BW);
```

```
x2 = max(c1);

x1 = min(c1);

ref_length = (x2 - x1);


pure = imbinarize(I,threshold_inner);%turns image into binary image with given

threshold (0.0-1.0)

BW = edge(pure); %detects edges in the grayscale image (only in gray scale)

[r1,c1] = find(BW);

x2 = max(c1);

x1 = min(c1);

y2 = max(r1);

y1 = min(r1);

bottom = y2;%where burner ends, flame attached


inner_height = burner_inner_diameter*(bottom - y1)/ref_length;

angle = atan(0.5*burner_inner_diameter/inner_height)*180/pi;

%{

if j==2

figure(5)

title_image = num2str(i);

figtitle='blow rep';

set(gcf,'numbertitle','off','name',figtitle)

subplot(2,2,k), imshowpair(image1,pure,'montage')
```

```
title(title_image);
%print('C:\Users\malet_000\Documents\MATLAB','-djpeg')
end
%}
if j==2
R_first(k,:,:,:,:,:) = [ i inner_height ref_length i i angle];
else
   R_second(c,:,:,:,:,:) = [ i inner_height ref_length i i angle];
end



pure = imbinarize(I,threshold_outer);%turns image into binary image with given
threshold (0.0-1.0)
BW = edge(pure); %detects edges in the grayscale image (only in gray scale)
[r1,c1] = find(BW);
x2 = max(c1);
x1 = min(c1);
max_Width=x2-x1;
y1 = min(r1);
outer_height=(bottom - y1);
%{
if j==2
figure(6)
```

```
title_image = num2str(i);
figtitle='blow rep';
set(gcf,'numbertitle','off','name',figtitle)
subplot(2,2,k), imshowpair(image1,pure,'montage')
title(title_image);
%print('C:\Users\malet_000\Documents\MATLAB','-djpeg')
end
%}

if j==2
R_first(k,4)=[outer_height*burner_inner_diameter/ref_length];
R_first(k,5)=[max_Width*burner_inner_diameter/ref_length];
else
   R_second(c,4)=[outer_height*burner_inner_diameter/ref_length];
   R_second(c,5)=[max_Width*burner_inner_diameter/ref_length];
   c=c+1;
end

k=k+1;

end
   end
```

```
   %INITIAL with REPETITION
 for i=45:3:69
   if i==45 || i==54 || i==63 || i==69
 for d=0:4
images = strcat('C:\Users\malet_000\Google Drive\Combustion lab\',folder_name,
num2str(coflow),'% coflow\Initial frames\c_', num2str(i), 'i000', num2str(d), ' (',
num2str(j), ').jpg');
image1 = imread (images);

I = rgb2gray(image1);
pure = imbinarize(I,threshold_inner);%turns image into binary image with given
threshold (0.0-1.0)
BW = edge(pure); %detects edges in the grayscale image (only in gray scale)
[r1,c1] = find(BW);
x2 = max(c1);
x1 = min(c1);
y2 = max(r1);
y1 = min(r1);
bottom = y2;%where burner ends, flame attached

% loop through all elements of pure
for( s = (floor(bottom)):length(pure) )
   % set each element to 0
```

```
    pure(s,:) = 0;
end
for( s = 1:(floor(bottom)- ref_length_thickness))
    % set each element to 0
    pure(s,:) = 0;
end
BW = edge(pure); %detects edges in the grayscale image (only in gray scale)
[r1,c1] = find(BW);
x2 = max(c1);
x1 = min(c1);
ref_length = (x2 - x1);

pure = imbinarize(I,threshold_inner);%turns image into binary image with given
threshold (0.0-1.0)
BW = edge(pure); %detects edges in the grayscale image (only in gray scale)
[r1,c1] = find(BW);
x2 = max(c1);
x1 = min(c1);
y2 = max(r1);
y1 = min(r1);
bottom = y2;%where burner ends, flame attached

inner_height = burner_inner_diameter*(bottom - y1)/ref_length;
```

```
angle = atan(0.5*burner_inner_diameter/inner_height)*180/pi;



pure = imbinarize(I,threshold_outer);%turns image into binary image with given
threshold (0.0-1.0)
BW = edge(pure); %detects edges in the grayscale image (only in gray scale)
[r1,c1] = find(BW);
x2 = max(c1);
x1 = min(c1);
max_Width=x2-x1;
y1 = min(r1);

outer_height=(bottom - y1);

inner_height_initial_array(1,(d+1)) = inner_height;
outer_height_initial_array (1,(d+1))= outer_height;
angle_initial_array (1,(d+1))= angle;
max_Width_initial_array(1,(d+1)) = max_Width;
ref_length_initial_array (1,(d+1))= ref_length;
  end

inner_height=mean(inner_height_initial_array);
outer_height=mean(outer_height_initial_array);
```

```
angle=mean(angle_initial_array);
max_Width=mean(max_Width_initial_array);
ref_length=mean(ref_length_initial_array);

if j==2
R_first_initial(f,:,:,:,:,:) = [ i inner_height ref_length i i angle];
R_first_initial(f,4)=[outer_height*burner_inner_diameter/ref_length];
R_first_initial(f,5)=[max_Width*burner_inner_diameter/ref_length];

else
   R_second_initial(g,:,:,:,:,:) = [ i inner_height ref_length i i angle];
   R_second_initial(g,4)=[outer_height*burner_inner_diameter/ref_length];
   R_second_initial(g,5)=[max_Width*burner_inner_diameter/ref_length];
   g=g+1;
end
k=k+1;
f=f+1;

end
 end
end

filename = 'Blowouts test.xlsx';
```

```
warning('off','MATLAB:xlswrite:AddSheet');
T_blowout = array2table(A,'VariableNames',{'Gear' 'inner_Height' 'ref_length'
'outer_Height' 'max_Width' 'angle'})
T_blowout_first_rep = array2table(R_first,'VariableNames',{'Gear' 'inner_Height'
'ref_length' 'outer_Height' 'max_Width' 'angle'})
T_blowout_second_rep = array2table(R_second,'VariableNames',{'Gear' 'inner_Height'
'ref_length' 'outer_Height' 'max_Width' 'angle'})
T_initial = array2table(B,'VariableNames',{'Gear' 'inner_Height' 'ref_length'
'outer_Height' 'max_Width' 'angle'})
T_initial_first_rep = array2table(R_first_initial,'VariableNames',{'Gear' 'inner_Height'
'ref_length' 'outer_Height' 'max_Width' 'angle'})
T_initial_second_rep = array2table(R_second_initial,'VariableNames',{'Gear'
'inner_Height' 'ref_length' 'outer_Height' 'max_Width' 'angle'})
if coflow == 50
    original='A25';
    first_rep='A36';
    second_rep='A41';
elseif coflow==25
    original='A48';
    first_rep='A59';
    second_rep='A64';
else
    original='A71';
```

```
    first_rep='A82';
    second_rep='A87';
end
sheet_no_blowout=1;
sheet_no_initial=2;
writetable(T_blowout,filename,'Sheet',sheet_no_blowout,'Range',original)
writetable(T_blowout_first_rep,filename,'Sheet',sheet_no_blowout,'Range',first_rep)
writetable(T_blowout_second_rep,filename,'Sheet',sheet_no_blowout,'Range',second_r
ep)
writetable(T_initial,filename,'Sheet',sheet_no_initial,'Range',original)
writetable(T_initial_first_rep,filename,'Sheet',sheet_no_initial,'Range',first_rep)
writetable(T_initial_second_rep,filename,'Sheet',sheet_no_initial,'Range',second_rep)
```

MATLAB code for calculating liftoff height:

```
k=1;
burner_inner_diameter = 1.279; %centimeter
lift=zeros(10,4); %sets metrix to size 9x6
B=zeros(10,6); %sets metrix to size 9x6
coflow = 75;
lift(1,:)=coflow;
B(1,:)=coflow;
inner_height_initial_array = zeros(1,5);
outer_height_initial_array = zeros(1,5);
```

```
angle_initial_array = zeros(1,5);

bottom_initial_array = zeros(1,5);

max_Width_initial_array = zeros(1,5);

ref_length_initial_array = zeros(1,5);

liftoff_length_array=zeros(1,20);

array_zeros = zeros; %returns a row of 0s and 1s - 0 if the row of pure contains no 1s, 1
vice versa

threshold_inner = 0.4;

threshold_outer=0.07;

threshold_inner_lifted=0.21;

ref_length_thickness = 10;

folder_name='Jet A blowouts\Jet A pure\'

for i=45:3:69

%INITIAL

for j=0:4

images = strcat('C:\Users\malet_000\Google Drive\Combustion lab\',folder_name,
num2str(coflow),'% coflow\Initial frames\c_', num2str(i), 'i000', num2str(j),'.jpg');

image1 = imread (images);

%image1 = imread('C:\Users\malet_000\Desktop\testing batch\c_45g0000.jpg');

I = rgb2gray(image1);

pure = imbinarize(I,threshold_inner);%turns image into binary image with given
threshold (0.0-1.0)

BW = edge(pure); %detects edges in the grayscale image (only in gray scale)
```

```
[r1,c1] = find(BW);
y2 = max(r1);
y1 = min(r1);
bottom = y2; %where burner ends, flame attached

% loop through all elements of pure
for( s = (floor(bottom)):length(pure) )
   % set each element to 0
   pure(s,:) = 0;
end
for( s = 1:(floor(bottom)- ref_length_thickness))
   % set each element to 0
   pure(s,:) = 0;
end
BW = edge(pure); %detects edges in the grayscale image (only in gray scale)
[r1,c1] = find(BW);
x2 = max(c1);
x1 = min(c1);
ref_length = (x2 - x1);
%{
if j==0
figure(5)
title_image = num2str(i);
```

```
figtitle='initial';
set(gcf,'numbertitle','off','name',figtitle)
subplot(3,3,k), imshowpair(image1,pure,'montage')
title(title_image);
%print('C:\Users\malet_000\Documents\MATLAB','-djpeg')
end
%}

pure = imbinarize(I,threshold_inner);%turns image into binary image with given
threshold (0.0-1.0)
BW = edge(pure); %detects edges in the grayscale image (only in gray scale)
[r1,c1] = find(BW);
x2 = max(c1);
x1 = min(c1);
y2 = max(r1);
y1 = min(r1);
bottom = y2; %where burner ends, flame attached


inner_height = burner_inner_diameter*(bottom - y1)/ref_length;
angle = atan(0.5*burner_inner_diameter/inner_height)*180/pi;

%{
```

```
if j==0
figure(1)
title_image = num2str(i);
figtitle='initial';
set(gcf,'numbertitle','off','name',figtitle)
subplot(3,3,k), imshowpair(image1,pure,'montage')
title(title_image);
%print('C:\Users\malet_000\Documents\MATLAB','-djpeg')
end
%}


pure = imbinarize(I,threshold_outer);%turns image into binary image with given
threshold (0.0-1.0)
BW = edge(pure); %detects edges in the grayscale image (only in gray scale)
[r1,c1] = find(BW);
x2 = max(c1);
x1 = min(c1);
max_Width=x2-x1;
y1 = min(r1);


outer_height=(bottom - y1);
```

```
inner_height_initial_array(1,(j+1)) = inner_height;
outer_height_initial_array (1,(j+1))= outer_height;
angle_initial_array (1,(j+1))= angle;
bottom_initial_array (1,(j+1))= bottom;
max_Width_initial_array(1,(j+1)) = max_Width;
ref_length_initial_array (1,(j+1))= ref_length;
end
inner_height=mean(inner_height_initial_array);
outer_height=mean(outer_height_initial_array);
angle=mean(angle_initial_array);
max_Width=mean(max_Width_initial_array);
ref_length=mean(ref_length_initial_array);
bottom = mean(bottom_initial_array);

B(k+1,:,:,:,:,:) = [ i inner_height ref_length i i angle];
B(k+1,4)=[outer_height*burner_inner_diameter/ref_length];
B(k+1,5)=[max_Width*burner_inner_diameter/ref_length];

%LIFT OFF
for z=0:19
   if z<10
      suffix ='g000';
```

```
    else
        suffix = 'g00';
    end
images = strcat('C:\Users\malet_000\Google Drive\Combustion lab\',folder_name,
num2str(coflow), '% coflow\Frames\c_', num2str(i), suffix, num2str(z), '.jpg');
image1 = imread (images);
I = rgb2gray(image1);
pure = imbinarize(I,threshold_inner_lifted);%turns image into binary image with given
threshold (0.0-1.0)
BW = edge(pure); %detects edges in the grayscale image (only in gray scale)
[r1,c1] = find(BW);
x2 = max(c1);
x1 = min(c1);
y2 = max(r1);
y1 = min(r1);

[rr lc]=size(pure);
array_zeros = zeros(rr,1);
length(pure);
% fill up array_zeros
for( s = 1:rr )
    % set rows with 1 to 1
    for( p = 1:lc)
```

```
        if pure(s,p) == 1
            array_zeros(s,1) = 1;
        end
    end
end


for( s = 1:(length(array_zeros)-7) )
    if array_zeros (s,1)==1
        if array_zeros(s+1,1)==0 && array_zeros(s+2,1)==0 && array_zeros(s+7,1)==0
            offset = s+1;
            break
        end
    end
end









%{
if z==0
figure(1)
```

```
%title_image = num2str(i);
title_image = num2str(i);
figtitle='lifted';
set(gcf,'numbertitle','off','name',figtitle)
subplot(3,3,k), imshowpair(image1,pure,'montage')
title(title_image);
end

if i==69 && z==0
figure(2)
title_image = num2str(i);
figtitle='lifted 45';
set(gcf,'numbertitle','off','name',figtitle)
imshowpair(image1,pure,'montage')
title(title_image);
array_zeros;
end
%}


% loop through all elements of pure
for( s = offset:length(pure) )
   % set each element to 0
```

```
    pure(s,:) = 0;
end

%{
if i==45 && z==0
figure(3)
title_image = num2str(i);
figtitle='corrected';
set(gcf,'numbertitle','off','name',figtitle)
imshow(pure)
title(title_image);
%print('C:\Users\malet_000\Documents\MATLAB','-djpeg')
end
%}
BW = edge(pure); %detects edges in the grayscale image (only in gray scale)
[r1,c1] = find(BW);
x2 = max(c1);
x1 = min(c1);
y2 = max(r1);
y1 = min(r1);

if i==57 && z==0
figure(2)
```

```
title_image = num2str(i);
figtitle='lifted 57';
set(gcf,'numbertitle','off','name',figtitle)
imshowpair(image1,pure,'montage')
title(title_image);
array_zeros;
end


if i==57
figure(3)
%title_image = num2str(i);
title_image = num2str(z+1);
figtitle='corrrected';
set(gcf,'numbertitle','off','name',figtitle)
subplot(5,4,z+1), imshow(image1)
title(title_image);
end


liftoff_length = burner_inner_diameter*(bottom-y2)/ref_length;
%angle = atan(0.5*burner_inner_diameter/inner_height)*180/pi;
```

```
liftoff_length_array(1,(z+1))=liftoff_length;



end

liftoff_length = mean(liftoff_length_array);



lift(k+1,:,:,:,:,:) = [ i liftoff_length ref_length  bottom];

k=k+1;
end



%REPETITION starts HERE
k=1;
R_first=zeros(4,4); %sets metrix to siza 4x4
R_second=zeros(4,4); %sets metrix to siza 4x4
R_first_initial=zeros(4,6); %sets metrix to siza 4x6
R_second_initial=zeros(4,6); %sets metrix to siza 4x6
f=1;
g=1;
```

```
for j=2:3
     %INITIAL with REPETITION
 for i=45:3:69
   if i==45 || i==54 || i==63 || i==69
 for d=0:4
images = strcat('C:\Users\malet_000\Google Drive\Combustion lab\',folder_name,
num2str(coflow),'% coflow\Initial frames\c_', num2str(i), 'i000', num2str(d), ' (',
num2str(j), ').jpg');
image1 = imread (images);

I = rgb2gray(image1);


pure = imbinarize(I,threshold_inner);%turns image into binary image with given
threshold (0.0-1.0)
BW = edge(pure); %detects edges in the grayscale image (only in gray scale)
[r1,c1] = find(BW);
y2 = max(r1);
y1 = min(r1);
%inner_tip = y2;
bottom = y2;%where burner ends, flame attached
```

```
% loop through all elements of pure
for( s = (floor(bottom)):length(pure) )
   % set each element to 0
   pure(s,:) = 0;
end
for( s = 1:(floor(bottom)- ref_length_thickness))
   % set each element to 0
   pure(s,:) = 0;
end
BW = edge(pure); %detects edges in the grayscale image (only in gray scale)
[r1,c1] = find(BW);
x2 = max(c1);
x1 = min(c1);
ref_length = (x2 - x1);

pure = imbinarize(I,threshold_inner);%turns image into binary image with given
threshold (0.0-1.0)
BW = edge(pure); %detects edges in the grayscale image (only in gray scale)
[r1,c1] = find(BW);
x2 = max(c1);
x1 = min(c1);
y2 = max(r1);
y1 = min(r1);
```

```
bottom = y2; %where burner ends, flame attached

inner_height = burner_inner_diameter*(bottom - y1)/ref_length;
angle = atan(0.5*burner_inner_diameter/inner_height)*180/pi;


pure = imbinarize(I,threshold_outer);%turns image into binary image with given
threshold (0.0-1.0)
BW = edge(pure); %detects edges in the grayscale image (only in gray scale)
[r1,c1] = find(BW);
x2 = max(c1);
x1 = min(c1);
max_Width=x2-x1;
y1 = min(r1);

outer_height=(bottom - y1);


inner_height_initial_array(1,(d+1)) = inner_height;
outer_height_initial_array (1,(d+1))= outer_height;
angle_initial_array (1,(d+1))= angle;
max_Width_initial_array(1,(d+1)) = max_Width;
ref_length_initial_array (1,(d+1))= ref_length;
```

```
bottom_initial_array (1,(d+1))= bottom;
  end

inner_height=mean(inner_height_initial_array);
outer_height=mean(outer_height_initial_array);
angle=mean(angle_initial_array);
max_Width=mean(max_Width_initial_array);
ref_length=mean(ref_length_initial_array);
bottom = mean(bottom_initial_array);

if j==2
R_first_initial(f,:,:,:,:,:) = [ i inner_height ref_length i i angle];
R_first_initial(f,4)=[outer_height*burner_inner_diameter/ref_length];
R_first_initial(f,5)=[max_Width*burner_inner_diameter/ref_length];

else
   R_second_initial(g,:,:,:,:,:) = [ i inner_height ref_length i i angle];
   R_second_initial(g,4)=[outer_height*burner_inner_diameter/ref_length];
   R_second_initial(g,5)=[max_Width*burner_inner_diameter/ref_length];
   g=g+1;
end

f=f+1;
```

```
%LIFTOFF with REPETITION
 for z=0:19
 if z<10
       suffix ='g000';
   else
       suffix = 'g00';
 end

images = strcat('C:\Users\malet_000\Google Drive\Combustion lab\',folder_name,
num2str(coflow), '% coflow\Frames\c_', num2str(i), suffix, num2str(z), ' (', num2str(j),
').jpg');
image1 = imread (images);
I = rgb2gray(image1);
pure = imbinarize(I,threshold_inner_lifted);%turns image into binary image with given
threshold (0.0-1.0)
BW = edge(pure); %detects edges in the grayscale image (only in gray scale)
[r1,c1] = find(BW);
x2 = max(c1);
x1 = min(c1);
y2 = max(r1);
y1 = min(r1);
```

```
[rr lc]=size(pure);
array_zeros = zeros(rr,1);
length(pure);
% loop through all elements of pure
for( s = 1:rr )
   % set each element to 0
   for( p = 1:lc)
      if pure(s,p) == 1
         array_zeros(s,1) = 1;
      end
   end
end

for( s = 1:(length(array_zeros)-7) )
   if array_zeros (s,1)==1
      if array_zeros(s+1,1)==0 && array_zeros(s+2,1)==0 && array_zeros(s+7,1)==0
         offset = s+1;
         break
      end
   end
end

% loop through all elements of pure
```

```
for( s = offset:length(pure) )
      pure(s,:) = 0; % set each element to 0
end
BW = edge(pure); %detects edges in the grayscale image (only in gray scale)
[r1,c1] = find(BW);
x2 = max(c1);
x1 = min(c1);
y2 = max(r1);
y1 = min(r1);

liftoff_length = burner_inner_diameter*(bottom-y2)/ref_length;
liftoff_length_array(1,(z+1))=liftoff_length;
end

liftoff_length = mean(liftoff_length_array);

if j==2
R_first(k,:,:,:) = [ i liftoff_length ref_length  bottom];
else
   R_second((k-4),:,:,:,:,:) = [ i liftoff_length ref_length  bottom];
 end
```

```
k=k+1;


end
end
end



filename = 'Blowouts test.xlsx';
warning('off','MATLAB:xlswrite:AddSheet');
T_liftoff = array2table(lift,'VariableNames',{'Gear' 'liftoff_length' 'ref_length'
'bottom'})
T_liftoff_first_rep = array2table(R_first,'VariableNames',{'Gear' 'liftoff_length'
'ref_length'  'bottom'})
T_liftoff_second_rep = array2table(R_second,'VariableNames',{'Gear' 'liftoff_length'
'ref_length'  'bottom'})
T_initial = array2table(B,'VariableNames',{'Gear' 'inner_Height' 'ref_length'
'outer_Height' 'max_Width' 'angle'});
T_initial_first_rep = array2table(R_first_initial,'VariableNames',{'Gear' 'inner_Height'
'ref_length' 'outer_Height' 'max_Width' 'angle'});
T_initial_second_rep = array2table(R_second_initial,'VariableNames',{'Gear'
'inner_Height' 'ref_length' 'outer_Height' 'max_Width' 'angle'});
if coflow == 75
    original='A2';
```

```
    first_rep='A13';
    second_rep='A18';
elseif coflow == 50
    original='A25';
    first_rep='A36';
    second_rep='A41';
elseif coflow==25
    original='A48';
    first_rep='A59';
    second_rep='A64';
else
    original='A71';
    first_rep='A82';
    second_rep='A87';
end
sheet_no_liftoff=1;
sheet_no_initial=2;
writetable(T_liftoff,filename,'Sheet',sheet_no_liftoff,'Range',original)
writetable(T_liftoff_first_rep,filename,'Sheet',sheet_no_liftoff,'Range',first_rep)
writetable(T_liftoff_second_rep,filename,'Sheet',sheet_no_liftoff,'Range',second_rep)
writetable(T_initial,filename,'Sheet',sheet_no_initial,'Range',original)
writetable(T_initial_first_rep,filename,'Sheet',sheet_no_initial,'Range',first_rep)
writetable(T_initial_second_rep,filename,'Sheet',sheet_no_initial,'Range',second_rep)
```